Solveig Fadnes

Two-Dimensional Blood Velocity Estimation for Intracardiac Flow Assessment

Thesis for the degree of Philosophiae Doctor

Trondheim, September 2014

Norwegian University of Science and Technology
Faculty of Medicine
Department of Circulation and Medical Imaging

NTNU – Trondheim
Norwegian University of
Science and Technology

NTNU
Norwegian University of Science and Technology

Thesis for the degree of Philosophiae Doctor

Faculty of Medicine
Department of Circulation and Medical Imaging

ISBN 978-82-326-0432-6 (printed ver.)
ISBN 978-82-326-0433-3 (electronic ver.)
ISSN 1503-8181

Doctoral theses at NTNU, 2014:260

Printed by NTNU-trykk

Måling av blodstrømshastigheter i hjertet

Ultralyd (ekkokardiografi) og fargedoppler er viktige verktøy som brukes for å detektere og visualisere medfødt hjertefeil. To av de mest vanlige formene for medfødt hjertefeil er atrie- og ventrikkelseptumdefekter, som er hull i hjerteveggen (septum) mellom forkamrene eller hjertekamrene. Et slikt hull gjør vanligvis at blod kan strømme direkte fra venstre til høyre side av hjertet som igjen kan føre til økt belastning i lungekretsløpet. Hastigheten til blodstrømmen gjennom hullet er et av målene som brukes til å avgjøre defektens alvorlighetsgrad. Denne målingen blir kun nøyaktig med konvensjonelle ultralydmetoder hvis ultralydstrålen har samme retning som blodstrømmen. Dette er på grunn av en fundamental begrensning ved konvensjonell ultralyd; bare den endimensjonale hastighetskomponenten langs ultralydstrålen blir målt. Utvikling av nye ultralydmetoder som kan måle to eller tre hastighetskomponenter av den tredimensjonale blodstrømsvektoren er derfor av klinisk nytteverdi og vil både kunne bedre visualiseringen av den komplekse blodstrømningen gjennom hjertet og gi bedre kvantitative mål på blodstrømshastigheten.

Grunnlaget for arbeidet som er presentert i denne avhandlingen er de teknologiske nyvinningene som gjør at vi nå kan avbilde med en mye høyere bilderate enn før. Den høye bilderaten oppnås ved å sende ufokuserte (plane) i stedet for fokuserte lydbølger og ved å bruke parallell stråleforming som gjør at vi kan lage et ultralydbilde etter bare én utsendt lydbølge. I denne avhandlingen brukte vi en metode kalt *speckle tracking* for å estimere de todimensjonale blodstrømshastighetene. Ekkoet fra blod (og vev) gir et unikt intensitetsmønster i ultralydbildet og en kan derfor spore dette specklemønsteret fra bilde til bilde for å finne forflytningen til blodet og estimere blodstrømshastigheten. I den første studien ble nyfødte med hjertefeil undersøkt med den nye teknikken, og resultatene indikerer at den nye metoden kan brukes til å kvantifisere blodstrømshastigheter gjennom atrie- og ventrikkelseptumdefekter og bedre visualiseringen av blodstrømsretningen i hjertet.

En annen begrensing ved ultralydavbildning av blodstrøm er *clutterfiltrering* som brukes for å skille det svake ekkoet fra blod fra det sterke ekkoet fra vev. Vevsekkoet må filtreres vekk før blodstrømsavbildning er mulig, men filtreringen vil også begrense den laveste blodhastigheten som kan måles. I den andre studien viser vi at en mulig løsning på problematikken rundt clutterfiltrering er å vinkle de utsendte planbølgene og kombinere hastighetsestimatene fra de ulike vinklene. I den tredje studien undersøker vi hvordan clutterfiltreringen påvirker specklemønsteret og hastighetsestimeringen, og hvordan den økte bilderaten kan brukes til å forbedre clutterfiltreringen og øke hastighetsspennet som kan måles.

Solveig Fadnes
Institutt for sirkulasjon og bildediagnostikk
Hovedveileder: Lasse Løvstakken
Biveileder: Hans Torp
Finansieringskilde: MI Lab

Ovennevnte avhandling er funnet verdig til å forsvares offentlig for graden Philosophiae Doctor (PhD) i medisinsk teknologi. Disputas finner sted i Auditoriet, Medisinsk teknisk forskningssenter, fredag 19. september 2014 kl 12:15.

Abstract

Ultrasound echocardiography and color flow imaging are important tools for detection and visualization of congenital heart disease. Two of the most common forms of congenital heart disease are atrial and ventricular septal defects, which are holes (shunts) in the septal wall between heart chambers. The peak velocity of the shunt blood flow is of diagnostic value, but may not be measured accurately with conventional ultrasound methods unless the ultrasound beam axis is aligned with the blood flow direction through the shunt. This is due to one of the fundamental limitations of the conventional methods; only the 1-D velocity component along the ultrasound beam axis is measured. Development of 2-D blood velocity methods providing quantitative information of the blood velocities in intracardiac flow is therefore of interest, and is the clinical aim of this thesis. Three contributions are included in this thesis. These chapters are written in article form and can be read individually. An introduction to ultrasound blood flow imaging and the clinical application of this thesis is also included in a separate chapter.

The basis of the work presented in this thesis is the technological advances which have allowed for a substantial increase in the acquisition rate of ultrasound images. These advances have made multi-dimensional flow imaging highly relevant due to possibilities for increased robustness and accuracy in the velocity estimation. High-frame-rate speckle tracking was used for 2-D velocity quantification, and it was shown that it was feasible to acquire peak shunt velocities in atrial and ventricular septal defects in newborns. A major limitation in blood velocity estimation is, however, the clutter filtering procedure to remove the strong signal from tissue from the blood signal. If the tissue signal is not sufficiently removed, the blood velocity estimates may be corrupted. In addition, also blood velocities may be removed by the clutter filter, limiting the lowest measurable velocity and the blood flow visualization. Two of the contributions were therefore devoted to investigate this issue. A possible solution to achieve robust speckle tracking velocity estimates was proposed using two scan angles and a compounding algorithm, and an improved flow depiction was achieved in the *in vivo* recordings. In addition, different clutter filters influence on the performance of the speckle tracking technique was thoroughly investigated. The high-frame-rate imaging technique allows for improved clutter filter design, minimizing the filter influence on the velocity estimates and resulting in reasonable tracking results even for near-perpendicular ultrasound beam-to-blood flow angles.

Preface

This thesis is submitted in partial fulfillment of the requirements for the degree of *Philosophiae Doctor* (Ph.D.) at the Faculty of Medicine of the Norwegian University of Science and Technology (NTNU). The research was funded by the *Medical Imaging Laboratory* (MI-Lab), and was carried out at the Department of Circulation and Medical Imaging. The main supervisor has been PhD Lasse Løvstakken, and co-supervisor has been Professor Hans Torp, both from the Department of Circulation and Medical Imaging, NTNU.

Acknowledgements

First of all, I would like to thank my main supervisor Lasse for introducing me to the world of ultrasound and blood flow imaging. You have always been great at motivating me and seeing possibilities instead of problems, and I always feel inspired leaving your office. I would also like to thank my co-supervisor Hans for his useful input on my work, and his thorough knowledge in the field of ultrasound. A sincere thank you must also be given to Siri Ann for all the invaluable help with the clinical studies. You have increased my knowledge of congenital heart disease and given me useful insight to your work as a pediatric cardiologist.

I have had many great colleagues during my years as a PhD student, and they have all contributed to a great working environment. We have traveled to many conferences and had a lot of fun together, and I have enjoyed getting to know each and everyone of you! A special thank you to Tonje, who made me apply for the PhD position, and have been my closest friend and colleague all these years, sitting next to me and keeping my spirits high. Furthermore, I must thank my mentor and hero Ingvild, who have taught me so much, and always been willing to explain and help with my problems.

I would also like to thank my parents and brothers for their love and support, and my friends, especially Gina and Kristina, for their interest in my work. Finally, I have to thank my dear Tore; your love, patience and encouragement have been invaluable, and my sweet little boy, Vebjørn, you have been the best distraction and my greatest motivation this last year.

Table of Contents

Abbreviations

B-mode	Brightness mode
CCA	Common carotid artery
CFD	Computational fluid dynamics
CFI	Color flow imaging
CW	Continuous wave
ECA	External carotid artery
FIR	Finite impulse response
$F_{\#}$	F-number
fps	Frames per second
ICA	Internal carotid artery
IIR	Infinite impulse response
IQ	In-phase Quadrature
LA	Left atrium
LV	Left ventricle
LVOT	Left ventricular outflow tract
PRB	Parallel receive beams
PRF	Pulse repetition frequency
PW	Pulsed wave
RA	Right atrium
RF	Radio frequency
RV	Right ventricle
Rx	Receive
SAD	Sum of absolute differences
SNR	Signal-to-noise ratio
SSD	Sum of squared differences
ST	Speckle tracking
Tx	Transmit
VD	Vector Doppler

Chapter 1

Introduction

Diagnostic ultrasound came into clinical practice in the 1970s, but it was various historical events at the beginning of the 1900s that kick-started the research on object detection using sound waves. Shortly after the sinking of the *Titanic* in 1912, the British meteorologist Lewis Richardson patented the use of *echolocation* to discover icebergs [1]. With World War I, detecting enemy submarines became an urgent aim, which the French scientist Paul Langevin successfully achieved using sound waves in 1915. His research has been considered to be the starting point of sonar (SOund Navigation And Ranging) and modern ultrasound [2].

Ultrasound is sound waves above the audible range of 20 kHz, and in medical diagnostics the typical range is from 2-10 MHz. The sound waves are transmitted into the body and the speed of sound in tissue is approximately equal to the speed of sound in water ($\sim 1500\,\mathrm{m/s}$). The timing and intensity of the received echo is used to identify the different internal structures and to form a 2-D *brightness* (B-mode) image which is displayed in real-time (continuously updated). Development and technological advances in many fields such as material science, transducer design, electronics and statistical signal processing have contributed to the important position ultrasound have in medical technology today. Ultrasound imaging is used in a wide range of clinical settings, from obstetrics and gynecology to neurology and in cardiovascular imaging [3]. Much of the success of ultrasound imaging is related to the fact that it is a non-invasive, safe, low-cost and portable technique.

Christian Doppler's theory from 1842 was 100 years later put into use in medicine when Satomura reported detection of heart wall movement based on the Doppler shift in the 1950s [4, 5] and shortly after detecting blood motion [6]. Doppler techniques for blood flow imaging are today implemented on most commercial ultrasound systems, and are important clinical tools, especially for diagnosing cardiovascular disease. The blood velocity estimates can be displayed either as a spectrum of velocities or as a *color flow map* in a region of interest. The spectral methods display all velocities present in a small region as a function of time and are either based on transmission of continuous wave (CW) or pulsed wave (PW) ultrasound. Color flow imaging (CFI), on the other hand, color encodes the measured velocities in a larger two- or three-dimensional region of interest, giving an impression of both spatial and temporal distribution of blood flow in real-time.

The conventional Doppler methods have some fundamental limitations which restrict their usefulness in diagnostic settings. The methods only measure the velocity

vector component parallel to the ultrasound beam axis, and, therefore, merely contain 1-D information of the 3-D blood flow velocities. The measurements are thus *angle-dependent* and the beam-to-flow angle must be known to estimate the true blood flow velocity vector. In addition, CFI and PW Doppler are based on pulsed emissions of ultrasound waves to achieve spatial information of the origin of the echo. Multiple transmissions in the same direction are needed to estimate the blood velocity, called the *ensemble size* of the signal. The pulse repetition frequency (PRF) introduced with pulsed emissions limits the highest measurable velocity according to the Nyquist sampling theorem. Velocities above the Nyquist limit are commonly encountered and results in *aliasing* artifacts in the image where the high velocities are not estimated or displayed correctly.

The echo from tissue is much stronger than the echo from blood scatterers and will completely corrupt the blood flow estimation unless the tissue and blood signals are separated. The tissue is stationary or slowly-moving, and the tissue echo may therefore be attenuated by applying a high-pass filter (clutter filter) to the received signal. The conventional line-by-line acquisition limits the maximum frame rate and ensemble size in color flow imaging. The typical ensemble size of 8-16 makes it difficult to achieve the sharp clutter filter desired for an efficient separation of clutter and blood signal, and the minimum measurable blood velocity is in practice limited by the clutter filter cut-off velocity. The limited velocity range, the angle-dependency and clutter filtering may lead to signal drop-outs, biased velocity estimates and ambiguous images which may be difficult to interpret [7–9].

Peak-velocity estimates and related pressure differences are of diagnostic value in many clinical settings, for example in stenotic arteries, valve abnormalities and shunt flows, and may be obtained with spectral Doppler if the ultrasound beam is aligned with the blood flow direction. Manual angle-correction is also possible, however, the blood flow direction may be difficult to predict as it is not necessarily parallel with the vessel wall as usually assumed. Angle-correcting the velocity estimates using the estimated beam-to-flow angle may therefore give inaccurate and not reproducible peak-velocity estimates [10].

An accurate description of blood flow dynamics in the circulatory system would be of value in the clinic and for research in pathophysiology. Intracardiac blood flow follows an efficient path in healthy hearts, and quantification of abnormal flow patterns and its connection to the heart function may therefore give insight of the disease and help develop tools for an early diagnosis [11–13]. Methods which quantify velocities in two or three dimensions and increase the measurable velocity range are of high interest, and may initially increase diagnostic certainty and increase pathophysiological knowledge, and thus serve as foundation for new diagnostic tools in the future.

Multi-dimensional flow velocity estimation

Techniques for multi-dimensional flow estimation where two- or three-dimensional blood velocity vectors are measured have been investigated since the 1970s [14–20]. Multi-dimensional flow velocity estimation may overcome the angle-dependency of the conventional Doppler-based methods, but has not yet been established for clinical

use. Ch. 2 includes a short review of the most common and recent 2-D velocity estimators and only a brief summary is given here. The main research lines have been vector Doppler [19] and speckle tracking [20] techniques. Firstly, vector Doppler techniques use several transmit and/or receive angles to obtain the Doppler shift from two or more beam-to-flow angles. The known separation angle between the Doppler estimates makes it possible to triangulate the lateral velocity component. The techniques have been evaluated for numerically simulated flow patterns [21], and also real-time implementations have been evaluated *in vitro* in flow phantoms and *in vivo* in human vessels [22, 23]. Still, the technique has not yet been developed for routine clinical applications. Related techniques were developed in 1998 by Jensen and Munk (transverse oscillation) [24] and Anderson (spatial quadrature) [25], in which the lateral velocity component is estimated using a lateral modulation introduced by complex apodization schemes on receive. The transverse oscillation technique has been implemented on a commercial ultrasound system (BK Medical, Herlev, Denmark), which has been utilized in recent studies [26, 27].

Speckle tracking techniques are the other main research line. The speckle is an intensity pattern in the 2-D ultrasound image caused by the constructive and destructive interference in the backscattered echoes. The blood speckle pattern movement from frame to frame is correlated with the blood flow in the image plane and may be tracked to obtain the 2-D velocity estimates. A similar technique is echo particle imaging velocimetry (echo PIV) [28], in which the ultrasound image is enhanced with contrast agents injected into the blood to increase the signal-to-noise ratio, and tracking techniques known from optical PIV are used to estimate the lateral velocity component. Alternative techniques have also been suggested, where a more recent method is echo-dynamography or vector flow mapping, which estimates the lateral velocity component specifically in the left ventricle, based on assumptions of in-plane flow and restrictions from the continuity equation [29, 30].

Recent advances in ultrasound technology make it possible to increase the frame rate for ultrasound imaging significantly by transmitting plane or diverging waves and constructing multiple image lines simultaneously [31]. The increased acquisition rate has made multi-dimensional blood velocity estimation highly relevant as the acquisition rate typically was a limiting factor in the suggested 2-D methods. The high acquisition rate allows for both a high frame rate, which makes it possible to capture complex and fast-varying flow, and an increased ensemble size. A larger ensemble size makes it easier to optimize the clutter filter as higher order filters may be used. As a result, the robustness and accuracy of the velocity estimates may be increased. Several authors have reported an increased robustness in 2-D velocity estimation using plane wave imaging for vector Doppler estimation in vascular imaging [32–34], and for speckle tracking in simulations and experiments [31, 35]. Plane or diverging transmit beams are also utilized in other applications such as shear wave elastography [36, 37] and coherent compound Doppler imaging [38].

Clinical application

The work summarized in this thesis exploits the possibilities that have arisen from plane wave imaging and parallel receive beamforming. The main clinical application discussed is congenital heart disease (CHD). Nearly one-third of all major congenital anomalies are congenital heart disease. The severity of a defect must be established quickly to ensure the best possible plan for treatment and follow-up of the patient. In pediatric cardiology today, 2-D echocardiography with color flow imaging is used to detect and visualize CHD, and the spectral Doppler methods are used to obtain peak-velocity estimates. The limitations of the conventional methods, and the possible misinterpretations which may arise [39], have been the motivation for this thesis. Utilizing plane wave imaging, speckle tracking velocity estimation has the potential to overcome these limitations. This thesis is devoted to develop high-frame-rate speckle tracking techniques to obtain robust, angle-independent velocity estimates for 2-D vector velocity visualization of intracardiac blood flow patterns, as well as for calibrated peak velocity estimates.

1.1 Aims of study

The overall aim of this thesis is to develop techniques for quantification of intracardiac blood flow. The work aims to overcome the limitations of conventional ultrasound color flow imaging using plane wave imaging and speckle tracking velocity estimation. We hypothesize that plane wave imaging and high-frame-rate speckle tracking can provide quantitative 2-D velocity estimates of clinical value in the evaluation of congenital heart disease. Specifically, the clinical focus has been on atrial and ventricular septal defects (hole or *shunt* in the septum between cardiac chamber), which are common congenital heart defects. The peak velocity in the shunt flow is of important diagnostic value, and angle-independent, robust velocity estimates would increase the certainty and reduce intra- and interobserver variability in the peak velocity estimation.

The aims are summarized in the following bullet points:

- To develop and evaluate blood speckle tracking methods for plane wave imaging.
- Address and suggest solution to clutter filtering issues related to speckle tracking and 2-D blood flow velocity estimation.
- Evaluate high-frame-rate speckle tracking for quantification of intracardiac blood flow.

1.2 Thesis outline

The thesis is organized as follows. The next section provides a summary of the contributions included in this thesis. A general discussion of the results and concluding remarks are given in Sec. 1.4 and 1.5. At the end of this chapter a list of publications including written and oral contributions to national and international conferences

is included. Chapter 2 is a background chapter which include a short introduction to ultrasound flow imaging and congenital heart disease physiology, diagnosis and treatment. Chapters 3, 4 and 5 contain the three studies included in this thesis.

1.3 Summary of contributions

1.3.1 Shunt Flow Evaluation of Congenital Heart Disease Based on Two-Dimensional Speckle Tracking

Atrial and ventricular septal defects are two of the most common types of congenital heart disease. Small defects may close without external help, whereas more severe defects must be repaired by catheter closure or corrective surgery. The diagnostic procedure involves color flow imaging to detect and visualize septal defects and continuous wave or pulsed wave Doppler to estimate the peak velocity. The peak shunt velocity is used to evaluate the shunt flow, and will, together with the location and size of the defect, hemodynamic consequences, associated defects and symptomatology of the patient, decide the further management of the defect.

The conventional Doppler methods have fundamental limitations and artifacts which may lead to undetected defects and misdiagnoses. Only the velocity component along the beam direction is measured and manual angle-correction must be done to obtain calibrated velocities. The Doppler methods based on pulsed ultrasound waves, are also limited by aliasing of velocities above the Nyquist limit.

In this work, 2-D speckle tracking is used both to get the spatial position of the septal defect and to achieve angle-independent shunt velocity estimates. Plane wave transmissions and parallel receive beamforming made it possible to acquire full field-of-view images at high frame rates, providing near-instantaneous images of blood flow in a large region of interest. A research scanner with a duplex acquisition scheme was used, where separate acquisition setups were implemented for flow and B-mode imaging to ensure a high image quality for both modalities.

Two neonatal patients with septal defects from the on-going feasibility study were included in this study. The shunt position was automatically tracked in B-mode images and further utilized in blood speckle tracking to obtain calibrated shunt flow velocities throughout the cardiac cycle in both patients. Validation towards conventional Doppler methods showed that high-frame-rate blood speckle tracking could be used to obtain calibrated shunt flow velocities throughout the cardiac cycle. A larger velocity span could be obtained using speckle tracking than conventional Doppler methods, since speckle tracking velocity estimates are less biased by clutter filtering and not limited by the Nyquist range. The results showed that complex intraventricular flow velocity patterns could be quantified which potentially can help increase diagnostic accuracy and decrease interobserver variability when measuring peak velocities in shunt flows.

This paper is in press for publication in Ultrasound in Medicine and Biology, and is presented here in its original form. The candidate was the main contributor to

all aspects of the work, except the important part of getting the study approved by the Regional Committee of Ethics and Medical Health, and carrying out the patient examinations, for which MD Siri Ann Nyrnes is gratefully acknowledged.

1.3.2 Robust Angle-Independent Blood Velocity Estimation Based on Dual-Angle Plane Wave Imaging

Ultrasound imaging is a widely used clinical tool to visualize and quantify blood velocities. However, the conventional methods have fundamental limitations and general improvements to minimize the need of interpreting the images would increase the diagnostic certainty. Multi-dimensional blood flow imaging, where two or all three components of the blood velocity vector are estimated, would allow for measuring the absolute blood velocity and visualizing complex blood flow patterns. Speckle tracking and vector Doppler are the two most common 2-D flow estimators and have recently become relevant in the context of plane or diverging wave imaging, where full field-of-view and multi-angle imaging can be achieved at very high frame rates. The high acquisition rates allow for both a high ensemble size and a high frame rate which will increase the accuracy of the 2-D flow estimators. High-pass filtering of the received signal is, however, still necessary to separate the blood signal from the strong tissue signal. The clutter filter will influence velocity estimates for flow at near-perpendicular beam-to-flow angles and remains a major limitation in 2-D blood velocity estimation.

In this work, a solution to the clutter filtering limitation on the beam-to-flow angle is proposed. Dual-angle plane wave imaging is utilized to obtain two independent flow velocity images from speckle tracking. The regions of corrupted velocities, due to the clutter filter, will differ for the two images. The corrupted velocities can therefore be discarded, and one compounded flow image can be obtained where only the valid velocity estimates are kept. The dual-angle acquisition also allows for direct comparison, and potentially also combination, with vector Doppler imaging.

Simulations of a rotating flow phantom were used to evaluate the compounding speckle tracking method and compare it with conventional speckle tracking and vector Doppler. A significant increase of accuracy was observed for the compounding speckle tracking method. The methods were further evaluated *in vivo* for vascular and neonatal cardiac imaging. The results showed that both speckle tracking and vector Doppler velocity estimation was possible for both *in vivo* scenarios. The vector Doppler technique is more sensitive to clutter filtering than the speckle tracking methods, whereas sufficient signal-to-noise ratio is important for the accuracy of the speckle tracking estimates. Generally, the compounded speckle tracking technique gave a more consistent flow depiction compared with vector-Doppler and the conventional speckle tracking technique based on only one scan angle.

This paper has been submitted to IEEE Transactions on Ultrasonics, Ferroelectrics and Frequency Control, and is presented here in its current form. The candidate was the main contributor to all aspects of the work, except the important part of patient examination, for which MD Siri Ann Nyrnes is gratefully acknowledged.

1.3.3 Clutter Filtering Influence on Blood Velocity Estimation Using Speckle tracking

Clutter filtering remains a major limitation in two-dimensional blood velocity estimation. For blood speckle tracking (BST), the clutter filter influences the speckle appearance and speckle tracking performance, and limits the minimum measurable velocity. To obtain low blood velocities, the clutter filter must sufficiently attenuate the clutter signal, have a narrow transition region and a low cut-off frequency. Such filter frequency responses may be difficult to achieve for short ensemble signals. The increased frame rates obtained with plane wave imaging and parallel receive beamforming may be used to increase the temporal ensemble lengths. This provides possibilities for improved clutter filtering, because filter orders can be increased and a steep transition region obtained.

In this work, we investigate clutter filter design and its influence on speckle appearance and tracking performance in simulations and *in vitro*. The overall aim is to measure all blood velocities for all beam-to-flow angles. Simulation results showed that the speckle pattern was significantly smeared in the filter transition region due to a reduced imaging bandwidth, resulting in reduced tracking accuracy for increasing beam-to-flow angles. However, for a perpendicular beam-to-flow angle, a lateral amplitude modulation was introduced in the speckle which increased the lateral tracking accuracy in our data.

Comparing the performance of speckle tracking with color flow imaging (CFI) for varying beam-to-flow angles, we found that BST could track well below clutter filter velocity cut-off, where CFI becomes significantly biased. BST was mainly limited by the high variance inferred by the low signal-to-noise ratio due to filter attenuation. Analysis further showed that time-variant clutter filters could be used to improve filtering and reduce variance for BST, but only for high slow-time ensembles, which were achieved using plane wave imaging in this work. The improved frequency responses, which may be obtained with longer ensemble signals, reduced the filter attenuation of the blood signal, thereby lowering the minimum measurable velocity. This was confirmed in *in vitro* straight-tube recordings, where lower velocities could be measured from a high beam-to-flow angle of 83° with a polynomial regression filter and a high ensemble size of 36 compared with a conventional ensemble size of 12 and a 4th order finite impulse response filter.

This paper has been submitted to IEEE Transactions on Ultrasonics, Ferroelectrics and Frequency Control, and is presented here in its current form. The candidate was the main contributor to all aspects of the work, except the theoretical approach in Sec. II.B, for which Dr. Steinar Bjærum is gratefully acknowledged.

1.4 Discussion of results

The aim of all the work summarized in this thesis was to achieve robust 2-D blood velocity estimates for quantitative flow analysis when evaluating congenital heart disease. High-frame-rate speckle tracking for blood velocity estimation was investigated through simulations, *in vitro* and *in vivo* recordings. For numerically simulated flows, the true velocities are known at all points in space and in time, and in-depth analysis of the 2-D velocity estimator is possible. The true velocity can also, to some extent, be known in an experimental setting. Experimental testing offers a more realistic scenario for the 2-D estimator and was used to investigate the accuracy of the method compared with color flow imaging. *In vivo* recordings are, however, necessary to map the clinical feasibility of the method, and was in this work conducted using an ultrasound research system and with help from a skilled pediatric cardiologist.

Related work

For visualization of septal defects, transthoracic (through chest) echocardiography is the conventional imaging modality. However, in some complex cases, other modalities are used to achieve better images of the defect. Cardiac catheterization, computed tomography and magnetic resonance may provide additional information of diagnostic value, but as the first is invasive and the others are expensive and time-consuming, their use in daily clinical practice is limited. To obtain higher quality images, transesophageal echocardiography (TEE), where the ultrasound probe is lead down the patient's throat, may also be used. The probe may be positioned close to the heart allowing higher transmit frequencies which increases image quality. However, the need for general anesthesia in children limits its clinical applicability. More recently, real-time 3-D (transthoracic) echocardiography shows promising results for visualization of septal defect [40–43].

For blood velocity imaging, methods to visually enhance the true blood velocity direction has been suggested to increase diagnostic certainty for atrial septal defects [44, 45], but is only a qualitative method. Echo-dynamography/vector flow mapping has shown quantitative 2-D velocity results from cardiac imaging corresponding with phase-contrast MR velocity estimates [30, 46, 47], but these methods have so far focused on visualization of vortex formations in the left ventricle, and cannot directly be used for evaluation of shunt flows. Promising *in vivo* 2-D velocity imaging of intracardiac flow using echo PIV has also been presented [48, 49], but as previously mentioned, the need of contrast agent injection limits it use in pediatric cardiology. At the moment, the best modality for quantitative 3-D velocity estimates is phase-contrast magnetic resonance (MR). The 3-D velocity estimates allow for quantitative volume flow evaluations [50,51], however, MR imaging is not applicable for routine clinical use due to time and cost considerations, and the need of sedation for small children.

Advantages and disadvantages of plane wave imaging

The high frame rate achieved with plane wave imaging and parallel receive beamforming is the main advantage of the acquisition setup, but for blood flow imaging, the possibility to increase the temporal ensemble size is equally important. A packet-based acquisition is sensible for both CFI and multi-dimensional flow imaging, which works in duplex mode with sufficient quality of both B-mode and flow images. Sufficient B-mode quality is important for a good depiction of the internal structures when interpreting the flow images. Despite a packet-based acquisition, the ensemble size can be significantly increased using plane wave imaging compared with conventional ensemble sizes.

In contribution 1, we investigated shunt flow evaluation in cardiac imaging in newborns. A frame rate of 107 frames per second was obtained with an ensemble size of 32 with one plane wave transmit angle for a full field-of-view flow acquisition. In contribution 2, a flow acquisition setup with two transmit angles was used to increase the accuracy of the blood velocity estimates through compounding. The high frame rate achieved with plane wave imaging makes it possible to use multiple transmit angles and still achieve a sufficiently higher frame rate than in conventional line-by-line acquisitions. With two transmit angles, a high flow frame rate of 75 frames per second was obtained for cardiac imaging in newborns, with a pulse repetition frequency of 8 kHz and ensemble size of 32 as in contribution 1. The B-mode image frame was divided in two acquisitions and interleaved the flow acquisition to maximize the flow frame rate, resulting in a reduced B-mode frame rate. The B-mode frame rate of 54 frames per second in contribution 1 was, however, shown to be sufficient for tissue speckle tracking of the septal defects investigated.

The disadvantages of plane wave imaging compared with focused imaging are the loss in penetration and decrease in image contrast and lateral resolution. The latter is particularly visible in B-mode imaging, but is, in our experience, less deteriorating and often negligible for blood flow imaging in which the elevated side lobe level is often still below the noise floor. The penetration depth of 5 cm needed for cardiac imaging in newborns seems achievable, but a low signal-to-noise ratio is, however, potentially a problem with plane wave imaging in general, and in our initial studies specifically, as the research system used was not a high-end system. In contribution 2 and 3, the signal-to-noise ratio is discussed, and the results show that the speckle tracking method is more sensitive to a decrease in signal-to-noise ratio than color flow imaging. Another issue discussed in contribution 3, is the potential increase of grating lobes artifacts when using plane wave imaging. The loss of transmit focusing elevates the level of the grating lobes, resulting in increased artifacts, which may influence the velocity estimates. Extra care must therefore be taken regarding the transducer pitch (distance between element centers) and/or pulse frequencies when using plane or diverging transmit beams.

Clutter filtering issues

A sharp high pass clutter filter for an efficient separation of the tissue and blood signal may be difficult to obtain for short ensemble signals. The clutter filtering limits

therefore the minimum measurable blood velocity and results in corrupted velocity estimates for beam-to-flow angles close to 90°.

In contribution 2, a possible solution to the clutter filtering issues was presented and tested in simulations and *in vivo*. With plane wave transmissions from two angles of ±10 degrees, a compounding speckle tracking algorithm was proposed to discard corrupted velocity estimates and obtain robust 2-D velocity estimates in a wide region of interest. It was observed in the simulations that the bias and root-mean-square error were reduced significantly from 22 % and 4 cm/s to 11 % and 2 cm/s when compounding the speckle tracking velocity estimates compared with the speckle tracking estimates from a single transmit angle. The dual-angle acquisition also made it possible to compare the speckle tracking performance directly with vector Doppler imaging, and it was observed that the speckle tracking estimates were less influenced by the clutter filter compared with vector Doppler. Both simulations and *in vivo* results indicated that compounding the speckle tracking velocity estimates increased the robustness and decreased the clutter filtering issues of the speckle tracking velocity estimator.

In contribution 3, clutter filter design and influence on speckle appearance and tracking was discussed. To retain speckle correlation between image frames, time-invariant FIR filters are most suitable as clutter filters. However, it was shown that for increasing ensemble sizes, the speckle decorrelation introduced by time-variant filters is negligible, and the choice of clutter filter is therefore not limited to time-invariant filters. With the increased ensemble sizes obtained with plane wave imaging, higher order clutter filters may also be used, and a low cutoff frequency and narrow transition region may be obtained. A sharp clutter filter reduces the clutter filtering issues in 2-D velocity estimation and makes it possible to measure lower blood flow velocities than in conventional imaging. For speckle tracking, a sharp clutter filter means less smearing of the speckle pattern and less blood signal attenuation, the latter is especially important in low signal-to-noise cases where the variance of velocity estimates rapidly increases for increased signal attenuation. The approach of using adaptive clutter filtering was not considered in this work, but has previously been proposed for the specific case of speckle tracking velocity estimation [52].

Blood velocity estimation using speckle tracking

The performance of the speckle tracking approach was compared with color flow imaging (and vector Doppler when applicable) as this is the conventional blood flow imaging modality. Speckle tracking is more computational demanding than color flow imaging, but can measure blood velocities beyond the Nyquist limit and provides 2-D velocity estimates. The narrow-band autocorrelation method [53] used in color flow imaging and vector Doppler, is know to be robust with regards to signal-to-noise ratio. The speckle tracking method, on the other hand, is a wide-band approach where a short pulse (wide bandwidth) is preferable, also making it more susceptible to noise. This was confirmed in the results obtained in this thesis work. If no aliasing artifacts or clutter filter issues are present, the speckle tracking and the color flow estimates could be combined to further improve the robustness of the velocity estimates [54], especially in low signal-to-noise conditions.

The speckle tracking velocity estimation is, in our work, based on the same data as color flow imaging, and, unlike e.g. echo PIV techniques, no contrast agents have been used. With the specific clinical application of newborn cardiac imaging of this thesis, it has been important to develop a modality without the need for contrast agents, general anesthesia or sedation, and where a future implementation for routine clinical use is possible.

Clinical feasibility

The results demonstrated that 2-D speckle tracking may indeed provide angle-independent flow velocity estimates of (abnormal) flow in hearts of newborns. It was also shown that vascular imaging could benefit from 2-D velocity estimation using speckle tracking. The limited patient population in contribution 1 and 2, however, makes it difficult to draw general conclusions and evaluate the clinical impact of the method. In addition to a larger patient population, the clinical impact may first thoroughly be discussed when the method is implemented in real-time or close to real-time, so that an efficient comparison can be made between diagnoses based on the conventional methods and 2-D speckle tracking, especially considering peak shunt velocity estimations and shunt evaluations. A comparison should also be made regarding detection of small septal defects, which have been reported to be missed with conventional CFI [39].

The acquired 2-D velocities may be important for the peak shunt velocity estimate which is an already established clinical measurement when evaluating shunt flow. Further, the 2-D velocity vector maps may provide new information of the potentially complex flow patterns and dynamics that occur in congenital heart disease. The new descriptive flow information may increase our understanding of the disease and increase diagnostic certainty, but may also be used to develop new and perhaps more certain quantitative measures. Both healthy and diseased cases must be investigated with the new method to understand the value of the 2-D quantitative velocity measurements.

A linear probe was used in this work, since it can easily utilize plane transmit waves and parallel receive beamforming, and the depth and field of view needed for cardiac imaging in newborns were achievable. In cardiac imaging, the standard probe is, however, a smaller phased array which can image between the ribs and have a larger field-of-view, but for newborns it is possible to image through the ribs, and a linear array could therefore be used. Papadacci *et al.* [37] recently showed that high frame rates and reasonable image quality can be obtained using a phased array and diverging beams, however, it remains to be tested for blood velocity estimation for cardiac depths of newborns and adults.

1.5 Concluding remarks

This thesis has focused on quantification of blood flow velocities using 2-D speckle tracking. We have shown that high-frame-rate speckle tracking based on plane wave imaging may improve the measurement of peak velocities for the evaluation of shunt

flow in atrial and ventricular septal defects in newborns. The need for manual angle-correction was removed for quantitative measurements and the proposed technique may thus help increase diagnostic accuracy and decrease interobserver variability.

Clutter filtering remains as a major limitation in 2-D velocity estimation and limits the minimum measurable velocity. A compounding blood speckle tracking algorithm, based on plane wave imaging from two scan angles, was shown to increase the accuracy of the velocity estimates in simulations, and a more consistent flow depiction was seen in *in vivo* recordings. We demonstrated that both speckle tracking and vector Doppler velocity estimation may be used for vascular and neonatal cardiac imaging, and that clutter filter issues and corrupted velocity estimates could be avoided to achieve more robust velocity estimates with the compounding speckle tracking approach. The speckle tracking estimates were, however, sensitive to the signal-to-noise ratio.

It was shown that clutter filtering will smear out the speckle and reduce the signal-to-noise ratio when parts of the Doppler signal are in the clutter transition region. This results in increased bias and variance of the speckle tracking estimates. However, for sufficient SNR, reasonable tracking results were achieved for all beam-to-flow angles. It was also shown that the bias of the axial speckle tracking velocity estimates were significantly lower than the bias of the velocity estimates in color flow imaging in the filter transition region, which indicated that the speckle tracking method is less influenced by clutter filtering than color flow imaging.

Time-variant clutter filters introduce a decorrelation in the speckle between image frames, because of changing filter frequency response. It was, however, shown that the increased ensemble sizes achieved with plane wave imaging significantly reduced the decorrelation between image frames, and it was concluded that also time-variant polynomial regression filters can be used for speckle tracking velocity estimation. A sharper clutter filter may be achieved with larger ensemble sizes, because higher filter order may be used, and it was shown that a lower filter frequency cutoff and a narrower transition region reduced the clutter filter influence on the speckle pattern and lowered the minimum measurable velocity.

Further work

Plane wave imaging has introduced new possibilities for multi-dimensional blood flow imaging, and with the increasing computational power available in research systems and commercial scanners, the near future will bring many advances in the field of real-time multi-dimensional blood flow imaging.

The methods developed and discussed in this thesis may be improved on many levels. Both processing and visualization parts can be refined. The work should continue to aim for real-time blood velocity tracking by increasing the efficiency of the tracking code through parallel implementation utilizing the increasing GPU power available. In addition, the method should be implemented for diverging beams and phased-array transducers to investigate if the high-frame-rate speckle tracking approach is feasible for cardiac imaging of adults.

Coherent plane wave compounding to improve image quality and signal-to-noise ratio has recently been proposed [55], and has been tested in simulations for speckle

tracking blood velocity estimation [56]. The coherent compounding technique allows for a continuous acquisition, where high image quality B-mode images and high-frame-rate flow images can be acquired from the same acquisition. The continuous acquisition would also reduce problems concerning clutter filter design. However, the coherent compounding and speckle tracking blood velocity estimation has not yet been tested *in vivo* and the potential impact of motion artifacts on the velocity estimates remains to be investigated.

A larger patient study is needed to fully evaluate the clinical impact of blood velocity estimation using speckle tracking. A large patient recruitment potential is available through the collaboration and network between the hospital in Trondheim and our department, and a broad clinical study is already on-going. Further, methods to quantify volume flows using speckle tracking velocity estimates should be evaluated, as volume flow estimation could be of useful diagnostic information. To further understand the development of congenital heart disease, a study to follow up patients from fetal to the newborn stage should be carried out.

The natural next step is an expansion to 3-D speckle tracking for blood velocity estimation, which is, in theory, straight forward as long as 3-D data are available. The true blood flow is a 3-D flow, and out-of-plane flow is inevitable for 2-D imaging, therefore, 3-D velocity estimates are needed to fully understand the intracardiac flow. Methods to acquire and display 3-D color flow images have been proposed [57, 58], where the 3-D volume date are acquire from a series of image planes throughout the volume. The volume data can either be acquired by moving or tilting the 1-D transducer and track the position [59], or by using a 2-D transducer producing the volume data by electronic scanning [60]. For speckle tracking purposes, the challenge is to acquire sufficiently temporally and spatially sampled 3-D data from a large region of interest. The high frame rates needed to avoid decorrelation may perhaps be achieved with diverging transmit beams for a 2-D transducer. However, high acquisition rates will generate large amounts of data which must be handled.

1.6 List of publications

In addition to published and unpublished manuscripts included in this thesis, written and oral contributions have been made to national and international conferences. A list of the material to which the candidate has contributed is included in the following.

Papers included in the thesis

1. **Solveig Fadnes**, Siri Ann Nyrnes, Hans Torp and Lasse Løvstakken, "Shunt Flow Evaluation in Congenital Heart Disease Based on Two-Dimensional Speckle Tracking", accepted for publication in *Ultrasound in Medicine and Biology*.

2. **Solveig Fadnes**, Ingvild Kinn Ekroll, Siri Ann Nyrnes, Hans Torp and Lasse Løvstakken, "Robust Angle-Independent Blood Velocity Estimation Based on Dual-Angle Plane Wave Imaging", submitted to *IEEE Transactions on Ultrasonics, Ferroelectrics and Frequency Control*.

3. **Solveig Fadnes**, Steinar Bjœrum and Lasse Løvstakken, "Clutter Filtering Influence on Blood Velocity Estimation Using Speckle Tracking", submitted to *IEEE Transactions on Ultrasonics, Ferroelectrics and Frequency Control*.

Conference proceedings

1. **Solveig Fadnes**, Abigail Swillens, Patrick Segers, Hans Torp and Lasse Løvstakken, "Clutter filtering issues in speckle tracking for two-dimensional blood velocity estimation - a potential solution based on compounded imaging", *IEEE International Ultrasonics Symposium Proceedings 2011*

2. **Solveig Fadnes**, Siri Ann Nyrnes, Abigail Swillens, Hans Torp and Lasse Løvstakken, "Shunt quantification in congenital heart disease based on two-dimensional speckle tracking", *IEEE International Ultrasonics Symposium Proceedings 2012*

Presentations and posters

1. **Solveig Fadnes**, Hans Torp and Lasse Løvstakken, "Biomechanical simulation and multi-dimensional flow imaging of cardiac flow", *Joint National PhD Conference in Medical Imaging and the Annual MedViz Conference, 2011.*

2. **Solveig Fadnes**, Hans Torp and Lasse Løvstakken, "Multi-dimensional flow quantification of cardiac flow patterns", *The Artimino Conference on Medical Ultrasound Technology, 2011.*

3. **Solveig Fadnes**, Abigail Swillens, Patrick Segers, Hans Torp and Lasse Løvstakken, "Clutter filtering issues in speckle tracking for two-dimensional blood velocity estimation - a potential solution based on compounded imaging", *2011 IEEE International Ultrasonics Symposium.*

4. **Solveig Fadnes**, Siri Ann Nyrnes, Abigail Swillens, Hans Torp and Lasse Løvstakken, "Shunt quantification in congenital heart disease based on two-dimensional speckle tracking", *2012 IEEE International Ultrasonics Symposium*

5. **Solveig Fadnes**, Siri Ann Nyrnes, Abigail Swillens, Hans Torp and Lasse Løvstakken, "Shunt quantification in congenital heart disease based on two-dimensional speckle tracking", *National PhD conference in Medical Imaging, 2012*

References

[1] L. Richardson, "British patent no. 11,125," 1913.

[2] P. Newman and G. Rozycki, "The history of ultrasound," *Surgical clinics of north America*, vol. 78, no. 2, pp. 179–195, 1998.

[3] D. H. Evans and W. N. McDicken, *Doppler ultrasound: physics, instrumentation, and signal processing*. Wiley, 2 ed., 2000.

[4] S. Satomura, S. Matsubara, and M. Yoshioka, "A new method of mechanical vibration measurement and its application," *Memoirs of the Institue of Scientific and Industrial Research Osaka University*, no. 13, pp. 125–133, 1956.

[5] S. Satomura, "Ultrasonic Doppler method for the inspection of cardiac functions," *The Journal of the Acoustical Society of America*, vol. 29, no. 11, pp. 1181–1185, 1957.

[6] S. Satomura, "Study of the flow patterns in peripheral arteries by ultrasonics.," *J.Acoust.Soc, Japan*, vol. 15, pp. 151–155, 1959.

[7] K. Ferrara and G. DeAngelis, "Color Flow Mapping," *Ultrasound in Medicine and Biology*, vol. 23, no. 3, pp. 321–345, 1997.

[8] C. Tysoe and D. Evans, "Bias in mean frequency estimation of Doppler signals due to wall clutter filters," *Ultrasound in medicine & biology*, no. 5, pp. 671–677, 1995.

[9] D. Evans and W. McDicken, "Signal Processing for Colour Flow Imaging," in *Doppler Ultrasound: Physics, Instrumentation and Signal Processing*, pp. 246–250, 2000.

[10] E. Y. L. Lui, A. H. Steinman, R. S. C. Cobbold, and K. W. Johnston, "Human factors as a source of error in peak Doppler velocity measurement.," *Journal of vascular surgery*, vol. 42, pp. 972–9, Nov. 2005.

[11] G. Pedrizzetti and F. Domenichini, "Nature Optimizes the Swirling Flow in the Human Left Ventricle," *Physical Review Letters*, vol. 95, p. 108101, Sept. 2005.

[12] P. J. Kilner, G. Z. Yang, a. J. Wilkes, R. H. Mohiaddin, D. N. Firmin, and M. H. Yacoub, "Asymmetric redirection of flow through the heart.," *Nature*, vol. 404, pp. 759–61, Apr. 2000.

[13] M. Gharib, E. Rambod, A. Kheradvar, D. J. Sahn, and J. O. Dabiri, "Optimal vortex formation as an index of cardiac health.," *Proceedings of the National Academy of Sciences of the United States of America*, vol. 103, pp. 6305–8, Apr. 2006.

[14] P. Peronneau, M. Xhaard, and A. Nowicki, "Pulsed Doppler ultrasonic flowmeter and flow pattern analysis," in *Blood flow measurements* (C. Roberts, ed.), ch. 2, pp. 24–28, Baltimore: Williams & Wilkins, 1972.

[15] S. Johnson, J. Greenleaf, C. Hansen, W. Samayoa, M. Tanaka, A. Lent, D. Christensen, and R. Woolley, "Reconstructing Three-Dimensional Fluid Velocity Vector Fields from Acoustic Transmission Measurements," in *Acoustical Holography* (L. W. Kessler, ed.), pp. 307–326, Springer US, 1977.

[16] G. E. Trahey, J. W. Allison, and O. T. von Ramm, "Angle independent ultrasonic detection of blood flow.," *IEEE transactions on bio-medical engineering*, vol. 34, pp. 965–967, Dec. 1987.

[17] G. E. Trahey, S. M. Hubbard, and O. T. von Ramm, "Angle independent ultrasonic blood flow detection by frame-to-frame correlation of B-mode images.," *Ultrasonics*, vol. 26, pp. 271–276, Sept. 1988.

[18] L. N. Bohs, B. J. Geiman, M. E. Anderson, S. M. Breit, and G. E. Trahey, "Ensemble tracking for 2D vector velocity measurement: Experimental and initial clinical results.," *IEEE transactions on ultrasonics, ferroelectrics, and frequency control*, vol. 45, pp. 912–24, Jan. 1998.

[19] B. Dunmire, K. W. Beach, K. Labs, M. Plett, and D. E. Strandness, "Cross-beam vector Doppler ultrasound for angle-independent velocity measurements.," *Ultrasound in medicine & biology*, vol. 26, pp. 1213–35, Oct. 2000.

[20] L. N. Bohs, B. J. Geiman, M. E. Anderson, S. C. Gebhart, and G. E. Trahey, "Speckle tracking for multi-dimensional flow estimation.," *Ultrasonics*, vol. 38, pp. 369–75, Mar. 2000.

[21] A. Swillens, P. Segers, H. Torp, and L. Lø vstakken, "Two-dimensional blood velocity estimation with ultrasound: speckle tracking versus crossed-beam vector Doppler based on flow simulations in a carotid bifurcation model.," *IEEE transactions on ultrasonics, ferroelectrics, and frequency control*, vol. 57, pp. 327–39, Jan. 2010.

[22] M. Scabia, M. Calzolai, L. Capineri, L. Masotti, and A. Fart, "A real-time two-dimensional pulsed-wave Doppler system," *Ultrasound in Medicine and Biology*, vol. 26, no. 1, pp. 121–131, 2000.

[23] A. Pastorelli, G. Torricelli, M. Scabia, E. Biagi, and L. Masotti, "A real-time 2-D vector Doppler system for clinical experimentation.," *IEEE transactions on medical imaging*, vol. 27, pp. 1515–24, Oct. 2008.

[24] J. A. Jensen and P. Munk, "A new method for estimation of velocity vectors.," *IEEE transactions on ultrasonics, ferroelectrics, and frequency control*, vol. 45, pp. 837–51, Jan. 1998.

[25] M. E. Anderson, "Multi-dimensional velocity estimation with ultrasound using spatial quadrature.," *IEEE transactions on ultrasonics, ferroelectrics, and frequency control*, vol. 45, pp. 852–61, Jan. 1998.

[26] M. M. l. Pedersen, M. J. Pihl, P. Haugaard, J. M. Hansen, K. L. Hansen, M. B. Nielsen, and J. r. A. Jensen, "Comparison of real-time in vivo spectral and vector velocity estimation.," *Ultrasound in medicine & biology*, vol. 38, pp. 145–51, Jan. 2012.

[27] K. L. Hansen, M. M. l. Pedersen, H. Mø ller Sø rensen, J. Kjaergaard, J. C. Nilsson, J. T. Lund, J. r. A. Jensen, and M. B. Nielsen, "Intraoperative cardiac ultrasound examination using vector flow imaging.," *Ultrasonic imaging*, vol. 35, pp. 318–32, Oct. 2013.

[28] H. B. Kim, J. R. Hertzberg, and R. Shandas, "Development and validation of echo PIV," *Experiments in Fluids*, vol. 36, pp. 455–462, Mar. 2004.

[29] S. Ohtsuki and M. Tanaka, "The flow velocity distribution from the Doppler information on a plane in three-dimensional flow," *Journal of visualization*, vol. 9, no. 1, pp. 69–82, 2006.

[30] D. Garcia, J. C. Del Alamo, D. Tanne, R. Yotti, C. Cortina, E. Bertrand, J. C. Antoranz, E. Perez-David, R. Rieu, F. Fernandez-Aviles, and J. Bermejo, "Two-dimensional intraventricular flow mapping by digital processing conventional color-Doppler echocardiography images.," *IEEE transactions on medical imaging*, vol. 29, pp. 1701–13, Oct. 2010.

[31] J. Udesen, F. Gran, K. L. Hansen, J. A. Jensen, C. Thomsen, and M. B. Nielsen, "High frame-rate blood vector velocity imaging using plane waves: simulations and preliminary experiments.," *IEEE transactions on ultrasonics, ferroelectrics, and frequency control*, vol. 55, pp. 1729–43, Aug. 2008.

[32] I. K. Ekroll, A. Swillens, P. Segers, T. Dahl, H. Torp, and L. Lovstakken, "Simultaneous quantification of flow and tissue velocities based on multi-angle plane wave imaging.," *IEEE transactions on ultrasonics, ferroelectrics, and frequency control*, vol. 60, pp. 727–38, Apr. 2013.

[33] I. K. Ekroll, T. r. Dahl, H. Torp, and L. Lø vstakken, "Combined vector velocity and spectral Doppler imaging for improved imaging of complex blood flow in the carotid arteries.," *Ultrasound in medicine & biology*, vol. 40, pp. 1629–40, July 2014.

[34] S. Ricci, L. Bassi, and P. Tortoli, "Real-time vector velocity assessment through multigate Doppler and plane waves.," *IEEE transactions on ultrasonics, ferroelectrics, and frequency control*, vol. 61, pp. 314–24, Feb. 2014.

[35] S.-Y. Wu, S.-L. Wang, and P.-C. Li, "Tracking in High-Frame-Rate Imaging," *Ultrasonic Imaging*, vol. 32, pp. 1–15, Jan. 2010.

[36] M. Tanter, J. Bercoff, L. Sandrin, and M. Fink, "Ultrafast compound imaging for 2-D motion vector estimation: application to transient elastography.," *IEEE transactions on ultrasonics, ferroelectrics, and frequency control*, vol. 49, pp. 1363–74, Oct. 2002.

[37] C. Papadacci, M. Pernot, M. Couade, M. Fink, and M. Tanter, "High-contrast ultrafast imaging of the heart.," *IEEE transactions on ultrasonics, ferroelectrics, and frequency control*, vol. 61, pp. 288–301, Mar. 2014.

[38] J. Bercoff, G. Montaldo, T. Loupas, D. Savery, F. Mézière, M. Fink, and M. Tanter, "Ultrafast compound Doppler imaging: providing full blood flow characterization.," *IEEE transactions on ultrasonics, ferroelectrics, and frequency control*, vol. 58, pp. 134–47, Jan. 2011.

[39] O. J. Benavidez, K. Gauvreau, K. J. Jenkins, and T. Geva, "Diagnostic errors in pediatric echocardiography: development of taxonomy and identification of risk factors.," *Circulation*, vol. 117, pp. 2995–3001, June 2008.

[40] T. O. Cheng, M.-X. Xie, X.-F. Wang, Y. Wang, and Q. Lu, "Real-time 3-dimensional echocardiography in assessing atrial and ventricular septal defects: an echocardiographic-surgical correlative study.," *American heart journal*, vol. 148, pp. 1091–5, Dec. 2004.

[41] P. Acar and S. Abadir, "3D Echocardiography in Routine Paediatric Cardiology," pp. 24–27, 2008.

[42] K.-S. Hsieh, "Evaluation of Congenital Heart Diseases with Real-time Three-dimensional Echocardiography," *Journal of Medical Ultrasound*, vol. 16, pp. 101–112, Jan. 2008.

[43] J. M. Simpson and O. Miller, "Three-dimensional echocardiography in congenital heart disease.," *Archives of cardiovascular diseases*, vol. 104, pp. 45–56, Jan. 2011.

[44] L. Lovstakken, S. Bjaerum, D. Martens, and H. Torp, "Blood flow imaging–A new real-time, 2-D flow imaging technique.," *IEEE transactions on ultrasonics, ferroelectrics, and frequency control*, vol. 53, pp. 289–99, Feb. 2006.

[45] S. A. Nyrnes, L. Lovstakken, H. Torp, and B. r. O. Haugen, "Blood flow imaging-a new angle-independent ultrasound modality for the visualization of flow in atrial septal defects in children.," *Echocardiography (Mount Kisco, N.Y.)*, vol. 24, pp. 975–81, Oct. 2007.

[46] M. Tanaka, T. Sakamoto, S. S, N. H, K. Yoshiaki, S. Ohtsuki, and H. Kanai, "Blood flow structure and dynamics , and ejection mechanism in the left ventricle: Analysis using echo-dynamography," *Journal of Cardiology*, vol. 52, pp. 86–101, 2008.

[47] T. Kojima, T. Kameyama, H. Nakajima, E. Khmyrova, T. Kurokawa, and Y. Saijo, "Evaluation of vortex flow in left ventricle by echo-dynamography and phase contrast magnetic resonance angiography.," *Conference proceedings : ... Annual International Conference of the IEEE Engineering in Medicine and Biology Society. IEEE Engineering in Medicine and Biology Society. Conference*, vol. 2012, pp. 2676–9, Jan. 2012.

[48] V. Piro, N. Piro, and O. Piro, "Characterization of Intraventricular Blood Flow Using a Microbubble-Contrast Tracking Echo-Piv Technique," *Journal of the American College of Cardiology*, vol. 59, p. E1139, Mar. 2012.

[49] B. Meyers, J. Charanko, M. Pu, W. Little, and P. Vlachos, "Robust clinical cardiac Echo Particle Image Velocimetry (EchoPIV)," *10th International Symposium on Particle Image Velocimetry*, 2013.

[50] P. Beerbaum, H. Korperich, P. Barth, H. Esdorn, J. Gieseke, and H. Meyer, "Noninvasive Quantification of Left-to-Right Shunt in Pediatric Patients : Phase-Contrast Cine Magnetic Resonance Imaging Compared With Invasive Oximetry," *Circulation*, vol. 103, pp. 2476–2482, May 2001.

[51] R. Krishnamurthy, "Neonatal cardiac imaging.," *Pediatric radiology*, vol. 40, pp. 518–27, Apr. 2010.

[52] C. M. Gallippi and G. E. Trahey, "Adaptive Clutter Filtering via Blind Source Separation for Two-Dimensional Ultrasonic Blood Velocity Measurement," *Ultrasonic Imaging*, vol. 24, pp. 193–214, Oct. 2002.

[53] C. Kasai, K. Namekawa, A. Koyano, and R. Omoto, "Real-Time Two-Dimensional Blood Flow Imaging Using an Autocorrelation Technique," *IEEE Transactions on Sonics and Ultrasonics*, vol. 32, no. 3, pp. 458–464, 1985.

[54] A. Swillens, P. Segers, and L. Lovstakken, "Two-dimensional flow imaging in the carotid bifurcation using a combined speckle tracking and phase-shift estimator: a study based on ultrasound simulations and in vivo analysis.," *Ultrasound in medicine & biology*, vol. 36, pp. 1722–35, Oct. 2010.

[55] G. Montaldo, M. Tanter, J. Bercoff, N. Benech, and M. Fink, "Coherent plane-wave compounding for very high frame rate ultrasonography and transient elastography.," *IEEE transactions on ultrasonics, ferroelectrics, and frequency control*, vol. 56, pp. 489–506, Mar. 2009.

[56] C.-C. Shen, M.-Y. Pan, and M.-L. Li, "High frame-rate vector flow estimation using speckle tracking with recursive plane-wave compounding," *2010 IEEE International Ultrasonics Symposium*, pp. 1307–1310, Oct. 2010.

[57] Y. Miyagi, H. Masaoka, N. Akamatsu, and K. Sekiba, "Development of a three-dimenisonal color Doppler system," *Medical progress through technology*, vol. 18, no. 4, pp. 201–208, 1992.

[58] P. Picot, D. Rickey, and R. Mitchell, "Three-dimensional colour Doppler imaging," *Ultrasound in Medicine and Biology*, vol. 19, no. 2, pp. 95–104, 1993.

[59] S. Berg, H. Torp, B. O. Haugen, and S. Samstad, "Volumetric Blood Flow Measurement with the Use of Dynamic 3-Dimensional Ultrasound Color Flow Imaging," *Journal of the American Society of Echocardiography*, vol. 13, pp. 0393–0402, May 2000.

[60] H. Tsujino, M. Jones, and T. Shiota, "Real-time three-dimensional color Doppler echocardiography for characterizing the spatial velocity distribution and quantifying the peak flow rate in the left ventricular," *Ultrasound in Medicine and Biology*, vol. 27, no. 1, pp. 69–74, 2001.

Chapter 2

Background

This chapter contains a brief introduction to ultrasound blood flow imaging and covers the techniques and issues discussed in this thesis. For a more thorough introduction to ultrasound imaging, please refer to [1–4]. In Sec. 2.3, an introduction to the main clinical application of the thesis work is given.

2.1 Ultrasound image acquisition

2.1.1 Unfocused versus focused imaging

In conventional line-by-line imaging, one focused ultrasound pulse is transmitted at a time and the received echoes are used to form a single image line in the ultrasound image, as illustrated to the left in Fig. 2.1. Recent advances in ultrasound imaging technology allow for parallel beamforming of multiple receive beams, and multiple image lines may therefore be formed simultaneously. To utilize many multiple receive lines, a large region of interest must be insonified by the transmit wave. In plane wave imaging, unfocused ultrasound waves are transmitted instead of focused waves. If all elements are used to transmit one unfocused beam, a full field-of-view region is insonified, and all image lines may be generated in parallel, as illustrated to the right in Fig. 2.1. One image is constructed after one transmitted wave, compared to only a single image line in conventional imaging. A substantial increase in frame rate (number of images acquired per second) is therefore achieved with plane wave imaging and parallel receive beamforming.

Resolution

The resolution of an ultrasound image is the minimum distance between two objects which may be distinguished from each other. Fig. 2.2 illustrates an imaging setup where the wavelength and pulse length of an ultrasound pulse are indicated. The axial (z-direction in Fig. 2.2) resolution is proportional to the pulse length (number of cycles in the pulse $\times$ wavelength). The axial resolution may be increased by reducing the number of cycles in the ultrasound pulse or by increasing the transmit frequency (reducing the wavelength). The lateral (x-direction in Fig. 2.2) resolution is determined by the width of the transmit and receive beams. The beam width (distance from beam axis to a -3 dB drop in pressure amplitude) for a focused transducer is often

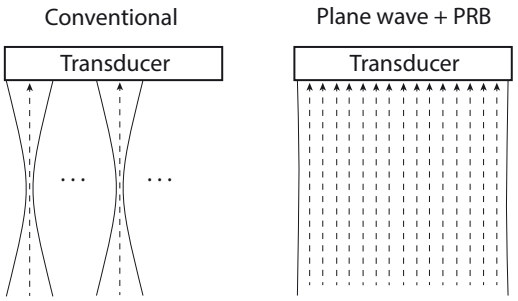

Figure 2.1: Left: Conventional line-by-line acquisition. One focused ultrasound beam is transmitted and the received echo form one image line in the ultrasound image. Right: One unfocused (plane) wave is transmitted using the whole transducer width. The received echo is used to form all image lines simultaneously.

given by

$$D_f = \frac{\lambda z_f}{D} = F_{\#}\lambda, \tag{2.1}$$

where λ is the wavelength, z_f is the focus depth, D is the size of the aperture, and the ratio between the focus distance and the aperture is the F-number, $F_{\#}$. If both transmit (tx) and receive (rx) beams are focused, the two-way $F_{\#}$ is given by

$$F_{\#\mathrm{txrx}} = \left(\frac{1}{F_{\#\mathrm{tx}}} + \frac{1}{F_{\#\mathrm{rx}}}\right). \tag{2.2}$$

When an unfocused beam is transmitted ($z_f \to \infty$), the two-way $F_{\#}$ is increased as $F_{\#\mathrm{tx}} = \frac{z_f}{D} \to \infty$ and $F_{\#\mathrm{txrx}} = F_{\#\mathrm{rx}}$, and the lateral resolution is reduced. The lack of transmit focusing will also lead to a decrease in penetration. The ultrasound energy is no longer concentrated, but spread out over a larger area.

The ultrasound wave is attenuated as it propagates through the tissue, and this attenuation is frequency-dependent: higher frequencies are more attenuated than lower frequencies. The transmit frequency (and spatial resolution) is therefore limited by the penetration depth needed. When imaging deep structures as the heart in adults, transmit frequencies down to 2-3 MHz are often used, but for children and newborns the propagation distance to the heart is shorter, and a higher transmit frequency may be used.

The noise in the ultrasound signal arises from different sources. Thermal noise arises in the transducer and front-end electronics, and acoustic noise may be caused by multiple reflections (reverberations) or distortion of the wave front (aberrations) due to changes in the speed of sound in inhomogeneous tissue. The signal-to-noise ratio can be increased by increasing the transmit power, but patient safety limits determines the maximum acoustic intensity which may be used [5, 6].

The geometry of the ultrasound transducer may also be a source of image quality corruption. The finite size of the aperture used to emit an ultrasound wave results

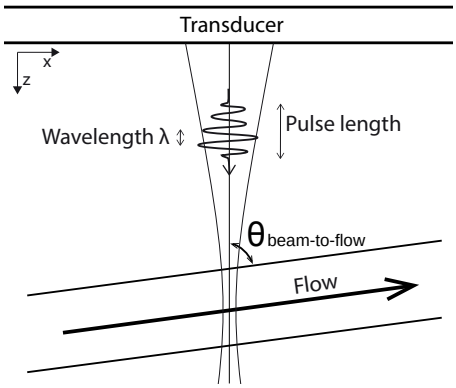

Figure 2.2: An ultrasound pulse traveling along the beam axis. The beam-to-flow θ is indicated.

in sidelobes. Echoes received from the sidelobes will be registered as if they were coming from the main lobe direction, and may degrade the image contrast. The amplitudes of the sidelobes are, however, much lower than the main beam. Another effect degrading the image contrast are grating lobes. The grating lobes arise from the regular spacing between the array elements which may cause constructive interference between neighboring elements in unwanted direction. The distance between the element centers must be less than $\lambda/2$ to completely avoid grating lobes for all steering angles (beam angle with respect to transducer). The grating lobes may lead to artifacts in the B-mode image and may also effect the blood flow estimates. The influence of grating lobes on blood velocity estimation is discussed in Ch. 5.

2.2 Ultrasound blood flow imaging

2.2.1 Conventional methods for blood flow estimation

The Doppler effect infers that when an observer is moving relative to a wave source, the frequency measured differs from the frequency of the emitted wave. In an everyday setting, you can notice the Doppler effect when an ambulance is passing. You hear a higher pitch of the siren when the ambulance is approaching than when it passes and moves away from you. When the ambulance is moving towards you, the sound waves are compressed (frequency is increased), whereas the waves are more spread out when the ambulance has passed. In ultrasound imaging, the blood is moving relative to the ultrasound transducer, so when an ultrasound wave is transmitted into the body, it will be scattered by the blood scatterers (red blood cells) and the backscattered echo will have a shift in frequency compared with the transmitted frequency. The Doppler shifts are actually in the audible range (0-20 kHz) and are made available to the physicians through loudspeakers on the ultrasound systems. The received signal from a given depth is a sum of contributions from a large ensemble of blood scatterers,

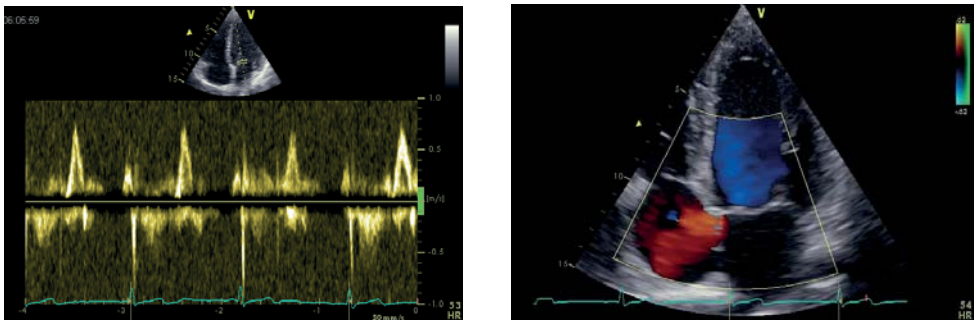

(a) PW Doppler spectrum

(b) Color flow image

Figure 2.3: (a) A PW Doppler spectrum from a sample volume in the heart is shown. The sample volume is indicated in the B-mode image in the upper part of the figure. The spectrum of velocities is shown as a function of time. (b) A color flow image of the heart is shown. The blood velocities are color encoded where red and blue indicates blood flow toward and away from the ultrasound transducer.

where each scatterer contributes with their own Doppler shift. The received signal is therefore a spectrum of velocities. The Doppler shifts correspond, however, only to the axial (along the beam axis) velocity component of the three-dimensional blood velocity vector. In Fig. 2.2, the ultrasound beam axis, the flow direction and the resulting beam-to-flow angle θ is indicated.

In conventional ultrasound blood imaging, the axial blood velocity estimates can be displayed either as a spectrum of velocities from a small region as a function of time or as a 2-D or 3-D parametric *color flow map* in a larger region of interest. The two spectral methods are continuous wave (CW) and pulsed wave (PW) Doppler. CW Doppler is continuously transmitting and receiving ultrasound and contains therefore all velocities along the ultrasound beam. In PW Doppler, pulsed transmission of ultrasound is used to obtain depth information of the received signal, and a small sample volume is placed at the region of interest. The PW Doppler spectrum displays the velocity information from this given sample volume. An example of a PW Doppler spectrum is given in Fig. 2.3a, where the corresponding sample volume is indicated in the B-mode image in upper part of the figure.

A color flow image of the heart is shown in Fig. 2.3b. The estimated mean axial blood velocities are displayed as a 2-D color map and overlaid a B-mode image. The colors correspond to the mean blood velocity component along the beam axis, where red colors typically indicate positive Doppler shifts (flow toward the transducer) and blue colors indicate negative Doppler shifts (flow away from the transducer).

Both PW Doppler and color flow imaging (CFI) use pulsed transmissions to obtain range (depth) resolution. Several ultrasound pulses are transmitted in each beam direction at a given pulse repetition frequency (PRF). The ultrasound pulse propagates in depth, and the received signal is sampled according to a given propagation depth in

the tissue. The required imaging depth may limit the highest PRF, because the echo must return before the next ultrasound pulse is transmitted. The time axis given by the pulse repetition time is called *slow-time*. In color flow imaging, a large 2-D region is imaged line-by-line, limiting the number of pulses in each beam direction to achieve acceptable image frame rates. The number of emitted pulses in each beam direction used to generate one image line is referred to as the (slow-time) ensemble size.

The movement of a scatterer between two pulses will result in a phase or time shift in the received signal in the slow-time direction which is used to estimate the velocity of the scatterer. In CFI, the blood velocity estimation is typically based on the autocorrelation method (ACM) suggested by Nakemawa and Kasai in the mid-eighties [7]. In this method, the mean axial velocity is estimated from the correlation of the Doppler signal from pulse to pulse (lag 1), $\hat{R(1)}$ as follows

$$\hat{v}_{\text{axial}} = \frac{c \cdot \text{PRF}}{4\pi f_0} \angle \hat{R}(1), \tag{2.3}$$

where c is the speed of sound and f_0 is the center frequency of the transmitted pulse. The autocorrelation function at lag 1 is given by

$$\hat{R}(1) = \frac{1}{N-1} \sum_{k=1}^{N-1} x(k)^* x(k+1), \tag{2.4}$$

where $x(k)$ is the Doppler signal from a given spatial position, * denotes the complex conjugate and N is the ensemble size. Even though CFI provides quantitative velocity information, the modality is mostly used to visualize blood flow and for the detection of abnormal flow, for example, heart valve insufficiencies, septum defects and artery plaque stenosis. The spectral Doppler methods are then used to quantify the velocities in a particular region of interest.

Limitations

The conventional Doppler estimators have been extensively validated and are used in a wide range of clinical settings. The limitations of the methods are also well known and are explained shortly in the following.

Angle-dependency: The conventional Doppler methods only measure one velocity component of the three-dimensional blood velocity vector; the velocity component along the ultrasound beam axis. The beam-to-flow angle must be known to find the true blood velocity vector, and the velocity estimates are therefore said to be *angle-dependent*.

Aliasing: For PW Doppler and color flow imaging, the pulse repetition frequency limits the highest measurable (axial) velocity according the Nyquist sampling theorem as follows

$$v_{\text{Nyquist}} = \frac{c \cdot \text{PRF}}{4 f_0}, \tag{2.5}$$

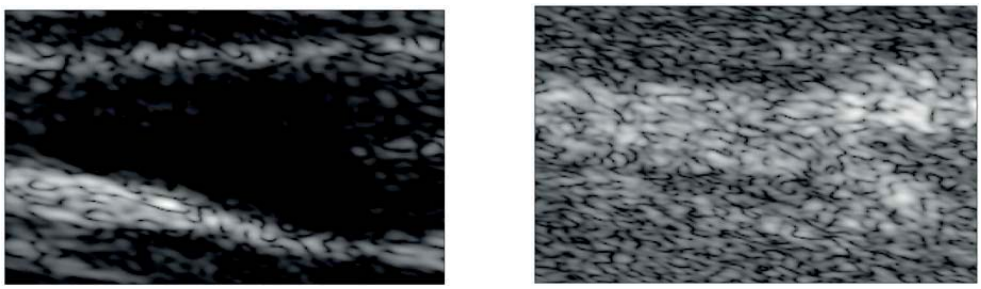

(a) Before clutter filtering. (b) After clutter filtering.

Figure 2.4: (a) The artery wall gives the strongest echo and the brightest parts of the image. The blood inside the artery results in much weaker echo and is the darkest region of the image. (b) Clutter filtering attenuates the strong echo from the tissue wall and the blood signal becomes visible in the ultrasound image.

where c is the speed of sound and f_0 is the pulse center frequency. Velocities above this limit will wrap around the velocity scale and be displayed as negative velocities in the spectrum or color flow image.

Flash artifacts: In color flow imaging, transducer movement during scanning or large tissue motion may result in phase-shifts which are not removed by the clutter filter. These phase-shifts can lead to color-flashes in the color flow image in areas which do not contain blood.

Color blooming: The colors in the color flow image may "bleed" into the tissue because of the limited spatial resolution of the color image compared to the B-mode image. The relative long pulses used in CFI increases SNR, but reduces the spatial resolution compared with B-mode imaging.

2.2.2 Clutter filtering

The echo from the blood scatterers are typically 40-80 dB weaker than the echo from surrounding tissue. Fig. 2.4 shows an ultrasound image of a carotid artery bifurcation before and after clutter filtering. Before clutter filtering, the tissue wall of the artery is the brightest part of the image, and is thus giving the strongest echo. Inside the artery, the image is almost completely dark. Echo coming from the blood flow inside the artery is much weaker than echo from the artery wall. After clutter filtering, however, the blood signal is visible and the echoes from the artery walls are attenuated. For blood velocity estimation, a sufficient separation of the tissue (clutter) and blood signals is necessary to obtain correct blood velocity estimates.

Clutter filtering is done in slow-time, where the movement of the blood flow has resulted in a phase or frequency shift in the blood signal, whereas the signal from surrounding stationary or slowly-moving tissue is located around zero frequency. This

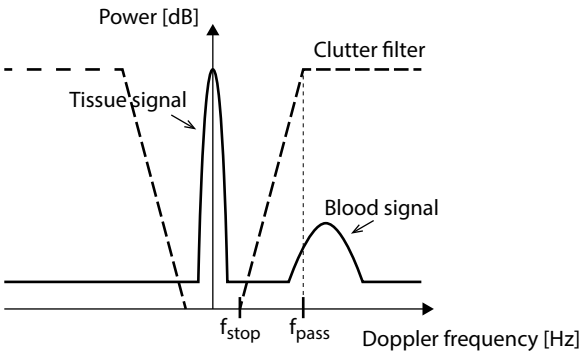

Figure 2.5: The movement of the blood scatterers result in a shift in Doppler frequency compared to the stationary or slowly-moving tissue. A high-pass filter may then be used to remove the tissue signal.

is illustrated in Fig. 2.5, where the blood signal has a shift in Doppler frequency compared with the tissue signal. The tissue signal is much stronger (higher amplitude), but may be attenuated by a high-pass clutter filter with a sufficient stopband region defined by f_{stop}. The region between the stopband f_{stop} and the passband f_{pass} of the filter is called the transition region. If parts of the blood signal are in this region, the clutter filter will attenuate the lowest blood velocities and limit the minimum measurable blood velocity. A steep transition region is therefore desired. For spectral blood velocity methods, very sharp frequency cut-offs can be implemented. For color flow imaging, however, the number of pulses in each direction is limited to achieve 2-D flow images at acceptable frame rates. The limited ensemble size restricts the clutter filter order and thus the sharpness of the filter cut-off.

Clutter filter design and its influence in color flow imaging, has previously been thoroughly investigated [8–10], and a short description of the common filter types will be given in the following.

Finite impulse response filters

Finite impulse response (FIR) filters are time-invariant and the output samples can be found from the following convolution sum

$$y(n) = \sum_{k=0}^{K} h(k)x(n-k), \quad n = 0, 1, ..., N \tag{2.6}$$

where $h(k)$ is the filter impulse response, K is filter order, N is the ensemble size and $x(n)$ and $y(n)$ are the input and output samples, respectively. The FIR filters have low computational complexity and only depend on present and past input samples. The number of valid output samples is $N - K$, because the first K samples must be discarded due to initialization.

Infinite impulse response filters

Output samples from infinite impulse response filters may be described by the following difference equation

$$y(n) = -\sum_{k=1}^{K} a_k y(n-k) + \sum_{k=0}^{K} b_k x(n-k), \tag{2.7}$$

where a_k and b_k are filter coefficients and K is the filter order. The output samples from an IIR filter depend on present and past input samples, and also past output samples. For short ensemble signals, it is important that the IIR filter is properly initialized to avoid a long transient response. Different initialization techniques have been proposed and investigated specifically for the short ensemble signals in color flow imaging [10, 11].

Polynomial regression filters

In polynomial regression filters, the clutter signal is approximated by a set of polynomial basis functions and subtracted from Doppler signal to obtain the blood signal. The output samples can be found from

$$\mathbf{y} = \left(\mathbf{I} - \sum_{k=0}^{K} \mathbf{b}_k \mathbf{b}_k^H \right) \mathbf{x}, \tag{2.8}$$

where $\mathbf{I}$ is the identity matrix, $\mathbf{b_k}$ are orthonormal basis vectors spanning the clutter signal subspace of dimension $K+1$. The filter order is K, and H is the conjugate transpose. The Legendre polynomials are often used as basis functions, because of the high stopband rejection [9]. The frequency response of the polynomial regression filter vary both with ensemble size and filter order, and, unlike FIR and IIR filtering, no output samples must be discarded after filtering.

2.2.3 Two-dimensional velocity estimation

Angle-correcting the 1-D velocity information obtained with the conventional Doppler methods may be difficult, and is not recommended when the beam-to-flow angle exceeds 60°. The potential errors in the estimate of the beam-to-flow angle have an increasing impact on the angle-corrected velocity estimates when the beam-to-flow angle is increasing. The angle-dependency and need for manual angle-correction, makes the velocity estimates operator-dependent [12]. For color flow imaging, a large range of beam-to-flow angles will be present, it is not feasible to angle-correct all the velocity estimates. The color flow images must therefore be interpreted to perceive the flow direction.

To overcome the angle-dependency in the conventional methods, several two-dimensional vector velocity techniques have been proposed to obtain both the axial and lateral velocity component in the imaging plane. The two main research lines have been vector Doppler and speckle tracking, which are the techniques used in this

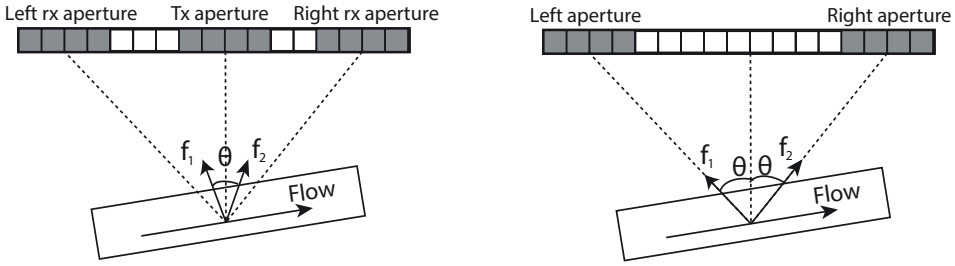

Figure 2.6: The lateral velocity component may be calculated from Doppler estimates, f_1 and f_2, from two transmit and/or receive angles. (a) A split aperture setup with one common transmit aperture and two receive aperture with different beam-to-flow angles. (b) A dual-angle setup with two transmit/receive apertures with different beam-to-flow angles.

thesis work. A brief introduction to these techniques and other more recently proposed methods are given below.

Vector Doppler

By transmitting and/or receiving the ultrasound beams from minimum two scan angles for the same sample volume, the lateral velocity component in that sample volume may be calculated from the two Doppler (axial) estimates obtained. Two typical vector Doppler setups are shown in Fig. 2.6. To the left, a split aperture setup is shown in which a transmit pulse is sent from the middle of the transducer and received from two receive apertures on the sides of the transducer. To the right, a dual-angle setup is shown in which the same aperture is used to transmit and receive beams from two different scan angles. The transmit pulses from the two scan angles can not be transmitted at the same time and the Doppler estimates from the two scan angles will therefore be obtained with a time-lag (unlike the Doppler estimates from the split aperture). However, the angle between the Doppler estimates obtained are larger than in the split aperture case, which increases the accuracy of the lateral velocity estimate.

A setup similar to that shown in Fig. 2.6b was used in the 2nd contribution in this thesis. When the two Doppler frequency estimates, f_1 and f_2, from this setup are found, the two velocity components can be calculated as follows [13]

$$\begin{aligned} v_x &= -\frac{c}{4f_0 \sin(\theta)}(\hat{f}_1 - \hat{f}_2) \\ v_z &= -\frac{c}{4f_0 \cos(\theta)}(\hat{f}_1 + \hat{f}_2) \end{aligned} \tag{2.9}$$

where c is the speed of sound, 2θ is the separation angle between the two scan directions, f_0 is the pulse center frequency and $\hat{f}_1$, $\hat{f}_1$ are the Doppler frequency estimates.

The vector Doppler technique has low computational complexity and may be expanded to 3-D velocity estimation if more scan angles are used. The depth is, however, limited by the aperture size and beam separation angle, because the velocity components can only be estimated in a beam overlapping region. A thorough review of the vector Doppler techniques can be found in [13]. Lately, real-time implementation on research systems have been done [14, 15], but the vector Doppler technique has not yet been established for clinical use.

Lateral modulation

A related approach to estimate both the axial and lateral velocity component was proposed by Jensen and Munk [16] (called transverse oscillation) and Anderson [17] (called spatial quadrature). In this method, a modulation in the lateral direction is introduced on receive using complex apodization schemes. The lateral modulation makes it possible to detect a phase-shift between parallel beams when lateral movement is present (similar to the phase shift in the axial direction caused by axial movement).

The transverse oscillation technique has been validated for both 2-D and 3-D velocity estimation in simulations and *in vitro* [18, 19], and has also been commercialized for linear array transducers on a ultrasound scanner from BK Medical (BK Medical, Herlev, Denmark), which has been used in recent studies [20, 21].

Doppler bandwidth

It has also been suggested to use the bandwidth of the received Doppler signal to estimate the lateral velocity component. The bandwidth is dependent on the spread of velocities and the corresponding observation time of the scatterers as they pass through the sample volume. The method have been investigated since the eighties [22, 23], but is still at an experimental stage. The method has several limitations, for example assumptions of stationary flow and the request of a spherically shaped Doppler sample volume.

Fourier-based

Wilson and Gill [24] extended their 1-D Fourier-based velocity estimator to two dimensions in 1993. The obtained Doppler signal from a 2-D region is a 3-D matrix consisting of the fast-time (depth) samples and the lateral (parallel beam) samples for several repetitions given by the slow-time ensemble size. In the Fourier domain, the 3-D power spectrum is located on a plane plane rotated in the 3-D Fourier space according to the lateral and axial velocities of the ultrasound scatterers. Wilson and Gill derived an estimator to utilize this information to obtain both the lateral and axial velocity components. Other estimators for this method have later been suggested and validated in simulations, *in vitro* and *in vivo* [25].

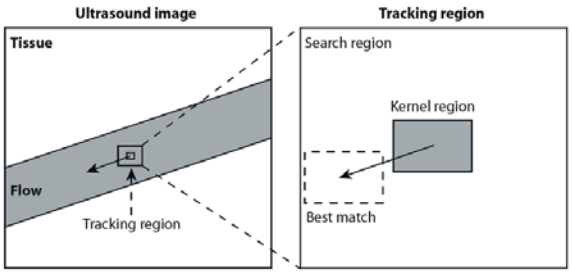

Figure 2.7: The basic principle of speckle tracking. A 2-D kernel is defined in the first image and the best match of this kernel is then search for in the next image.

Echodynamography/vector flow mapping

A more recent method combines measured axial velocities with regularization based on physical principles to estimate the lateral velocity component. Ohtsuki *et al.* [26] presented a method called echodynamography in 2006, where it was assumed that the flow along the wall could be divided in a laminar and vortical component. Assuming only in-plane flow, fluid dynamics theories can be used to estimate the lateral velocity component from the vortical flow component. Repeating the assumptions when moving away from the wall, a complete 2-D velocity map of the ventricular flow could be obtained. Later, a similar approach was proposed by Garcia *et al.* [27] in which the wall movement was estimated using speckle tracking and used together with the continuity equation to obtain the lateral flow velocities assuming in-plane flow. Again, the complete 2-D velocity map of the ventricular flow could be obtained by repeating the assumptions moving from the wall inwards in the ventricle.

Speckle tracking

In Fig. 2.4 in Sec. 2.2.2, the speckle pattern (intensity pattern) which appear in the ultrasound images is shown. The speckle is present in ultrasound images of both tissue and flow, and is a result of the constructive and destructive interference in the backscattered echo. The movement of the blood speckle pattern in the 2-D image is correlated with the movement of blood, and may be tracked from frame to frame to estimate the 2-D blood velocities. The 2-D speckle tracking technique was suggested by Trahey in 1987 [28], and the basic principle is shown in Fig. 2.7. A 2-D kernel is defined in the first image and the best match of this kernel is searched for in possible positions in a defined search region in the next (or a later) image. The velocity is estimated based on the displacement of the kernel and the known time between the image acquisitions and the size of the search region determines the maximum measurable velocity.

The tracking technique was originally suggested for radio-frequency (RF) signals, but because of the computational complexity of 2-D RF cross-correlation, new approaches have been suggested [29]. Other pattern matching algorithms than

normalized cross-correlation may be used, including sum of absolute differences (SAD) or sum of squared differences (SSD). The computational complexity of the tracking technique is reduced when SAD or SSD matching on the envelope data is used instead of RF cross-correlation [29].

The normalized cross-correlation algorithm is given by

$$\rho(u,v) = \frac{\sum_{x,y} \left(I(x+u,y+v) - \overline{I}_{u,v}\right)\left(K(x,y) - \overline{K}\right)}{\sqrt{\sum_{x,y}(I(x+u,y+v) - \overline{I}_{u,v})^2 \sum_{x,y}(K(x,y) - \overline{K})^2}}, \tag{2.10}$$

where K is the original kernel and I is the search region displaced (u,v) from the kernel K position for a subsequent frame. The averages are defined as

$$\begin{aligned} \overline{I}_{u,v} &= \frac{1}{N_x N_y} \sum_{x,y} I(x+u,y+v) \\ \overline{K} &= \frac{1}{N_x N_y} \sum_{x,y} K(x,y), \end{aligned} \tag{2.11}$$

where N_x and N_y are the kernel dimensions, so $x = [0, N_x - 1]$ and $y = [0, N_y - 1]$. The index of the maximum correlation value determines the most likely displacement of the kernel.

The simpler SAD algorithm is given by

$$d_{\mathrm{SAD}}(u,v) = \sum_{x,y} |I(x+u,y+v) - K(x,y)|, \tag{2.12}$$

where d_{SAD} is the SAD coefficient representing the error in the matching. The match with minimal error gives the displacement estimate. Similarly, the SSD algorithm is given by

$$d_{\mathrm{SSD}}(u,v) = \sum_{x,y} \left(I(x+u,y+v) - K(x,y)\right)^2, \tag{2.13}$$

where the minimum SSD-coefficient $d_{\mathrm{SSD}}(u_{\min}, v_{\min})$ reveals the most likely displacement of the kernel.

The accuracy of the velocity estimation is mainly limited by speckle decorrelation due to velocity gradients and low signal-to-noise conditions [29, 30]. Contrast agents would increased the signal-to-noise ratio, but is not applicable in all clinical settings.

Echo particle imaging velocimetry

Another recent approach related to speckle tracking is echo particle imaging velocimetry (echo PIV). This technique combining the optical imaging technique PIV with contrast-enhanced B-mode imaging was described by Kim *et al.* in 2004 [31]. Conventional optical PIV techniques are use to obtain reference flow fields in *in vitro* experiments. The PIV analysis techniques can be used to estimate the velocities of contrast agent particles from B-mode images. The contrast agents (microbubbles)

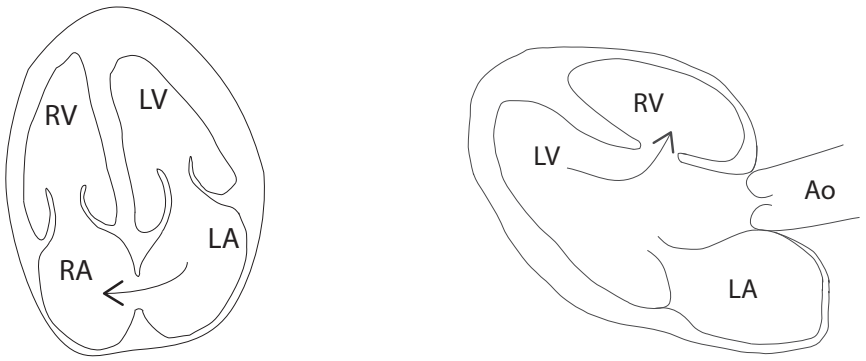

(a) ASD from an apical 4-chamber view.

(b) VSD from a parasternal long-axis view.

Figure 2.8: Illustration of atrial and ventricular septal defects in two typical imaging views. (a) The blood path through an ASD from the left to the right atrium is indicated with an arrow. (b) The blood path through the VSD from the left to the right ventricle is illustrated with an arrow. LV = left ventricle, LA = left atrium, RV = right ventricle, RA = right atrium, Ao = aorta

are injected into the blood pool intravenously and the strong backscattering from the microbubbles increases the signal-to-noise ratio significantly. Similar to speckle tracking, echo PIV use cross-correlation between subsequent image frames to obtain the particle displacement and estimate the 2-D blood velocities. The method has further been tested in both experimental and clinical settings and has been validated towards phase-contrast magnetic resonance showing promising results [32, 33].

It has also been suggested to use the PIV analysis techniques directly on the radio-frequency data [34, 35].

2.3 Congenital heart disease

Congenital heart disease (CHD) is the most common congenital abnormality, present in approximately 8 per 1000 live births [36]. Two of the most common types of CHD are ventricular septal defect (VSD) and atrial septal defect(ASD). A septal defect is a hole (shunt) in the wall (septum) between heart chambers, either between the atria in an ASD or between the ventricles in a VSD. There are different types of ASDs and VSDs depending on the position of the defect in the septum. Examples of an ASD and a VSD are illustrated in two typical ultrasound echocardiography views in Fig. 2.8. The ASD is shown from a four-chamber view (all four heart chambers are visible), whereas the VSD is shown from a parasternal long-axis view, in which the left atrium, the left ventricle, the right ventricle and the outflow to the aorta are visible. The septal defects usually allow (unwanted) blood flow from the left to the right side of the heart, increasing blood flow to the pulmonary circulation.

The septal defects may be discovered during pregnancy in a routine ultrasound

examination, or after birth if a heart murmur, or related symptoms (e.g. not gaining weight), is detected. Echocardiography is then used to examine the heart, and the goals of the examination include finding defect location and size, relationship with neighboring structures, flow direction, peak shunt velocity and potential enlarged ventricles [37]. A missed CHD or an erroneous diagnosis may at worst have a fatal outcome.

After birth, the circulatory system in neonates changes, and the pressure difference between the left and right side of the heart is small. The shunt flow velocities are therefore low and may be bidirectional (changing between left-to-right and right-to-left direction). As the circulatory system is normalized, the pressure difference between the left and right side of the heart increases, resulting in higher shunt velocities. In VSDs, an increase up to 4 m/s is typical and suggest that the pressure difference between the systemic and pulmonary circulation is normal. The pressure difference between the atria is small, so low shunt velocities are expected here. Many defects will, in the end, close by themselves, but large defects may have to be repaired by catheter closure or corrective surgery. In catheter closure, a permanent implant is inserted over the septal defect to close the hole and become a part of the heart wall. The device is placed using a catheter, which is lead into the heart through a large vein from the thigh. A catheter closure is favorable compared to open-heart surgery, but the location of the defect may not be suitable for catheter closure, making surgery the only alternative.

References

[1] D. H. Evans and W. N. McDicken, *Doppler ultrasound: physics, instrumentation, and signal processing*. Wiley, 2 ed., 2000.

[2] B. Angelsen and H. Torp, *Ultrasound Imaging - Waves, Signals and Signal processing in Medical Ultrasound*. Emantec, 2000.

[3] R. Cobbold, *Foundations of Biomedical Ultrasound*. Oxford University Press, Inc., 2007.

[4] P. R. Hoskins, K. Martin, and A. Thrush, *Diagnostic Ultrasound: Physics and Equipment*. Cambridge University Press, 2nd ed., 2010.

[5] Laurel, *Medical Ultrasound Safety*. American Institue of Ultrasound in Medicine, 2nd ed., 2009.

[6] G. ter Haar, *Safe Use of Ultrasound in Medical Diagnosis*. British Medical Ultrasound Society and British Institute of Radiology, 3rd ed., 2012.

[7] C. Kasai, K. Namekawa, A. Koyano, and R. Omoto, "Real-Time Two-Dimensional Blood Flow Imaging Using an Autocorrelation Technique," *IEEE Transactions on Sonics and Ultrasonics*, vol. 32, no. 3, pp. 458–464, 1985.

[8] A. Hoeks, J. V. de Vorst, A. Dabekaussen, P. Brands, and R. Reneman, "An efficient algorithm to remove low frequency Doppler signals in digital Doppler systems," *Ultrasonic imaging*, vol. 144, pp. 135–144, 1991.

[9] H. Torp, "Clutter rejection filters in color flow imaging: a theoretical approach.," *IEEE transactions on ultrasonics, ferroelectrics, and frequency control*, vol. 44, pp. 417–24, Jan. 1997.

[10] S. Bjæ rum, H. Torp, and K. Kristoffersen, "Clutter filter design for ultrasound color flow imaging.," *IEEE transactions on ultrasonics, ferroelectrics, and frequency control*, vol. 49, pp. 204–16, Mar. 2002.

[11] R. B. Peterson, L. E. Atlas, and K. W. Beach, "A comparison of IIR initialization techniques for improved color Doppler wall filter performance," *Proceedings of IEEE Ultrasonics Symposium ULTSYM-94*, pp. 1705–1708 vol.3, 1994.

[12] E. Y. L. Lui, A. H. Steinman, R. S. C. Cobbold, and K. W. Johnston, "Human factors as a source of error in peak Doppler velocity measurement.," *Journal of vascular surgery*, vol. 42, pp. 972–9, Nov. 2005.

[13] B. Dunmire, K. W. Beach, K. Labs, M. Plett, and D. E. Strandness, "Cross-beam vector Doppler ultrasound for angle-independent velocity measurements.," *Ultrasound in medicine & biology*, vol. 26, pp. 1213–35, Oct. 2000.

[14] A. Pastorelli, G. Torricelli, M. Scabia, E. Biagi, and L. Masotti, "A real-time 2-D vector Doppler system for clinical experimentation.," *IEEE transactions on medical imaging*, vol. 27, pp. 1515–24, Oct. 2008.

[15] S. Ricci, L. Bassi, and P. Tortoli, "Real-time vector velocity assessment through multigate Doppler and plane waves.," *IEEE transactions on ultrasonics, ferroelectrics, and frequency control*, vol. 61, pp. 314–24, Feb. 2014.

[16] J. A. Jensen and P. Munk, "A new method for estimation of velocity vectors.," *IEEE transactions on ultrasonics, ferroelectrics, and frequency control*, vol. 45, pp. 837–51, Jan. 1998.

[17] M. E. Anderson, "Multi-dimensional velocity estimation with ultrasound using spatial quadrature.," *IEEE transactions on ultrasonics, ferroelectrics, and frequency control*, vol. 45, pp. 852–61, Jan. 1998.

[18] J. Udesen and J. r. A. Jensen, "Investigation of transverse oscillation method.," *IEEE transactions on ultrasonics, ferroelectrics, and frequency control*, vol. 53, pp. 959–71, May 2006.

[19] M. J. Pihl and J. A. Jensen, "Measuring 3D velocity vectors using the Transverse Oscillation method," *2012 IEEE International Ultrasonics Symposium*, pp. 1881–1885, Oct. 2012.

[20] M. M. l. Pedersen, M. J. Pihl, P. Haugaard, J. M. Hansen, K. L. Hansen, M. B. Nielsen, and J. r. A. Jensen, "Comparison of real-time in vivo spectral and vector velocity estimation.," *Ultrasound in medicine & biology*, vol. 38, pp. 145–51, Jan. 2012.

[21] K. L. Hansen, M. M. l. Pedersen, H. Mø ller Sø rensen, J. Kjaergaard, J. C. Nilsson, J. T. Lund, J. r. A. Jensen, and M. B. Nielsen, "Intraoperative cardiac ultrasound examination using vector flow imaging.," *Ultrasonic imaging*, vol. 35, pp. 318–32, Oct. 2013.

[22] V. L. Newhouse, D. Censor, T. Vontz, J. a. Cisneros, and B. B. Goldberg, "Ultrasound Doppler probing of flows transverse with respect to beam axis.," *IEEE transactions on bio-medical engineering*, vol. 34, pp. 779–89, Oct. 1987.

[23] P. Tortoli, G. Guidi, L. Mantovani, and V. L. Newhouse, "Velocity magnitude estimation with linear arrays using Doppler bandwidth.," *Ultrasonics*, vol. 39, pp. 157–61, Apr. 2001.

[24] L. S. Wilson and R. W. Gill, "Measurement of two-dimensional blood velocity vectors by the ultrasonic speckle projection technique," *Ultrasound Imaging*, vol. 15, no. 4, pp. 286–303, 1993.

[25] N. Oddershede, L. Lø vstakken, H. Torp, and J. r. A. Jensen, "Estimating 2-D vector velocities using multidimensional spectrum analysis.," *IEEE transactions on ultrasonics, ferroelectrics, and frequency control*, vol. 55, pp. 1744–54, Aug. 2008.

[26] S. Ohtsuki and M. Tanaka, "The flow velocity distribution from the Doppler information on a plane in three-dimensional flow," *Journal of visualization*, vol. 9, no. 1, pp. 69–82, 2006.

[27] D. Garcia, J. C. Del Alamo, D. Tanne, R. Yotti, C. Cortina, E. Bertrand, J. C. Antoranz, E. Perez-David, R. Rieu, F. Fernandez-Aviles, and J. Bermejo, "Two-dimensional intraventricular flow mapping by digital processing conventional color-Doppler echocardiography images.," *IEEE transactions on medical imaging*, vol. 29, pp. 1701–13, Oct. 2010.

[28] G. E. Trahey, J. W. Allison, and O. T. von Ramm, "Angle independent ultrasonic detection of blood flow.," *IEEE transactions on bio-medical engineering*, vol. 34, pp. 965–967, Dec. 1987.

[29] L. N. Bohs, B. J. Geiman, M. E. Anderson, S. C. Gebhart, and G. E. Trahey, "Speckle tracking for multi-dimensional flow estimation.," *Ultrasonics*, vol. 38, pp. 369–75, Mar. 2000.

[30] B. H. Friemel, L. N. Bohs, K. R. Nightingale, and G. E. Trahey, "Speckle decorrelation due to two-dimensional flow gradients.," *IEEE transactions on ultrasonics, ferroelectrics, and frequency control*, vol. 45, pp. 317–27, Jan. 1998.

[31] H. B. Kim, J. R. Hertzberg, and R. Shandas, "Development and validation of echo PIV," *Experiments in Fluids*, vol. 36, pp. 455–462, Mar. 2004.

[32] G.-R. Hong, G. Pedrizzetti, G. Tonti, P. Li, Z. Wei, J. K. Kim, A. Baweja, S. Liu, N. Chung, H. Houle, J. Narula, and M. a. Vannan, "Characterization and quantification of vortex flow in the human left ventricle by contrast echocardiography using vector particle image velocimetry.," *JACC. Cardiovascular imaging*, vol. 1, pp. 705–17, Nov. 2008.

[33] F. Zhang, C. Lanning, L. Mazzaro, A. J. Barker, P. E. Gates, W. D. Strain, J. Fulford, O. E. Gosling, A. C. Shore, N. G. Bellenger, B. Rech, J. Chen, J. Chen, and R. Shandas, "In vitro and preliminary in vivo validation of echo particle image velocimetry in carotid vascular imaging.," *Ultrasound in medicine & biology*, vol. 37, pp. 450–64, Mar. 2011.

[34] B. Beulen, N. Bijnens, M. Rutten, P. Brands, and F. Vosse, "Perpendicular ultrasound velocity measurement by 2D cross correlation of RF data. Part A:

validation in a straight tube," *Experiments in Fluids*, vol. 49, pp. 1177–1186, Apr. 2010.

[35] B. Beulen, A. C. Verkaik, N. Bijnens, M. Rutten, and F. Vosse, "Perpendicular ultrasound velocity measurement by 2D cross correlation of RF data. Part B: volume flow estimation in curved vessels," *Experiments in Fluids*, vol. 49, pp. 1219–1229, Apr. 2010.

[36] D. van der Linde, E. E. M. Konings, M. a. Slager, M. Witsenburg, W. a. Helbing, J. J. M. Takkenberg, and J. W. Roos-Hesselink, "Birth prevalence of congenital heart disease worldwide: a systematic review and meta-analysis.," *Journal of the American College of Cardiology*, vol. 58, pp. 2241–7, Nov. 2011.

[37] G. A. Forbus and G. S. Shirali, "Anomalies of the Ventricular Septum," in *Echocardiography in Pediatric and Congenital Heart Disease* (W. W. Lai, L. L. Mertens, M. S. Cohen, and T. Geva, eds.), ch. 12, p. 179, Chichester: Wiley-Blackwell, 2009.

Chapter 3

Shunt Flow Evaluation in Congenital Heart Disease Based on Two-Dimensional Speckle Tracking

Solveig Fadnes[1], Siri Ann Nyrnes[1,2], Hans Torp[1], and Lasse Løvstakken[1]
[1] MI Lab and Dept. of Circulation and Medical Imaging, NTNU, Norway
[2] Dept. of Pediatrics, St. Olav's University Hospital, Trondheim, Norway

High-frame-rate ultrasound speckle tracking was used for quantification of peak velocities in shunt flows resulting from septal defects in congenital heart disease. In a duplex acquisition scheme implemented on a research scanner, unfocused transmit beams and full parallel receive beamforming were used to achieve a frame rate of 107 frames/s for full field-of-view flow images with high accuracy, while also ensuring high quality focused B-mode tissue imaging. The setup was evaluated *in vivo* for neonates with atrial and ventricular septal defects.

The shunt position was automatically tracked in B-mode images and further used in blood speckle tracking to obtain calibrated shunt flow velocities throughout the cardiac cycle. Validation toward color flow imaging and pulsed wave Doppler with manual angle correction indicated that blood speckle tracking could provide accurate estimates of shunt flow velocities. The approach was less biased by clutter filtering compared with color flow imaging and was able to provide velocity estimates beyond the Nyquist range. Possible placements of sample volumes (and angle corrections) for conventional Doppler resulted in a peak shunt velocity variation of 0.49-0.56 m/s for the ventricular septal defect of patient 1 and 0.38-0.58 m/s for the atrial septal defect of patient 2. In comparison, the peak velocities found from speckle tracking were 0.77 and 0.33 m/s for patient 1 and patient 2, respectively.

Results indicated that complex intraventricular flow velocity patterns could be quantified using high-frame-rate speckle tracking of both blood and tissue movement. This could potentially help increase diagnostic accuracy and decrease inter-observer variability when measuring peak velocity in shunt flows.

3.1 Introduction

Atrial (ASDs) and ventricular (VSDs) septal defects are the two most common forms of congenital heart defects [1]. The natural history of small septal defects may be regression or spontaneous closure [2, 3], whereas more severe defects must be repaired by catheter closure or corrective surgery. The management of an ASD or VSD depends on the location, size, hemodynamic consequences, associated defects and the symptomatology of the patient. Generally, the clinical approach is to repair an isolated ASD or VSD when there is a large left-to-right shunt [4]. In pediatric cardiology today, 2-D echocardiography with color flow imaging (CFI) is used to detect and visualize septal defects. Continuous wave Doppler and pulsed wave (PW) Doppler are utilized to estimate the peak velocity and evaluate the shunt flow [5].

Color flow imaging, continuous wave and pulsed wave Doppler have been extensively validated and are used in a wide range of clinical settings, but the methods have fundamental limitations. The frequency shifts between the transmitted and received ultrasound waves are used to estimate the blood velocity components along the ultrasound beam axis. The velocity estimates are thus limited to one component of the velocity vector and dependent on the angle between the ultrasound beam and the blood flow direction, and the resulting color flow images can be difficult to interpret. In addition, CFI and PW Doppler are based on pulsed transmission of ultrasound waves, and the pulse repetition frequency limits the highest measurable velocities according to the Nyquist sampling theorem. Velocities above the Nyquist limit are commonly encountered and will give aliasing artifacts in the image where high velocities will not be displayed correctly. These fundamental limitations may lead to undetected defects and misdiagnosis [6].

To improve imaging and evaluation of shunt flows, other modalities have been suggested. Real-time 3-D echocardiography has yielded promising results in the visualization of septal defects [7, 8], but the blood flow estimation is still angle dependent. In transesophageal echocardiography, the probe is led down the patient's esophagus, and cardiac images of higher quality are achieved. Also, cardiac magnetic resonance imaging is a useful modality, not limited by the acoustic window, but the need for general anesthesia or sedation in these methods limits their use in pediatric cardiology [9].

Several flow velocity estimators for estimating both the axial and lateral velocity components have been proposed. Speckle tracking [10] and vector Doppler [11] are the two main research lines for 2-D flow estimation, but recently new techniques as echo particle image velocimetry (PIV) [12,13] have been suggested. For the latter, the need of contrast agents makes it currently not suitable for pediatric imaging. The speckle tracking technique uses the speckle in the ultrasound image, which is a result of the constructive and destructive interference from the backscattered echoes, to estimate the velocity of the scatterers. The movement of the blood speckle is correlated with the movement of the blood, and the speckle can be tracked from frame to frame to obtain information on blood velocities. The vector Doppler technique combines the Doppler estimates from two transmit and/or receive angles to obtain angle-independent velocity measurements. Several studies have been performed to evaluate the speckle tracking

and vector Doppler techniques for numerically simulated flow patterns, *in vitro* flow phantoms and *in vivo* in human vessels [14–19]. However, neither speckle tracking nor vector Doppler has yet been established for clinical use in blood flow estimation. This can, in our experience, be attributed to a lack of robustness and limitations related to data acquisition and processing capabilities for real-time imaging.

Recent developments in ultrasound imaging technology provide a substantially higher acquisition rate which offers new possibilities in 2-D flow estimation. By transmitting broad unfocused ultrasound pulses, parallel receive beamforming can be used to increase the acquisition rate, resulting in instantaneous full field-of-view images at high frame rates. The technique has been suggested for elastography [20], compound Doppler imaging [21] and vector velocity imaging [22]. The high acquisition rate also makes it possible to have a higher ensemble size for improved clutter filtering possibilities and to achieve more robust velocity estimates without compromising a high frame rate, which is advantageous when imaging complex blood flow [23].

Quantitative vector velocity imaging has, to the author's knowledge, not previously been evaluated for use in pediatric cardiology. However, a qualitative method based on the direct visualization of blood speckle has been suggested, and was shown to increase the certainty in ASD shunt flow evaluation [24, 25]. In this work, we investigate 2-D speckle tracking for quantitative blood flow velocity estimation in ASDs and VSDs in newborns. The overall objective was to achieve angle-independent peak shunt flow velocity estimates for better shunt evaluation. To find the true peak velocity throughout the cardiac cycle, we further propose the use of tissue speckle tracking to follow the shunt position in the 2-D image plane throughout the cardiac cycle.

3.2 Methods

Two patients from the ongoing feasibility study are the subjects in this study. Patient 1, a boy, was 8 days old and 3340 g at the time of the ultrasound recordings. He had a perimembranous VSD, which was focused on in this study. He was also born with a secundum ASD, a pulmonary artery sling (the left pulmonary artery anomalously originating from the right pulmonary artery) and an anal atresia. Patient 2, a girl, was born prematurely at 31+4 weeks and diagnosed with a secundum ASD. She was 25 days old and 2165 g when included and had no additional congenital malformations. Written informed consent was obtained from the parents of the participants before the examination. The study was approved by the Norwegian Regional Committee for Medical and Health Research Ethics, and patient safety measurements were within the guidelines from the U.S. Food and Drug Administration.

3.2.1 *In vivo* and *in vitro* setup

We used a SonixMDP ultrasound scanner (Ultrasonix, Richmond, BC, Canada) with a 4- to 9- MHz linear transducer and a Sonix DAQ for channel data acquisition for *in vivo* and *in vitro* recordings. In the duplex acquisition scheme implemented, separate acquisition setups were used for B-mode and flow imaging to ensure sufficient image

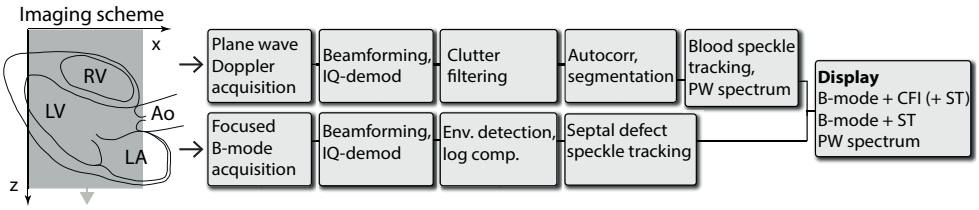

Figure 3.1: Schematic overview of data acquisition and post-processing setup. The channel data are acquired, and beamforming is done off-line. The plane wave data are clutter filtered before blood velocity estimation is done using the autocorrelation approach and speckle tracking. The B-mode images are used for septal defect speckle tracking. On the left is a parasternal long-axis view of a heart where the left atrium (LA), left ventricle (LV), right ventricle (RV) and outflow tract to the aorta (Ao) are visible. One plane transmit beam is covering the region of interest. CFi = color flow imaging, ST = speckle tracking, PW = pulsed wave.

quality for both modalities. Fig. 3.1 is a schematic of data acquisition and post-processing used in this work, where the top and bottom line represent acquisition and processing of blood flow images and B-mode images, respectively.

Unfocused transmit beams transmitted at a pulse repetition frequency (PRF) of 8 kHz were used for the flow imaging with an ensemble size of 32. The transmit beams covered a region equal to the transducer width, and full parallel receive beamforming was used, achieving a frame rate of 107 frames/s (fps) when interleaved with the separate B-mode scan sequence. Channel radiofrequency (RF) data (128 channels) were stored for up to 2 s (limited by 16 GB of channel data memory), and beamforming and processing were done off-line. The data were beamformed using a hamming apodization window over the active receive aperture to reduce side lobes. A high-pass clutter filter was applied to separate the blood signal from the strong tissue signal, before blood velocity estimation. Conventional Doppler and 2-D speckle tracking estimation of the blood velocity were done after clutter filtering. The color flow power and velocity estimates and the intensity in the B-mode images were used for segmentation of areas containing blood. Threshold values were set empirically for the given data sets.

The B-mode scan sequence was interleaved the flow acquisition, and two interleave groups of 64 focused pulses were used to cover the whole transducer width, resulting in a B-mode frame rate of 54 fps. A PRF of 12 kHz was used for the B-mode images. Additional imaging parameters for the duplex acquisition are given in Table 1.

An in vitro flow phantom was used to validate and investigate the accuracy of the speckle tracking blood flow estimation algorithm. The setup consisted of a pump (PhysioPulse 100 Flow System, Shelley Medical Imaging Technologies, London, ON, Canada) connected to a straight-tube flow phantom (ATS Laboratories, Bridgeport, CT, USA) with a blood-mimicking fluid [26]. The tube had a diameter of 6 mm, and a stationary flow scenario with a beam-to-flow angle of 60 degrees and a maximum

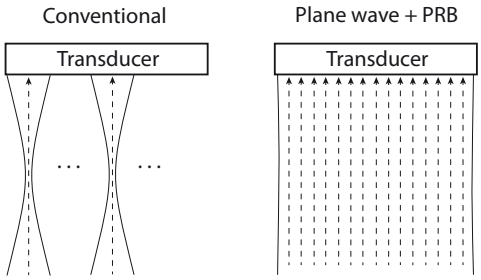

Figure 3.2: Comparison of conventional ultrasound acquisition scheme with parallel receive beamforming (PRB). Left: In the conventional set up, one focused transmit line and one focused receive line are acquired at a time. Right: A broad unfocused wave is transmitted and multiple image lines are received simultaneously.

velocity of approximately 1 m/s was investigated. We used the same acquisition and processing setup used for the *in vivo* recordings. The reference velocities used for comparison were calculated under the assumption of a fully developed laminar flow and based on the tube diameter and the programmed volume flow rate.

3.2.2 Data acquisition

In conventional ultrasound imaging, the image is built line by line. One focused pulse is transmitted at the time, and the received echoes form one line in the image as illustrated to the left in Fig. 3.2. Recent development in ultrasound technology allows for multiple image lines to be generated in parallel [22]. The approach may to some extent be used for focused transmit pulses, but to cover a wide imaging region, unfocused or diverging beams must be emitted.

Today's research scanners can store and process the RF data from all the channels in the transducer. When the channel data are available, any number of receive lines can be beamformed simultaneously in software, and a full image may result from the transmission of just one full field plane wave, as illustrated to the right in Fig. 3.2. The ultrahigh acquisition rate obtained by plane wave imaging and parallel receive beamforming makes it possible to have a wide region of interest, with dense lateral image sampling at high frame rates. The highly dynamic and complex blood flow in the heart makes high frame rates crucial and plane wave imaging favorable for blood flow imaging. There is, however, a loss in penetration with plane wave imaging, compared with focused imaging, and also a decrease in image contrast and lateral resolution. The latter is particularly visible in B-mode imaging, but is, in our experience, less deteriorating and often negligible for blood flow imaging, where the dynamic range is significantly lower; that is, the elevated side lobe level is often below the noise floor, and the parametric image display typically uses a low dynamic range.

3.2.3 Conventional color flow imaging and processing

In CFI, the estimated axial blood velocity is displayed as a 2-D color map, where the colors correspond to the blood velocity component along the beam axis. The image region is scanned line by line, where a series of ultrasound pulses are emitted in each beam direction at a given PRF. The movement of the blood scatterers indicates a shift in the received signal from pulse to pulse. The part of the received signal coming from the stationary tissue is called the clutter signal, whereas the signal originating from the moving blood scatterers is called the Doppler signal. The Doppler signal is separated from the clutter signal using a high-pass filter, for example, a polynomial regression, FIR or IIR filter [10]. The number of emitted pulses in each beam direction used to generate one image line is referred to as the ensemble size. The blood velocity estimation is typically based on the autocorrelation method (ACM), where the mean velocity is estimated from the correlation of the Doppler signal from pulse to pulse (lag 1), $\hat{R(1)}$ [27],

$$\hat{v}_{\text{axial}} = \frac{c \times \text{PRF}}{4\pi f_0} \angle \hat{R}(1), \tag{3.1}$$

where c is the speed of sound and f_0 is the center frequency of the transmitted pulse. The autocorrelation function is calculated as follows,

$$\hat{R}(1) = \frac{1}{N_p} \sum_{0}^{Np-1} x(k)^* x(k+1), \tag{3.2}$$

where $x(k)$ is a fixed spatial position, * denotes the complex conjugate and N_p is the ensemble size. The autocorrelation function is also spatially averaged to decrease estimator variance. In this work, a polynomial regression filter of order 2 was chosen as the clutter filter for the autocorrelation estimation, with a -3 dB cutoff at 0.05 m/s.

3.2.4 Blood flow estimation using speckle tracking

Speckle is an interference pattern in the back-scattered signal from many subresolution scatterers, for example, the red blood cells. The movement of the speckle pattern is correlated with the movement of the scatterer ensemble, and the 2-D blood velocities can thus be estimated by tracking the movement of the blood speckle pattern from frame to frame using pattern matching techniques [10]. The speckle tracking principle is illustrated in Fig. 3.3. A kernel region is defined in a first image acquisition and the best pattern match of the kernel is searched for in a following image, determining the displacement of the kernel.

Different pattern matching algorithm can be used, for example, 2-D normalized cross-correlation, sum-of-absolute-differences and sum-of-squared-differences. When the most likely displacement is found, the velocity can be estimated given the time between the two acquisitions. After this process is repeated for the whole imaging area, a vector velocity map of the blood flow is obtained.

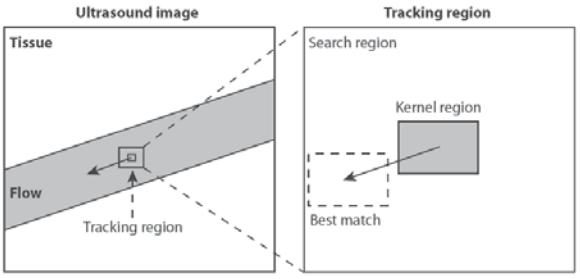

Figure 3.3: Speckle tracking principle. A kernel is defined in the first acquisition, and the best match of this kernel is searched for in the next acquisition.

In this work, pattern matching was done using the sum-of-squared-differences (SSD) algorithm,

$$d(\alpha,\beta) = \sum_{x,y} \left(I(x+\alpha, y+\beta) - K(x,y)\right)^2, \tag{3.3}$$

where I is the image displaced (α,β) from the original kernel position, and K is the original kernel. The minimum SSD-coefficient, $d(\alpha_{min},\beta_{min})$, reveals the most likely displacement of the kernel. The minimum measurable velocity is limited by the sampling resolution in the data, which can be quite crude. Linear interpolation of the IQ data and parabolic subsample interpolation of the estimated displacement were used to improve the velocity resolution. If $f_1 = d(\alpha_{min},\beta_{min})$ and f_0 and f_2 are the two nearest neighbors, the subsample offset correction for the estimated displacement is given by [28]

$$\hat{\delta} = \frac{f_0 - f_2}{2(f_0 - 2f_1 + f_2)}. \tag{3.4}$$

The maximum measurable velocity is determined by the size of the search region. The velocity estimates were subjected to median averaged over the temporal ensemble of 32 to minimize the effect of spurious tracking errors. The acquisition rate of 8 kHz made averaging over a large packet of 32 pulses possible while still achieve a high flow frame rate. Additional temporal averaging over five flow frames was done in a non-causal way according to the weights [0.1 0.2 0.4 0.2 0.1] to smooth the flow patterns throughout the cardiac cycle. The velocity estimates were also spatially averaged in a region of 2×2 mm to reduce the variance of the estimates.

A time-invariant clutter filter is preferable for speckle tracking methods to ensure that every speckle image is filtered equally. This is important in order to maximize temporal and spatial correlation. In this work, a fourth-order FIR filter with a -3 dB cut-off at $0.33 \times V_{\text{Nyquist}} = 0.2$ m/s was used.

The accuracy of the speckle tracking velocity estimation was investigated for stationary flow in an *in vitro* flow phantom. After one recording of 130 flow frames, the velocity estimates were averaged as described above, where N=26 independent

realizations were used to estimate the expected value and standard deviation of the method *in vitro*.

To validate the velocity estimates in the *in vivo* cases, PW spectra were made retrospectively from the same recording used for speckle tracking and autocorrelation estimation. The Doppler ensemble lengths of 32 are sufficient to make conventional PW spectrum for the intended use of validation in this work. A PW spectrum could thus be made from any given point in the image and was estimated using the discrete Fourier transform

$$\hat{P}(\omega) = \frac{1}{RB} \sum_{r=0}^{R-1} \sum_{b=0}^{B-1} \left| \sum_{n=0}^{N_p-1} w(n) x_{r,b}(n) e^{-i\omega n} \right|^2 , \tag{3.5}$$

where $x_{r,b}(n)$ is the IQ signal from a range, beam position for a given ensemble sample n, $w(n)$ is a smooth window function, R is the number of range samples, B is the number of receive beams and N_p is the ensemble length. In this work, a Hamming window was used and the averaging region was 1 mm in the axial direction and 0.5 mm in the lateral direction.

3.2.5 Semi-automatic tracking of septal defect using speckle tracking

The objective of this work was to estimate shunt flow velocities. During the contraction and relaxation of the myocardium, the shunt is shifted in the ultrasound image plane, and the shunt size may also vary. To keep track of the velocities in the shunt flow, it is therefore important to track the septal defect position during the cardiac cycle. The same speckle tracking algorithm was used for tissue tracking by utilizing a larger kernel region and assuming a maximum tissue velocity of 5-10 cm/s. The kernel size was 1.1 mm in the lateral direction and 1.3 mm in the axial direction. An area of 45 overlapping kernel regions were defined around the start and end points of the septal defect in the image, as indicated with two squares in Fig. 3.4. The median of all the displacement vectors in each of the squares defined the start or end point of the defect in the next frame.

The septal defect position was manually marked in two different frames, corresponding to end-systole and end-diastole. These known positions were used as attractors to assure robust tracking results throughout the cardiac cycle. The new position of the septal defect found from speckle tracking was for each frame corrected using the predefined positions $(x, z)_{\text{systole}}$ and $(x, z)_{\text{diastole}}$ as follows,

$$\Delta x_{\text{attractor}}(t) = (x(t) - x_{\text{s}})k_s(t) + (x(t) - x_{\text{d}})k_d(t) \tag{3.6}$$

$$x_{\text{corrected}}(t) = x(t) - \Delta x_{\text{attractor}}(t), \tag{3.7}$$

where $x(t)$ and $x_{\text{corrected}}(t)$ are the shunt positions before and after the correction. The attraction parameters $k_s(t)$ and $k_d(t)$ have values between 0 and 1, as illustrated in Fig. 3.5, and describe the attraction strength as a function of time. At end-systole

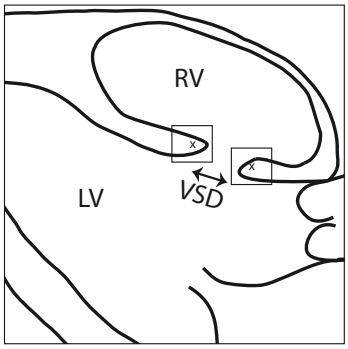

Figure 3.4: Tissue speckle tracking of a ventricular septal defect (VSD) in the septum between the left (LV) and right (RV) ventricles. The defect is marked in the first acquisition. Many overlapping large kernels are defined around the marked beginning and end of the defect in the image (inside the *squares* indicated).

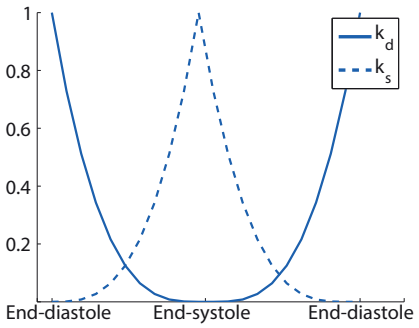

Figure 3.5: Shunt tracking attractor parameters, k_s and k_d, as a function of time. The parameters define the attraction strength.

and end-diastole, k_s and k_d are equal to 1, respectively, and the shunt positions are thus equal to the predefined positions for these frames.

The shunt tissue tracking approach was validated by visual inspection of the example data used in this work. Based on the tissue tracking of the shunt position, it was possible to have a PW Doppler sample volume automatically moving with the maximum velocity in the shunt for all frames in the cardiac cycle. This differs from conventional PW Doppler, where a fixed sample volume is manually placed where the seemingly highest axial shunt velocities are present according to the color flow images.

Table 3.1: Image acquisition parameters

Probe	UX L9-4/38	
Probe type	128 element linear array	
	Flow	B-mode
Pulse center frequency [MHz]	5	6.67
Transmit aperture [cm]	3.89	1.5
Transmit F-number	-	2
Receive F-number	1.1	1.1
Pulse repetition frequency [Hz]	8000	12000
Ensemble size	32	-
Frame rate [Hz]	107	54

3.3 Results

3.3.1 Speckle tracking of blood flow

To the left in Fig. 3.6 is a color flow image of stationary flow in an *in vitro* tube phantom, with the speckle tracking estimates overlaid as arrows. Speckle tracking and angle-corrected autocorrelation velocity estimates from the region marked by dashed lines at 25 mm depth were used to estimate velocity profiles and standard deviations for N=26 independent realizations. To the right in Fig. 3.6, the velocity profiles are compared with the expected parabolic profile for a fully developed laminar flow.

For a 1 mm×1 mm area in the middle of the tube, the mean axial velocity was 0.50 ± 0.02 m/s for the autocorrelation method and 0.51 ± 0.01 m/s for speckle tracking. The mean lateral velocity was 0.88 ± 0.03 m/s for speckle tracking. The resulting absolute velocity was 0.99 ± 0.04 m/s for the angle-corrected ACM and 1.02 ± 0.02 m/s for speckle tracking. The reference velocity in the same region was 0.98 m/s.

To the left in Fig. 3.7 is a color flow image of blood flow in the heart of patient 1, a newborn with a VSD. The image is acquired from a parasternal long-axis view, in which the left atrium, the left ventricle and the right ventricle were visible. The septum between the ventricles is distinct, and the shunt flow is clearly visible in the image (marked by the white dashed line). The color flow image contains only the 1-D velocity information along the beam direction, underlined here by the superimposed arrows. To the right in the figure is the same image frame, with the colors representing the absolute velocities found from speckle tracking instead of the autocorrelation estimates. The direction of the speckle tracking estimates is indicated by arrows.

As can be observed, the shunt flow is differently highlighted in the image when the absolute velocities are displayed. The highest absolute velocities are found in the shunt region, but because of a large lateral component that is not measured with CFI, this is not directly seen in the color flow image. In addition, the direction of the flow is not easily interpreted from the color flow image, which consequently makes it difficult to correctly angle-correct the autocorrelation estimates. The speckle tracking estimates directly give the information about directions and absolute velocities of the blood flow in the image plane. In addition, it was observed that the speckle tracking method

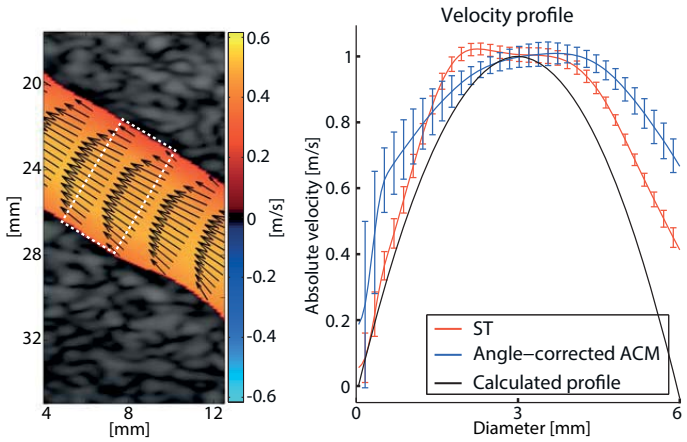

Figure 3.6: Stationary flow in an *in vitro* straight-tube phantom with a beam-to-flow angle of 60 degrees. Left: Color flow image with speckle tracking estimates overlaid as arrows. Right: Mean speckle tracking and angle-corrected autocorrelation method (ACM) velocity profiles with standard deviations from 26 measurements compared with the calculated reference velocity profile. The velocity profiles are estimated from the area indicated by the dashed lines.

tracked beyond the Nyquist limit in areas where aliasing artifacts were present in the color flow image.

In Fig. 3.8 are color flow and speckle tracking velocity images of patient 2 with an ASD. These images were acquired from a subcostal oblique long-axis view in which all four chambers are visible. The defect is in the septum between the atria in the lower part of the images. In the color flow image, uniform color distribution in the shunt area is seen. This could be mistaken for color blooming into the tissue for cases where the septal defect is not clearly visible in the B-mode image. The 2-D velocity information from speckle tracking to the right in this figure indicates the flow from the left to the right atrium.

3.3.2 Speckle tracking of septal defect

Fig. 3.9 provides examples of tissue tracking results of the VSD in patient 1 for three different frames corresponding to early diastole, late diastole and mid-systole. The frame times are 0.07, 0.18 and 0.31 s where 0.39 s is a full cycle. The starting and ending positions of the septal defect in the images were found for all B-mode frames and the maximum displacement in the image plane was 3-5 mm. The speckle tracking algorithm gave robust tracking results when the movement was in the image plane, and the end-systole and end-diastole attractors helped assure robust results even with out-of-plane-movement.

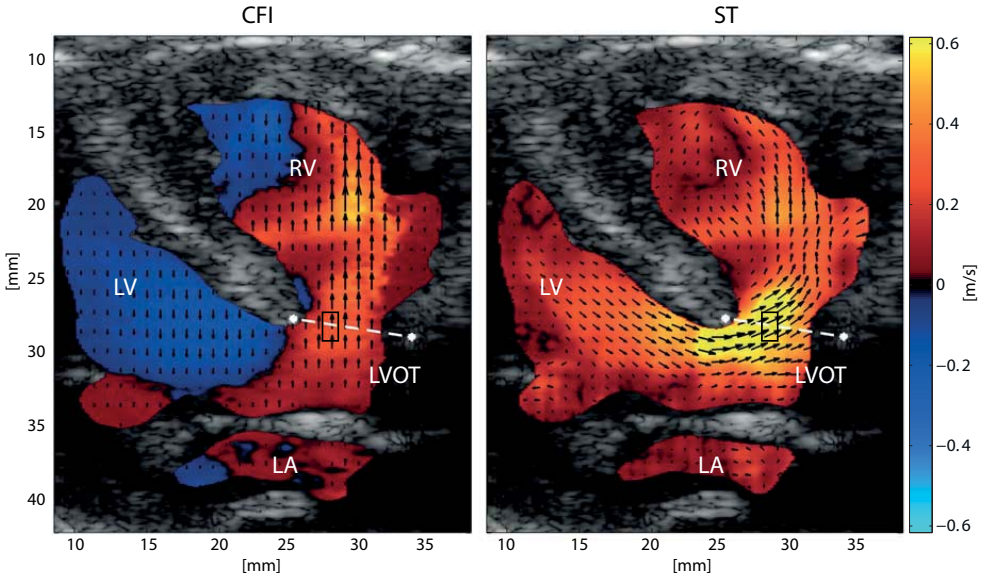

Figure 3.7: Color flow and speckle tracking images of patient 1 (8 days, 3340 g) indicating a ventricular septal defect from a parasternal long-axis view. The septal defect is approximately 6 mm wide in this view, and the left-to-right shunt flow is marked with a white dashed line. The sample volume for the retrospective pulsed wave spectrum in Fig. 3.10 is indicated in the shunt region. The superimposed arrows in the color flow image to the left underline the 1-D velocity information acquired from the autocorrelation estimates. The colors in the image to the right represent the absolute velocity found from speckle tracking. The arrows represent the direction and magnitude of the speckle tracking estimates. LV = left ventricle, RV = right ventricle, LA = left atrium, LVOT = left ventricular outflow tract.

3.3.3 Shunt flow evaluation

Both speckle tracking and autocorrelation velocity estimates were validated with retrospective PW Doppler. The velocity estimates were compared with those of conventional PW Doppler and PW Doppler from a moving sample volume based on shunt tracking. For the conventional PW Doppler, a fixed sample volume was placed manually by a pediatric cardiologist. In Fig. 3.10, the PW spectrum of the VSD is shown with and without a moving sample volume together with the velocity estimates from color flow and speckle tracking. When the sample volume is not moving with the septal defect in the image plane (right panel), potentially important shunt flow information is missed for parts of the cycle. In this example, the shunt is bidirectional, and the reversed flow from the right to the left ventricle is missed when the sample volume is fixed, as indicated by the yellow circle on the right in Fig. 3.10. The axial velocity estimates from speckle tracking agreed well with the PW spectrum and

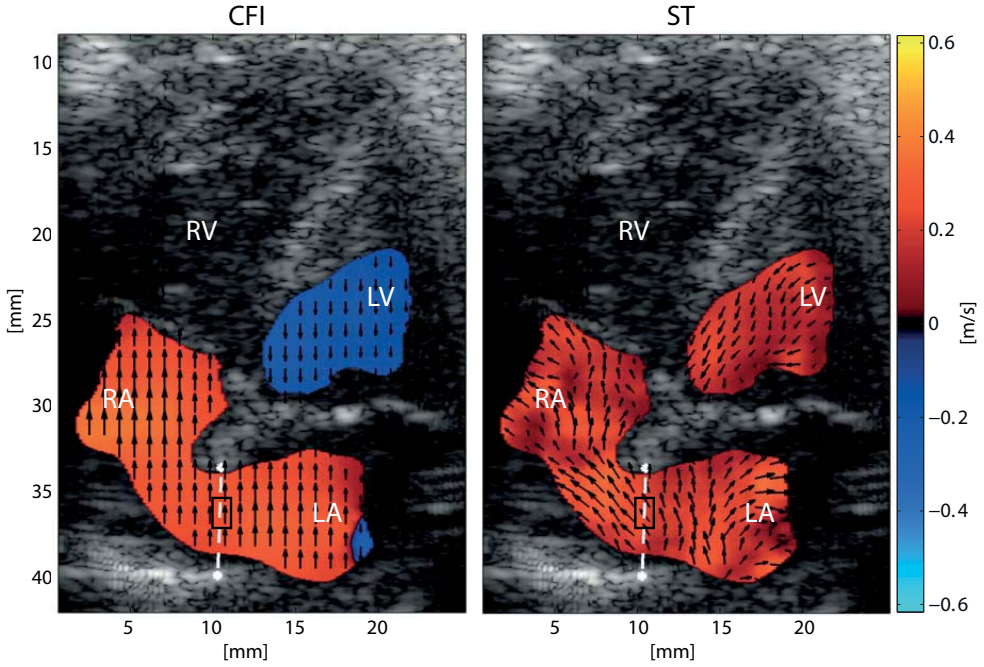

Figure 3.8: Color flow and speckle tracking images of patient 2 (premature, 2165 g) indicating an atrial septal defect from a subcostal oblique long-axis view. The septal defect is approximately 5 mm wide in this view, and the left-to-right shunt flow is marked with a white dashed line. The sample volume for the retrospective pulsed wave spectrum in Fig. 3.11 is indicated in the shunt region. The superimposed arrows in the color flow image to the left underline the 1-D velocity information acquired from the autocorrelation estimates. The colors in the image to the right represent the absolute velocities found from speckle tracking. The arrows represent the direction and magnitude of the speckle tracking estimates. LV = left ventricle, RV = right ventricle, LA = left atrium, RA = right atrium.

autocorrelation estimates.

In Fig. 3.11 is the PW spectrum of the ASD in patient 2 together with the speckle tracking and autocorrelation velocity estimates. The velocities in the ASD are lower than the velocities in the VSD and the beam-to-flow angle is high, resulting in axial velocities around the cut-off velocity of the FIR filter of 0.2 m/s. To the right in Fig. 3.11 the FIR filter was used for the autocorrelation estimates as well to compare the filter effect on the two estimators. The autocorrelation method overestimates the velocities in the filter transition region. A much better result is therefore obtained with the polynomial regression filter with a 0.05 m/s cut-off as seen to the left in Fig. 3.11. With this filter, the autocorrelation and speckle tracking estimates correspond better.

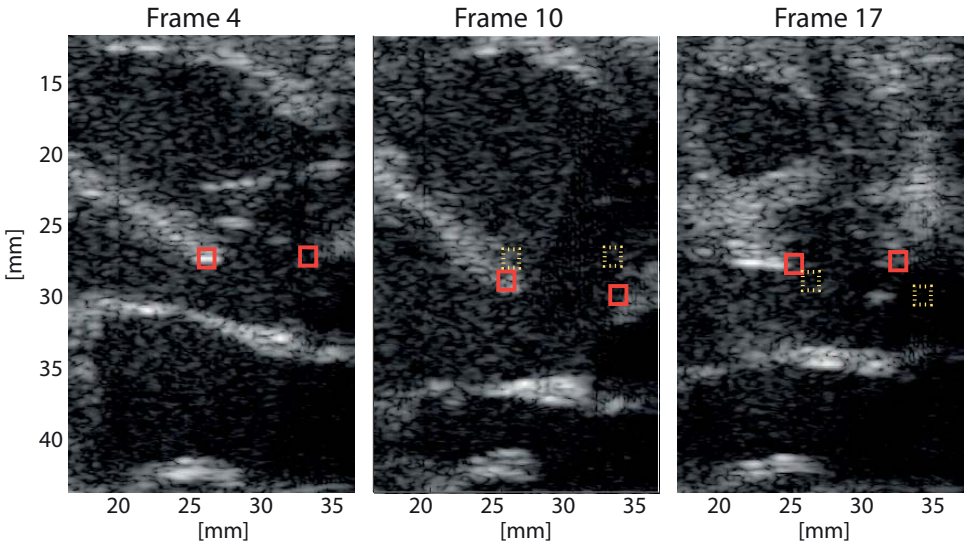

Figure 3.9: Three different time frames showing tissue tracking results of the ventricular septal defect in patient 1. The yellow dotted squares represent the defect's position at the previous displayed frame. Dynamic range is 50 dB.

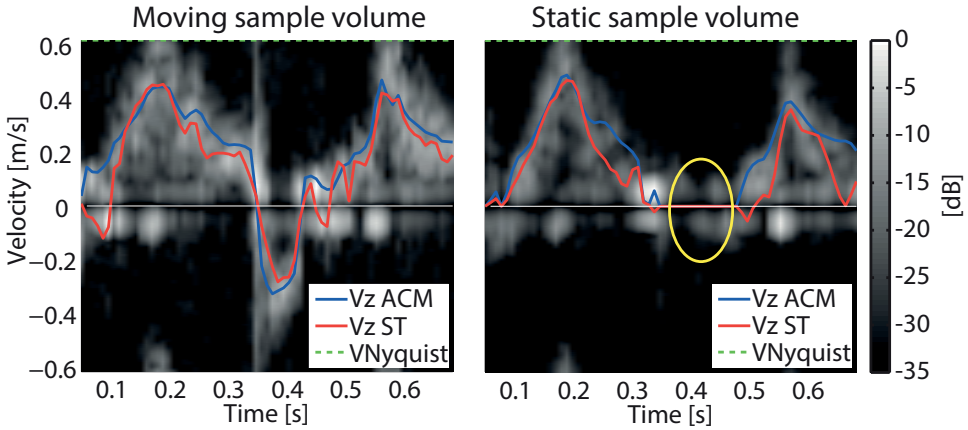

Figure 3.10: Retrospective pulsed wave spectrum from the shunt region in patient 1. The spectrum is shown together with the speckle tracking (ST) and autocorrelation method (ACM) velocity estimates from the same sample volume. Left: The sample volume is automatically placed at the location of the highest velocity in the shunt for all frames. Right: A static sample volume is manually placed in the shunt region.

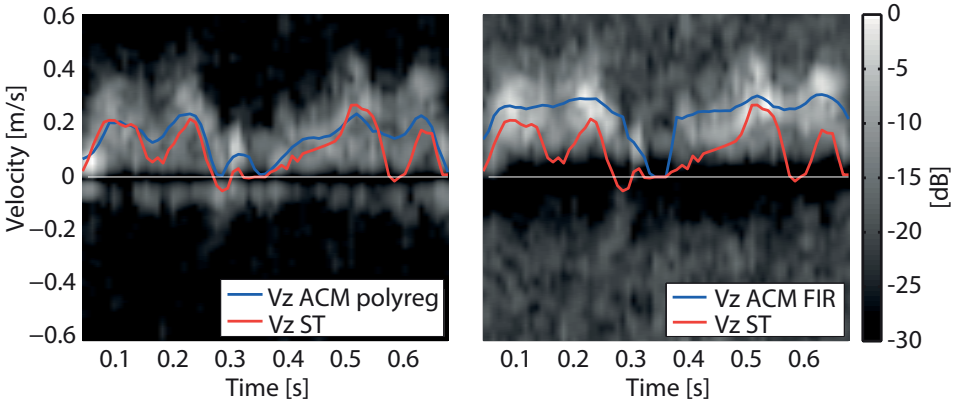

Figure 3.11: Retrospective pulsed wave spectrum from the shunt region in patient 2. The spectrum is shown together with the speckle tracking (ST) and autocorrelation method (ACM) estimates. Right: The FIR filter is used for both the Doppler and the speckle tracking estimates.

To the left in Fig. 3.12, the angle-corrected autocorrelation estimates from the moving sample volume in patient 1 are compared with the absolute velocities from speckle tracking for all frames. The angle correction factor was estimated for each frame based on the flow direction estimates from speckle tracking. The maximum left-to-right shunt velocity measured in this view was 0.77 m/s. The VSD was bidirectional and the maximum right-to-left shunt velocity measured was approximately 0.3 m/s. The gray region indicates the variation in manually angle-corrected autocorrelation estimates from different fixed sample volume positions. The peak velocity found manually varied from 0.49-0.56 m/s, an underestimation compared to the peak velocity found from speckle tracking.

To the right in Fig. 3.12 are the absolute velocities in the shunt for patient 2. The manually found absolute velocities from the autocorrelation method were in general higher than the absolute velocities found from speckle tracking. The peak velocity found manually varied from 0.38 to 0.58 m/s, compared with the speckle tracking peak velocity of 0.33 m/s.

The speckle tracking velocity profiles from the shunt region in the VSD and ASD are illustrated in Fig. 3.13. The red profiles in the VSD are from frames where the flow has been reversed and is going from the right ventricle into the left ventricle. In the VSD, the flow profile develops from a relatively flat to a more complex profile with skewed peak velocities as the velocity in the shunt increases. The velocity profiles are more plug-shaped throughout the cycle for the ASD, as seen to the right in Fig. 3.13.

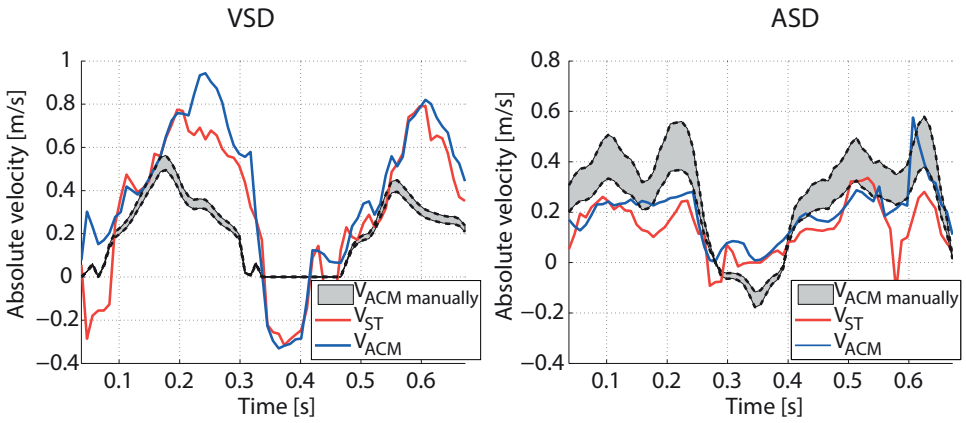

Figure 3.12: Comparison of absolute velocities from speckle tracking (V_{ST}) with angle-corrected autocorrelation estimates (V_{ACM}) from the moving sample volume in the ventricular septal defect in patient 1 and atrial septal defect in patient 2. The speckle tracking estimates were used to angle-correct the autocorrelation estimates. The variation in the absolute velocity estimation using manual angle-correction and a fixed sample volume is also indicated.

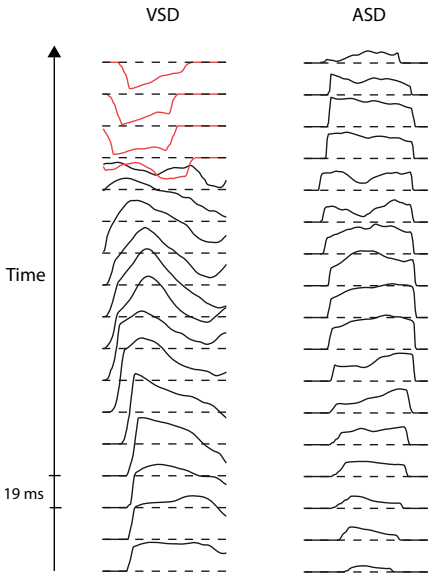

Figure 3.13: Estimated velocity profiles over the shunt region indicated by the white lines in Fig. 3.7 and 3.8 for one cardiac cycle. VSD = ventricular septal defect, ASD = atrial septal defect.

3.4 Discussion

In this work, our aim was to investigate if 2-D speckle tracking of blood velocities could be used to provide angle-independent velocity measurements in the context of shunt flow evaluation in congenital heart disease. In current clinical routine, peak velocity is one of the important measures in shunt evaluation. However, when peak velocity is measured with PW Doppler, a manual angle-correction is needed, leading to a potentially inaccurate measurement, especially for high beam-to-flow angles [29]. Further, several measurements from different image views may be needed to ensure that the peak velocity is found. With our acquisition scheme, high-frame-rate flow images are acquired where color flow imaging, blood flow speckle tracking and PW Doppler estimation can be done from the same data set. In addition, tissue speckle tracking based on B-mode images was used to provide the shunt position throughout the cardiac cycle to ensure that the true peak velocity was found in the imaging plane.

An *in vitro* flow phantom was used to test the acquisition setup and speckle tracking algorithm. The speckle tracking velocity estimates for the N=26 independent measurements had a low standard deviation (1-3 cm/s) and were in good agreement with the reference velocities as seen in Fig. 3.6. The increased deviation at the edges of the tube can be attributed to the limited spatial resolution of the imaging system, as well as to the clutter filter for low velocities.

The *in vivo* results indicate that speckle tracking may indeed provide angle-independent flow velocity estimates in ASD and VSD shunts throughout the cardiac cycle. The manual angle-correction in the Doppler-based methods may infer a variation in peak velocity estimate especially for large beam-to-flow angles as seen for the ASD in Fig. 3.12. For the VSD in Fig. 3.12, the timing of the peak velocity estimate was also observed to differ, where the absolute peak velocity occurred later in the cycle than that from the manual angle-corrected peak axial velocity. For the speckle tracking estimates, no angle-correction is needed, and improved measurements of peak velocities may therefore be acquired. The speckle tracking angle estimates can also be used to automatically angle-correct the PW Doppler estimates in more complex flow situations where the beam-to-flow angle is difficult to determine manually. Also, for cases where the beam-to-flow angle exceeds the recommended limit for angle-correction (60 degrees [29]), the angle-independent speckle tracking estimate still provides an estimate of the absolute velocity.

The 2-D velocity vector maps provide new information on the potentially complex flow patterns and dynamics that may occur in congenital heart disease. Vortex formation in the right ventricle caused by VSD shunt flow is, for example, visualized with the 2-D velocity vector maps. In color flow images, where only the axial velocity component is displayed, small defects can be missed as the shunt flow could be mistaken as color blooming into the tissue [6]. Further, the shunt position tracking made it possible to generate spatial velocity profiles from the shunt throughout the cardiac cycle and to automatically find the peak velocity in the shunt, for all frames. These flow profiles can provide new information on the shunt flow in general; for instance, it could be observed that the peak velocity was not necessarily found in the middle of the shunt in our data. The automatic shunt position tracking also provided an estimate

of the diameter of the shunt, which is typically also documented during the clinical evaluation.

The speckle tracking estimates were validated toward PW Doppler and autocorrelation estimates in this work. The axial velocities match the PW spectra well in Fig. 3.10 and 3.11. Other sample volumes were tested and gave similar results. Based on the current data, a statistical comparison between the axial velocity estimations from speckle tracking and autocorrelation cannot be made. The comparison was performed only as an initial validation of the axial speckle tracking. A general comparison of accuracy and robustness of the two methods needs a separate study. The absolute velocity profiles for the speckle tracking and angle-corrected autocorrelation estimates in Fig. 3.12 are reasonable and indicate that the tracking works in both the axial and lateral direction.

For near-transversal flow both the autocorrelation and speckle tracking estimates will suffer from clutter filter issues. In areas with a high beam-to-flow angle, the blood signal as well as the clutter signal will be attenuated by the clutter filter, and the image will suffer from signal dropouts. In addition, the autocorrelation estimates will be overestimated in the filter transition region, as seen to the right in Fig. 3.11, where the autocorrelation estimates were filtered using the same FIR filter as for the speckle tracking estimates. It was observed that the speckle tracking provided more consistent estimates well below the filter cutoff velocity. The speckle tracking approach is also capable of providing velocity estimates beyond the Nyquist range and, thus, exhibits a wider range of measurable velocity compared with the autocorrelation technique. If no aliasing artifacts or clutter filter issues are present, the axial velocity estimates from the autocorrelation method are, however, quite robust. In low signal-to-noise conditions, the speckle tracking and autocorrelation estimates could therefore be combined to further improve the robustness of the velocity estimates [16].

The limitation of speckle tracking is mainly speckle decorrelation leading to inaccurate tracking results. The speckle pattern decorrelate rapidly because of spatial and temporal velocity gradients, non-laminar flow and out-of-plane movement [30]. With ultrahigh frame rates equal to the PRF, where instantaneous images over a full field-of-view are acquired, the speckle decorrelation from frame to frame is reduced compared with what can be achieved based on a conventional imaging scheme. Out-of-plane movements were observed, but did not seem to influence the in-plane velocity estimates in our data. The ultrahigh frame rates are achieved with single plane wave emissions, and a loss in contrast and lateral resolution and a low signal-to-noise ratio is thus potentially a problem in our setup for flow imaging. Transducer surface heating constraints limited our transmission voltage and sequence (e.g., coded excitation was no applicable). However, newborns often have good acoustic windows for cardiac imaging (you can often image through their ribs) and fairly good signal-to-noise ratios were achieved in the data examples in this work. The loss of contrast and lateral resolution was minimized by apodization and dynamic focusing (F-number = 1.1) on receive, and for the blood speckle tracking results, the ultrahigh frame rate achieved was probably more important than the resolution reduction. A larger patient study, however, is needed to map the clinical feasibility of this approach.

The robustness of the tissue speckle tracking was dependent on a visual septum

during the cardiac cycle. Out-of-plane movement made the tracking more difficult. The frame rate of the B-mode images in our setup was sufficient to track the septal defect movement in our limited data material. However, to conclude on this matter, the method must be tested on a broader set of patients to evaluate robustness and usability.

A linear probe was used in this work, because it can easily use plane transmit waves and parallel receive beamforming, and the depth and field of view needed for cardiac imaging in newborns were achievable. Further work should include an evaluation of high-frame-rate speckle tracking using phased arrays as these probes are conventionally used in pediatric imaging. An imaging scheme in which diverging transmit beams are used together with parallel receive beamforming must then be implemented to achieve similar high-frame-rate flow images. Further work will also evaluate the potential clinical impact of the method for a larger patient population. In addition, methods for volume flow measurements will be included and potential solutions to the clutter filter issues will be investigated.

3.5 Conclusions

High-frame-rate speckle tracking based on plane wave imaging may improve the measurement of peak velocities for the evaluation of shunt flow in atrial and ventricular septal defects in newborns. The peak shunt velocity was more clearly visualized than in color flow imaging, and the need for manual angle correction was eliminated for quantitative measurements. Further, by adding spatial tracking of shunt position, the spatiotemporal peak velocity in the imaging plane could be found, which was shown to differ from that obtained based on Doppler estimates. The proposed technique may thus help increase diagnostic accuracy and decrease inter-observer variability.

References

[1] D. van der Linde, E. E. M. Konings, M. a. Slager, M. Witsenburg, W. a. Helbing, J. J. M. Takkenberg, and J. W. Roos-Hesselink, "Birth prevalence of congenital heart disease worldwide: a systematic review and meta-analysis.," *Journal of the American College of Cardiology*, vol. 58, pp. 2241–7, Nov. 2011.

[2] A. Hanslik, U. Pospisil, U. Salzer-Muhar, S. Greber-Platzer, and C. Male, "Predictors of spontaneous closure of isolated secundum atrial septal defect in children: a longitudinal study.," *Pediatrics*, vol. 118, pp. 1560–5, Oct. 2006.

[3] D. J. Penny and G. W. Vick, "Ventricular septal defect.," *Lancet*, vol. 377, pp. 1103–12, Mar. 2011.

[4] D. Driscoll, H. D. Allen, D. L. Atkins, J. Brenner, a. Dunnigan, W. Franklin, H. P. Gutgesell, P. Herndon, R. E. Shaddy, and K. a. Taubert, "Guidelines for evaluation and management of common congenital cardiac problems in infants, children, and adolescents. A statement for healthcare professionals from the Committee on Congenital Cardiac Defects of the Council on Cardiovascular Disease in the," *Circulation*, vol. 90, pp. 2180–2188, Oct. 1994.

[5] G. A. Forbus and G. S. Shirali, "Anomalies of the Ventricular Septum," in *Echocardiography in Pediatric and Congenital Heart Disease* (W. W. Lai, L. L. Mertens, M. S. Cohen, and T. Geva, eds.), ch. 12, p. 179, Chichester: Wiley-Blackwell, 2009.

[6] O. J. Benavidez, K. Gauvreau, K. J. Jenkins, and T. Geva, "Diagnostic errors in pediatric echocardiography: development of taxonomy and identification of risk factors.," *Circulation*, vol. 117, pp. 2995–3001, June 2008.

[7] T. O. Cheng, M.-X. Xie, X.-F. Wang, Y. Wang, and Q. Lu, "Real-time 3-dimensional echocardiography in assessing atrial and ventricular septal defects: an echocardiographic-surgical correlative study.," *American heart journal*, vol. 148, pp. 1091–5, Dec. 2004.

[8] P. Acar, S. Abadir, S. Paranon, G. Latcu, J. Grosjean, and Y. Dulac, "Live 3D echocardiography with the pediatric matrix probe.," *Echocardiography (Mount Kisco, N.Y.)*, vol. 24, pp. 750–5, Aug. 2007.

[9] J. M. Oliver-Ruiz and M. Bret-Zurita, "Magnetic resonance imaging in the evaluation of congenital intracardiac shunts.," *Revista española de cardiología*, vol. 60, pp. 895–8, Sept. 2007.

[10] L. N. Bohs, B. J. Geiman, M. E. Anderson, S. C. Gebhart, and G. E. Trahey, "Speckle tracking for multi-dimensional flow estimation.," *Ultrasonics*, vol. 38, pp. 369–75, Mar. 2000.

[11] B. Dunmire, K. W. Beach, K. Labs, M. Plett, and D. E. Strandness, "Cross-beam vector Doppler ultrasound for angle-independent velocity measurements.," *Ultrasound in medicine & biology*, vol. 26, pp. 1213–35, Oct. 2000.

[12] H. Zheng, L. Liu, L. Williams, J. R. Hertzberg, C. Lanning, and R. Shandas, "Real time multicomponent echo particle image velocimetry technique for opaque flow imaging," *Applied Physics Letters*, vol. 88, p. 261915, 2006.

[13] C. Poelma, J. M. Mari, N. Foin, M. X. Tang, R. Krams, C. G. Caro, P. D. Weinberg, and J. Westerweel, "3D Flow reconstruction using ultrasound PIV," *Experiments in Fluids*, vol. 50, pp. 777–785, 2009.

[14] L. Bohs, B. Friemel, and G. Trahey, "Experimental velocity profiles and volumetric flow via two-dimensional speckle tracking," *Ultrasound in medicine & biology*, vol. 21, no. 7, 1995.

[15] L. Bohs and S. Gebhart, "2-D motion estimation using two parallel receive beams," *IEEE transactions on ultrasonics, ferroelectrics, and frequency control*, vol. 48, pp. 392–408, Mar. 2001.

[16] A. Swillens, P. Segers, and L. Lovstakken, "Two-dimensional flow imaging in the carotid bifurcation using a combined speckle tracking and phase-shift estimator: a study based on ultrasound simulations and in vivo analysis.," *Ultrasound in medicine & biology*, vol. 36, pp. 1722–35, Oct. 2010.

[17] R. Steel, K. V. Ramnarine, a. Criton, F. Davidson, P. L. Allan, N. Humphries, H. F. Routh, P. J. Fish, and P. R. Hoskins, "Angle-dependence and reproducibility of dual-beam vector doppler ultrasound in the common carotid arteries of normal volunteers.," *Ultrasound in medicine & biology*, vol. 30, pp. 271–6, Feb. 2004.

[18] A. Pastorelli, G. Torricelli, M. Scabia, E. Biagi, and L. Masotti, "A real-time 2-D vector Doppler system for clinical experimentation.," *IEEE transactions on medical imaging*, vol. 27, pp. 1515–24, Oct. 2008.

[19] P. Tortoli, A. Dallai, E. Boni, L. Francalanci, and S. Ricci, "An automatic angle tracking procedure for feasible vector Doppler blood velocity measurements.," *Ultrasound in medicine & biology*, vol. 36, pp. 488–96, Mar. 2010.

[20] M. Tanter, J. Bercoff, L. Sandrin, and M. Fink, "Ultrafast compound imaging for 2-D motion vector estimation: application to transient elastography.," *IEEE transactions on ultrasonics, ferroelectrics, and frequency control*, vol. 49, pp. 1363–74, Oct. 2002.

[21] J. Bercoff, G. Montaldo, T. Loupas, D. Savery, F. Mézière, M. Fink, and M. Tanter, "Ultrafast compound Doppler imaging: providing full blood flow characterization.," *IEEE transactions on ultrasonics, ferroelectrics, and frequency control*, vol. 58, pp. 134–47, Jan. 2011.

[22] J. Udesen, F. Gran, K. L. Hansen, J. A. Jensen, C. Thomsen, and M. B. Nielsen, "High frame-rate blood vector velocity imaging using plane waves: simulations and preliminary experiments.," *IEEE transactions on ultrasonics, ferroelectrics, and frequency control*, vol. 55, pp. 1729–43, Aug. 2008.

[23] I. K. Ekroll, A. Swillens, P. Segers, T. Dahl, H. Torp, and L. Lovstakken, "Simultaneous quantification of flow and tissue velocities based on multi-angle plane wave imaging.," *IEEE transactions on ultrasonics, ferroelectrics, and frequency control*, vol. 60, pp. 727–38, Apr. 2013.

[24] L. Lovstakken, S. Bjaerum, D. Martens, and H. Torp, "Blood flow imaging–A new real-time, 2-D flow imaging technique.," *IEEE transactions on ultrasonics, ferroelectrics, and frequency control*, vol. 53, pp. 289–99, Feb. 2006.

[25] S. A. Nyrnes, L. Lovstakken, H. Torp, and B. r. O. Haugen, "Blood flow imaging-a new angle-independent ultrasound modality for the visualization of flow in atrial septal defects in children.," *Echocardiography (Mount Kisco, N.Y.)*, vol. 24, pp. 975–81, Oct. 2007.

[26] K. V. Ramnarine, D. K. Nassiri, P. R. Hoskins, and J. Lubbers, "Validation of a new blood-mimicking fluid for use in Doppler flow test objects," *Ultrasound in Medicine and Biology*, vol. 24, no. 3, pp. 451–459, 1998.

[27] C. Kasai, K. Namekawa, A. Koyano, and R. Omoto, "Real-Time Two-Dimensional Blood Flow Imaging Using an Autocorrelation Technique," *IEEE Transactions on Sonics and Ultrasonics*, vol. 32, no. 3, pp. 458–464, 1985.

[28] I. Cespedes, Y. Huang, J. Ophir, and S. Spratt, "Methods for estimation of subsample time delays of digitized echo signals," *Ultrasonic imaging*, 1995.

[29] A. Thrush, "Spectral Doppler ultrasound," in *Diagnostic Ultrasound: Physics and Equipment* (P. R. Hoskins, K. Martin, and A. Thrush, eds.), ch. 9, pp. 105–120, Cambridge University Press, 2nd ed., 2010.

[30] B. H. Friemel, L. N. Bohs, K. R. Nightingale, and G. E. Trahey, "Speckle decorrelation due to two-dimensional flow gradients.," *IEEE transactions on ultrasonics, ferroelectrics, and frequency control*, vol. 45, pp. 317–27, Jan. 1998.

Chapter 4

Robust Angle-Independent Blood Velocity Estimation Based on Dual-Angle Plane Wave Imaging

Solveig Fadnes[1], Ingvild Kinn Ekroll[1], Siri Ann Nyrnes[1,2], Hans Torp[1], and Lasse Løvstakken[1]
[1] MI Lab and Dept. of Circulation and Medical Imaging, NTNU, Norway
[2] Dept. of Pediatrics, St. Olav's University Hospital, Trondheim, Norway

Two-dimensional blood velocity estimation has shown potential to solve the angle-dependency of conventional ultrasound flow imaging. Clutter filtering, however, remains a major challenge for large beam-to-flow angles, leading to signal drop-outs and corrupted velocity estimates.
This work presents and evaluates a compounding speckle tracking (ST) algorithm to obtain truly angle-independent two-dimensional blood velocity estimates. A dual-angle plane wave imaging setup with full parallel receive beamforming is utilized to achieve high frame rate speckle tracking estimates from two scan angles, which may be compounded to obtain velocity estimates of increased robustness. The acquisition also allows direct comparison to vector Doppler (VD) imaging.
Absolute velocity bias and root-mean-square (RMS) error of the ST and VD estimations were investigated using simulations of a rotating flow phantom with low velocities ranging from 0 to 20 cm/s. In a challenging region where the estimates were influenced by clutter filtering, the bias and RMS error for VD were 36 % and 6 cm/s, whereas they were 22 % and 4 cm/s for conventional ST. However, compounding of the ST estimates reduced both the bias and RMS error significantly, to 11 % and 2 cm/s.
The method was also tested *in vivo* for vascular and neonatal cardiac imaging. In a carotid artery bifurcation the obtained blood velocity estimates showed that the VD estimates were more influenced by clutter filtering than compounded ST. The results from the cardiac case showed that the ST method was more affected by low SNR than VD. More consistent blood flow depiction was, however, observed for the compounded ST velocity estimates compared with conventional ST in both the carotid artery and cardiac case. Generally, more robust angle-independent blood velocity estimates may be obtained with compounded speckle tracking.

4.1 Introduction

Ultrasound imaging is a non-invasive tool used for blood flow velocity estimation and visualization in a wide range of clinical settings. The conventional Doppler methods detect and estimate frequency or phase shifts caused by moving blood scatterers, but are only able to measure the axial velocity component of the three-dimensional velocity vector. This leads to an angle-dependency on the beam-to-flow angle and is one of the fundamental limitations in current ultrasound methods for blood velocity estimation. In addition, the backscattered echo from blood is weak and must be separated from the strong clutter signal coming from surrounding tissue before velocity estimation. The tissue is stationary or slowly-moving and can be attenuated by applying a high-pass clutter filter to the received signal. Unfortunately, for slow flow and near-transversal flow, the blood signal will be attenuated as well. In color flow imaging (CFI), where the mean axial velocities are displayed as a two-dimensional parametric map in the region of interest, this will lead to signal drop-outs in the image, or biased blood velocity estimates [1, 2]. General improvements to avoid the angle-dependency and clutter filter issues would minimize the need of interpreting the images, and therefore increase the diagnostic certainty.

Multi-dimensional blood flow imaging where two or all three components of the blood velocity vector are estimated would allow for measuring the absolute blood velocity and visualizing complex blood flow patterns. Speckle tracking (ST) [3] and vector Doppler (VD) [4] have been the two main research lines for two-dimensional flow estimation. The speckle pattern in the ultrasound image is a result of the constructive and destructive interference from the backscattered echoes, e.g. from ensembles of red blood cells. As the movement of blood speckle is correlated with movement of blood, the speckle can be tracked from frame to frame using pattern matching techniques to estimate the two-dimensional blood velocities. The vector Doppler technique, on the other hand, combines the Doppler estimates from two or more transmit and/or receive angles to obtain both the axial and the lateral velocity components.

Alternative two-dimensional flow estimators have been proposed. In 1998 both Anderson [5] and Jensen and Munk [6] suggested to introduce a modulation in the lateral direction of the received ultrasound field using complex apodization schemes to obtain both the axial and the lateral velocity components. In 2004 Kim *et al.* [7] introduced echo PIV (particle image velocimetry) for tracking of contrast microbubbles in ultrasound images, similar to optical tracking of particles in *in vitro* flow setups. More recently, different techniques to visualize and identify vortex flow in the left ventricle called vector flow mapping (VFM) and vortography have been suggested [8–11]. The latter techniques utilize 2-D color Doppler information and 2-D flow assumptions to estimate the lateral velocity component.

Two-dimensional velocity vector imaging has recently become relevant in the context of plane or diverging wave imaging, where full field-of-view and multi-angle imaging can be achieved at very high frame rates [12–14], and also increase the accuracy of both VD and ST. Clutter filtering is, however, still necessary to separate the blood signal from the clutter signal, which results in corrupted blood velocity estimates for near-perpendicular beam-to-flow angles. The velocity estimates are thus

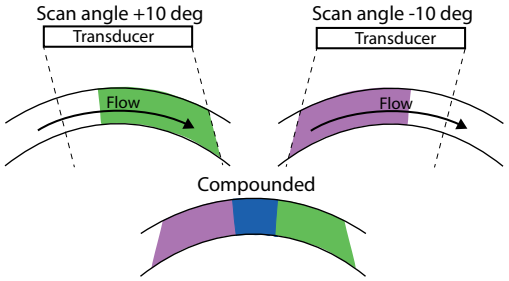

Figure 4.1: Scan setup with two transmit angles and corresponding segmentation maps. The compounded map illustrates where the final speckle tracking estimates is combined from the two scan angles (blue area) and where it only consists of estimates from one scan angle (purple and green).

still angle-dependent, and transversal flow will not be estimated correctly. Clutter filtering remains therefore as a major limitation in two-dimensional blood velocity estimation.

In this work, we investigate how dual-angle plane wave imaging (PWI) can be used to minimize clutter filtering issues for two-dimensional blood velocity estimation based on speckle tracking. As only one angle is needed to produce two-dimensional velocity estimates, the introduction of two opposite angled scans may be used to avoid dropouts and corrupted velocity estimates in the region of interest. With two scan angles, a truly angle-independent velocity estimator may thus be approached, where a minimum blood velocity can be measured for any given beam-to-flow angle. As the same acquisition sequence is used for vector Doppler imaging, we compare the performance of compounded ST to VD.

4.2 Methods

4.2.1 Tilted plane wave imaging setup

The proposed data acquisition setup is a dual-angle plane wave scan sequence, as illustrated in Fig. 4.1. The full aperture of a linear array is used to transmit tilted unfocused, full field-of-view ultrasound waves, and parallel receive beamforming [13] is utilized to generate all image lines in parallel. An ensemble of transmissions, N, for each scan angle was acquired for flow velocity estimation. The acquisition of the ensemble in the two scan directions can be interleaved or acquired subsequently. With subsequent acquisition, a higher pulse repetition frequency (PRF) within an ensemble can be achieved, but a time lag between the two ensembles will arise. For the *in vivo* recordings, a duplex acquisition scheme was used, where a separate B-mode setup was interleaved the plane-wave flow sequence to ensure high quality B-mode images. More information about the imaging setup is given in Sec. 4.2.6 and 4.2.7.

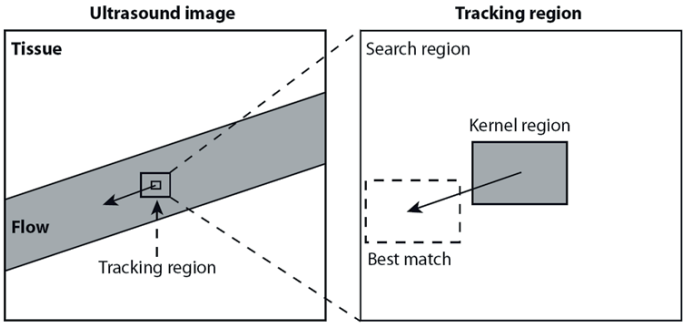

Figure 4.2: Speckle tracking principle. A kernel is defined in a first acquisition and the best match of this kernel is searched for in the next acquisition.

4.2.2 Speckle tracking

The basic concept in speckle tracking is shown schematically in Figure 5.11. A 2-D kernel region is defined in a given image and the best match of this kernel is searched for in a following image in time, determining the most likely displacement of the kernel. When the displacement is found, the velocity can be estimated given the time between the two image acquisitions. This process is repeated for the whole imaging area, and for all subsequent image samples in the temporal ensemble. The velocities are averaged over the ensemble and a vector velocity map of the blood flow is obtained [3].

The most likely displacement is found using normalized 2D cross-correlation on consecutive temporal samples of the envelope (detected) data,

$$\rho(u,v) = \frac{\sum_{x,y}\left(I(x+u,y+v) - \overline{I}_{u,v}\right)\left(K(x,y) - \overline{K}\right)}{\sqrt{\sum_{x,y}(I(x+u,y+v) - \overline{I}_{u,v})^2 \sum_{x,y}(K(x,y) - \overline{K})^2}} \tag{4.1}$$

where K is the original kernel and I is the comparison area displaced (u,v) from the kernel K position. The averages are defined as

$$\begin{aligned} \overline{I}_{u,v} &= \frac{1}{N_x N_y}\sum_{x,y} I(x+u,y+v) \\ \overline{K} &= \frac{1}{N_x N_y}\sum_{x,y} K(x,y), \end{aligned} \tag{4.2}$$

where N_x and N_y are the kernel dimensions, so $x = [0, N_x - 1]$ and $y = [0, N_y - 1]$. Parabolic subsample interpolation of the estimated displacement was used to improve the tracking resolution. If $d_1 = \rho(u_{max}, v_{max})$ is the region with highest correlation and d_0 and d_2 are the two nearest neighbor regions, the subsample offset correction

for the estimated displacement is given by [15]

$$\hat{\delta} = \frac{d_0 - d_2}{2(d_0 - 2d_1 + d_2)}. \tag{4.3}$$

The maximum measurable velocity is determined by the size of the search region.

4.2.3 Vector Doppler

The two-dimensional blood velocity vector can be obtained using the overlapping Doppler measurements from the two scan angles as follows [4]

$$\begin{aligned} \hat{v}_x &= -\frac{c}{4f_0 \sin(\theta)}(\hat{f}_1 - \hat{f}_2) \\ \hat{v}_z &= -\frac{c}{4f_0 \cos(\theta)}(\hat{f}_1 + \hat{f}_2) \end{aligned} \tag{4.4}$$

where c is the speed of sound, 2θ is the separation angle between the two scan directions, f_0 is the pulse center frequency and $\hat{f}_1$, $\hat{f}_1$ are the Doppler frequency estimates. The Doppler frequencies are estimated using the temporal autocorrelation function with lag one, $\hat{f} = \angle(\hat{R}(1)) \times \mathrm{PRF}/2\pi$ [16]. The autocorrelation function is calculated as follows,

$$\hat{R}(1) = \frac{1}{N-1} \sum_{k=1}^{N-1} x(k)^* x(k+1), \tag{4.5}$$

where $x(k)$ is a fixed spatial position, * denotes the complex conjugate and N is the ensemble size.

4.2.4 Compounded speckle tracking

Contrary to vector Doppler, only a single scan angle is needed to do velocity estimation using speckle tracking, since the method is based on 2-D correlation between speckle images within an ensemble. Two scan angles will therefore result in two independent flow velocity images at approximately the same time instant. The clutter filter will attenuate the signal at near-perpendicular beam-to-flow angles, resulting in drop-outs and poor velocity estimates in different regions for the two images. With two flow images available, the excessive information can be utilized by combining or discarding estimates from the two images depending on the robustness of the estimates. Finally, one flow image can be generated where the clutter filter impact is reduced.

The segmentation maps for discarding estimates were made as in conventional color flow segmentation by thresholding signal power and velocity after clutter filtering. In addition, the variance in the speckle tracking estimates over the ensemble was included as a discriminator. Thus, after the color flow segmentation, ST estimates with variance above a certain threshold were discarded. The concept is illustrated in Fig. 4.1, where the segmentation maps for the two scan angles are shown in green and purple. Estimates from regions with large beam-to-flow angles are discarded in

the final velocity estimates. The blue area illustrates the overlapping area of the segmentation maps where the estimates from the two scan angles have been combined in the final velocity estimate.

4.2.5 Clutter filtering setup

Clutter filtering is necessary to suppress the strong tissue echo prior to blood velocity estimation. The clutter filter frequency response will limit the lower measurable blood velocity, thus a filter with sufficient stop band attenuation and steep transition region is desired. The clutter filter is a high-pass filter and can be implemented as a polynomial regression, FIR or IIR filter [17]. Designing the appropriate clutter filter can be a challenge, but a high ensemble size makes it easier to achieve the desired filter frequency response as higher order filters can be employed. For speckle tracking, a time-invariant clutter filter is preferable to ensure that every speckle image is filtered equally, since the method is based on correlation between the speckle images. In this work a 10th order FIR filter was designed for the speckle tracking estimation with a $-3\,\mathrm{dB}$ velocity cut-off at $0.18 \cdot \mathrm{V_{Nyquist}}$. For the Doppler data, a time-variant, 3rd order polynomial regression filter with a steeper transition region was used as an alternative to the FIR filter. For the given ensemble lengths of 32 and 50, the $-3\,\mathrm{dB}$ velocity cut-off was $0.10 \cdot \mathrm{V_{Nyquist}}$ and $0.06 \cdot \mathrm{V_{Nyquist}}$, respectively. Both the FIR and polynomial regression filter were evaluated on the Doppler data to see how they affected the velocity estimates.

4.2.6 Simulation study

A simulation study was carried out to evaluate the tilted plane wave imaging setup and the ST and VD velocity estimation methods. The Field II [18] simulation software was used to simulate channel RF data of a cylindrical phantom with analytical Couette (circular) flow. The number of blood scatterers per resolution cell was approximately 10 to ensure a Gaussian distributed signal amplitude as expected from blood scatterers. The flow phantom allowed evaluation of the algorithm in a situation where all beam-to-flow angles were present for a span of velocities. The velocity range was 0-20 cm/s and the phantom was placed at a depth of 2 cm. The ensemble size was 50 at slow-time PRF of 4 kHz in each scan direction (i.e. 8 kHz firing rate in total). IQ-demodulation and beamforming were done in the exact same manner as for *in vivo* acquired channel RF data. The flow imaging parameters are listed in Table 1. White noise was added to give a signal-to-noise ratio of 30 dB and the 10th order FIR filter with a -3 dB cut-off at 5 cm/s was used to include clutter filter effects in the simulation.

To evaluate the robustness of the estimators, a total of 10 realizations of the flow phantom (each with an ensemble size of 50) were simulated. Both the VD and ST velocity estimates were spatially averaged in a region of 1 mm × 1 mm to reduce the variance of the estimates. Based on the 10 realizations, the bias and root-mean-square (RMS) error were calculated and compared.

Table 4.1: Image acquisition parameters

Probe	UX L9-4/38		
Probe type	128 element linear array		
Pitch [μm]	304		
Elevation focus [mm]	19		
	Flow	B-mode, carotid	B-mode, cardiac
Pulse center frequency [MHZ]	5	6.6	6.6
Pulse length	2.5	1	1.5
PRF [Hz]	8000	12000	12000
Ensemble size carotid/cardiac	50/32	-	-
Elements used on transmit	128	128	49
Transmit angle [deg]	± 10	-7.2 $\rightarrow$ 7.2	0
Transmit F-number	-	-	2
Transmit focus depth [mm]	-	-	30
Receive angle [deg]	± 10	0	0
Receive F-number	1.1	1.1	1.1

4.2.7 *In vivo* study

Two *in vivo* cases were included in this work to investigate imaging scenarios where the blood flow is typically lateral and where the estimated blood velocities may be corrupted by the clutter filter. The first case was vascular imaging of the carotid artery bifurcation of a healthy volunteer and the second case was cardiac imaging of a neonate. The neonate was 15 days and weighed 3065 g at the time of the recording and was born with a ventricular septal defect (VSD) of the muscular type. The VSD was placed in the mid part of the septum and was not visible in the left ventricular outflow tract which was the focus in this work.

A SonixMDP ultraound scanner (Ultrasonix, Richmond, BC, Canada) with a 4-9 MHz linear transducer and a Sonix DAQ was used for the *in vivo* channel RF data acquisition. Two different duplex (B-mode+flow) acquisition schemes were used for the two *in vivo* cases.

For vascular imaging, the flow sequence consisted of plane waves transmitted at a PRF of 8 kHz from alternating angles ($\pm 10^\circ$). The slow-time Doppler PRF was thus 4 kHz for each scan angle, and the ensemble size of the acquisition was 50. The B-mode image was acquired by coherent compounding of 43 transmitted plane waves with transmit angles ranging from $[-7.2, 7.2]$ degrees at a PRF of 12 kHz. The duplex frame rate after a total of $43 + 2\times50$ transmit events was 62 fps.

For cardiac imaging, the flow sequence consisted of *sequential* plane wave transmissions from -10° then $+10^\circ$ to achieve a slow-time Doppler PRF of 8 kHz for each scan angle. The ensemble size of the acquisition was 32 and an acquisition setup with focused B-mode imaging was used. The B-mode sequence was divided in two groups and interleaved the flow acquisition, resulting in twice as many flow frames as B-mode frames. Each interleave group consisted of 64 focused pulses transmitted

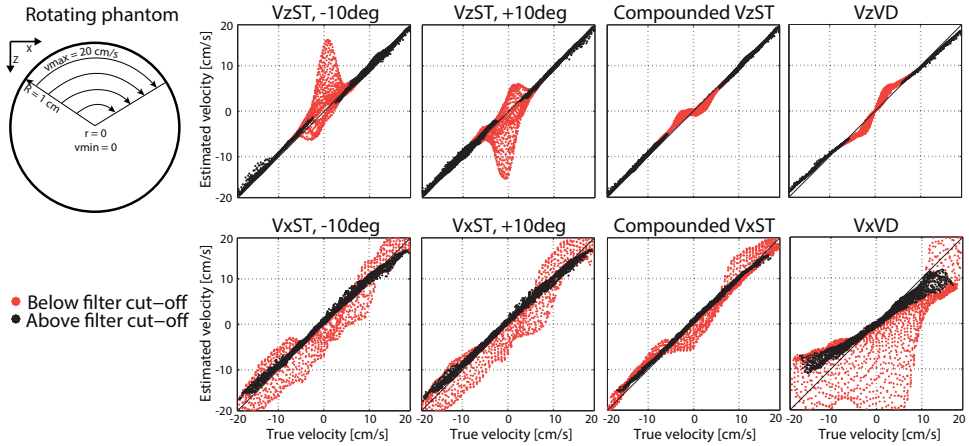

Figure 4.3: Scatter plot of speckle tracking estimates from the two scan angles compared to the compounded estimates and the vector Doppler estimates for the simulated rotating phantom.

at a PRF of 12 kHz. The flow frame rate after 64 + 2×32 transmit events was 75 fps whereas the B-mode frame rate was 38 fps.

Channel RF data (128 channels) were stored for up to 2 seconds duration (limited by 16 GB of channel data memory), and beamforming and post-processing were done offline. The RF data were IQ-demodulated and receive filtered to increase signal-to-noise ratio (SNR), and then beamformed using a hamming apodization window over the active receive aperture to reduce side lobes. The Doppler data were beamformed using a tilted receive angle equal to the transmit angle, so the separation angle between the Doppler scans was 20°. The flow estimates was spatially averaged 1 mm×1 mm in the carotid artery case and 2 mm×2 mm in the cardiac case. In addition the estimates were averaged over 3 flow frames to smooth the flow patterns in time throughout the cardiac cycle. Image acquisition parameters for the flow and B-mode sequences are listed in Table 1.

The study was approved by the Norwegian Regional Committee for Medical and Health Research Ethics. Written informed consent was obtained from the parents of the neonate before examination. The prior patient safety measurements were within the guidelines from the US Food and Drug Administration (FDA).

4.3 Results

4.3.1 Simulations

Fig. 4.3 shows an illustration of the simulated rotating phantom together with scatterplots of the estimated versus the reference velocity components. The speckle tracking estimates from the two scan angles, the compounded speckle tracking

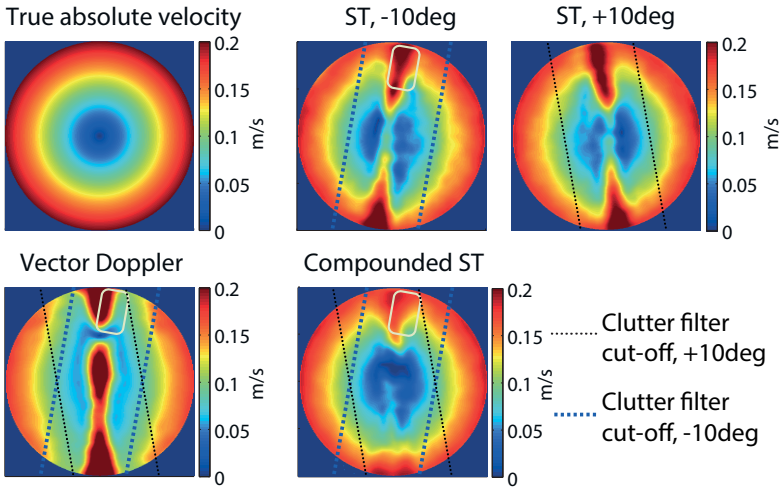

Figure 4.4: Absolute velocity comparison between the true velocity and the estimated using speckle tracking and vector Doppler. The ST estimates from a single scan angle ($\pm 10°$) are included in the upper right corner. The VD and the compounded ST estimates are shown in the lower panel. In the indicated white square the RMS error was 4 cm/s for the ST estimates from $-10°$ and 2 cm/s for the compounded ST estimates.

estimates, and the vector Doppler estimates are shown from left to right, respectively. The top and bottom panel further show the z and x velocity components. Velocity estimates below the clutter filter cut-off velocity at -3 dB are plotted in red, and show a higher variance compared with the velocities in the passband of the filter for all methods. For the compounded ST estimates this variance is lowered for all velocities and a higher agreement with the reference velocities is achieved. To the right in Fig. 4.3 the scatterplots for the V_z and V_x estimates from vector Doppler are shown. The V_z estimates have a low variance, but are overestimated in the vicinity of the clutter filter cut–off and are slightly underestimated for the highest velocities. The V_x estimates from vector Doppler are poor below clutter filter cut-off, and also have a higher variance than the ST estimates above filter cut-off, in addition to a clear underestimation.

The absolute velocity estimates of the rotating phantom are shown in Fig. 4.4. The true velocities in the phantom, ranging from 0 to 20 cm/s, are shown in the upper left corner. The absolute velocity estimates from speckle tracking for the two scan angles are shown in the upper right side of the figure. The dashed and dotted lines illustrate the clutter filter cut-off velocities in the phantom for scan angle $-10°$ and $+10°$, respectively. The axial velocities inside these lines are below the -3 dB clutter filter cut-off at 5 cm/s. An overestimation can be observed when the ST estimates are in the clutter filter transition region for either scan angle. In the lower right panel, the

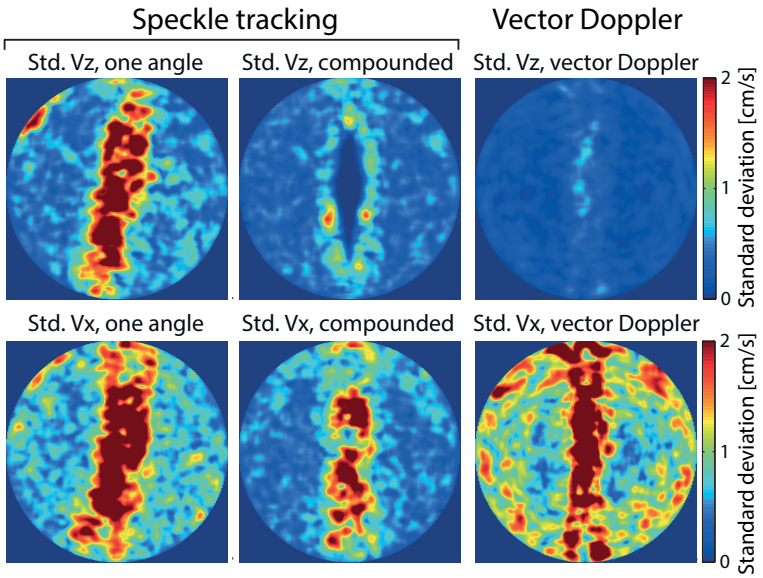

Figure 4.5: Standard deviation in cm/s of the V_z and V_x-components of the speckle tracking and vector Doppler velocity estimators over 10 realizations of the simulated phantom.

compounded ST absolute velocities are shown. Overall the compounded ST estimates have a better agreement with the true velocities. This can especially be observed in regions where the single angle ST estimates are clearly influenced by the clutter filter. Specifically, the absolute velocity bias and RMS error in the region defined by the white square were reduced from 22 % and 4 cm/s for the single angle ST estimates to 11 % and 2 cm/s for the compounded ST estimates.

In the lower left corner the vector Doppler estimates of the absolute velocities are shown. The VD estimates underestimates when either of the Doppler estimates is influenced by the clutter filter and overestimates when both Doppler estimates are below filter cut-off. The absolute velocity bias and RMS error in white square was 36 % and 6 cm/s for the VD estimates. The RMS error for the whole region where at least one Doppler angle was influenced by the clutter filter, was 7 cm/s for the VD estimates and 2 cm/s for the compounded ST estimates.

The standard deviations of the three estimators, the single angle ST, compounded ST and VD, were found for 10 realizations of the rotating phantom and are shown in Fig. 4.5. It was observed that a more robust estimator is achieved in the compounding ST compared with single-angle ST and VD estimation. The mean standard deviation of the whole phantom for the V_x-component was 1.1 cm/s, 0.7 cm/s and 1.4 cm/s for single-angle ST, compounding ST and VD, respectively. For the V_z-component the corresponding numbers were 0.8 cm/s, 0.4 cm/s and 0.2 cm/s.

4.3.2 *In vivo*

Fig. 4.6 and 4.7 show the carotid bifurcation of a healthy volunteer for one frame in diastole. The ST estimates from $\pm 10^\circ$ are compared with the compounded ST estimates and the VD estimates.

The yellow circles in Fig. 4.6a and 4.6b indicate problem areas for the two scan angles. It is observed that both color flow and ST estimates were corrupted by the clutter filter in these regions. By visual inspection the compounded ST velocity estimates in Fig. 4.7a show a more consistent depiction of the blood flow. In Fig. 4.7b the corresponding VD estimates of the absolute velocity are shown. In general, higher velocities than the compounded ST estimates are observed.

The timing of the frame in Fig. 4.6 and 4.7 is marked in Fig. 4.8, where the compounded ST and VD absolute velocity estimates from the common carotid are plotted in the upper panel. The VD estimates were in general higher than the compounded ST estimates when both were clutter filtered with the FIR filter. A polynomial regression clutter filter with a lower velocity cut-off (2 cm/s) was tested on the VD estimates and a better agreement was then achieved between the VD and ST estimates for the low velocities in diastole. In the lower panel of Fig. 4.8, the retrospective PW spectra made from the same data set are shown together with the Doppler estimates and the ST component in the scan directions.

Fig. 4.9 and 4.10 show the blood flow in the left ventricular outflow tract in the heart of a newborn. In this view, from parasternal long-axis, the flow in the left ventricular outflow tract has a large beam-to-flow angle for both scan angles. Fig. 4.9 shows the speckle tracking estimates overlaid the corresponding color flow images from the two scan angles. Some inconsistency and high variance estimates are indicated by the yellow circle for scan angle -10° in Fig. 4.9, and clearly corrupted estimates are observed in the yellow circle for scan angle $+10^\circ$. A seemingly more robust depiction of the blood flow is observed for the compounded ST estimates in Fig. 4.10. Again, higher velocity estimates are obtained from the vector Doppler estimator compared with the compounding ST estimator in the outflow tract where both scan angles have high beam-to-flow angles.

In the upper panel of Fig. 4.11 the compounded ST and VD absolute velocity estimates from a region right after the aortic valve are plotted and the timing of the frame in Fig. 4.9 and 4.10 is marked. The VD estimates were significantly higher than the compounded ST estimates using either clutter filter. The large difference is in the lateral component, since the PW spectra in the lower panel show an agreement between the Doppler estimates and the ST component in the scan directions.

4.4 Discussion

Clutter filtering results in corrupted velocity estimates for beam-to-flow angles close to 90° and remains a major limitation in two-dimensional blood velocity estimation. For approaches based on the autocorrelation method, a bias is induced in the filter transition region. For speckle tracking, the loss of signal power will degrade the speckle correlation. Signal drop-out and corrupted velocity estimates may influence

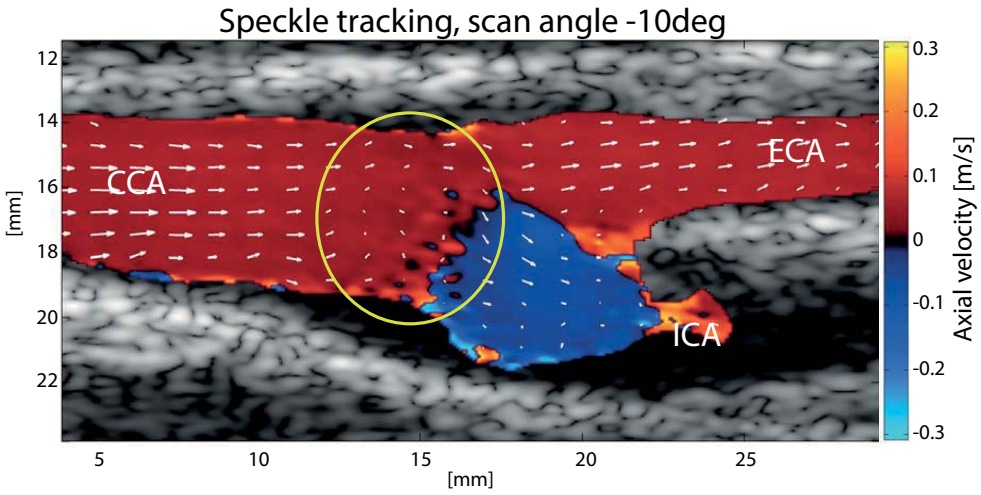

(a)

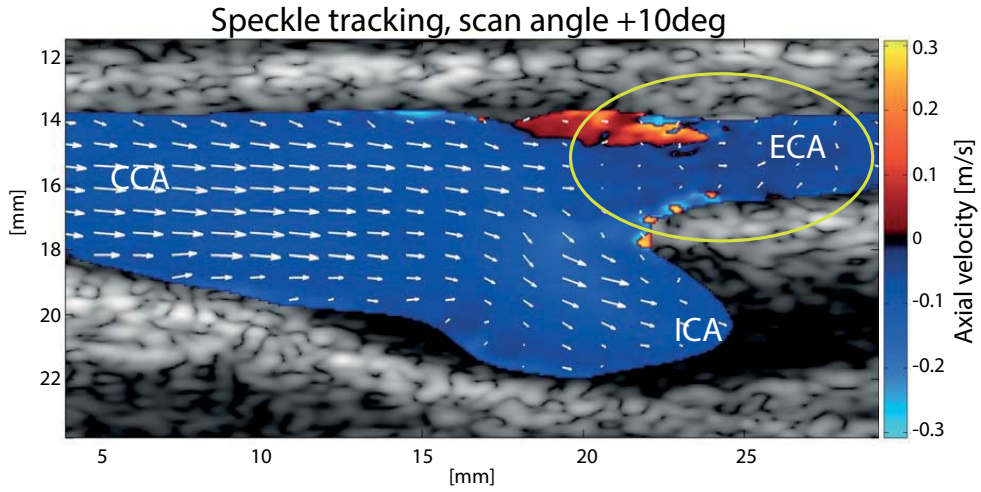

(b)

Figure 4.6: Blood flow in the carotid artery bifurcation of a healthy volunteer. The common, internal and external carotid arteries are indicated as CCA, ICA and ECA, respectively. The timing of the frame is given in Fig. 4.8. The speckle tracking results for angle $-10°$ and $+10°$ are shown as arrows overlaid the corresponding color flow image. The yellow circles indicate areas where the clutter filter destroys the velocity estimates.

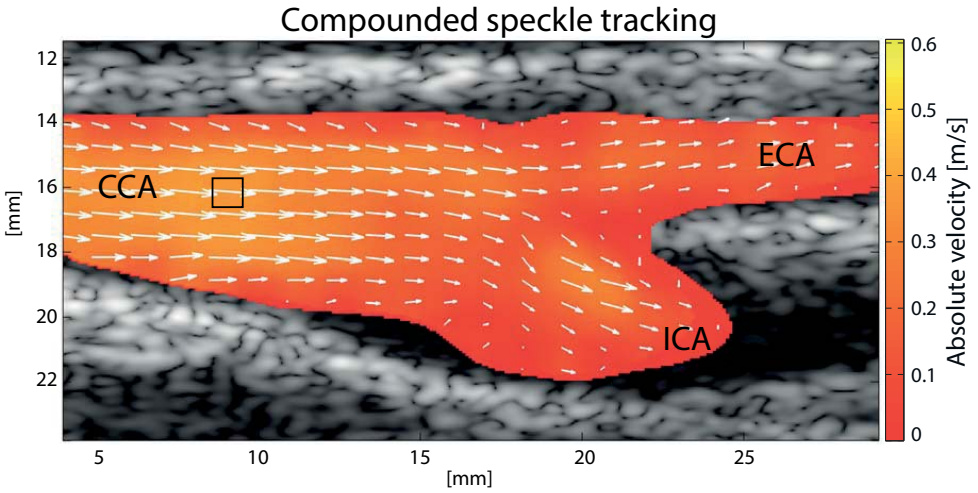

(a) Compounded ST estimates where the colors represent the absolute velocities.

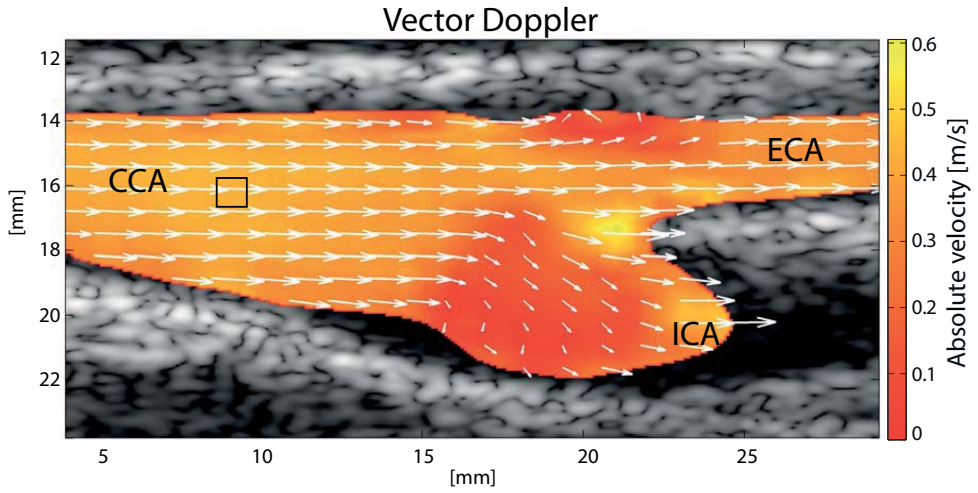

(b) VD estimates where the colors represent the absolute velocities.

Figure 4.7: Blood flow in the carotid artery bifurcation of a healthy volunteer. The common, internal and external carotid arteries are indicated as CCA, ICA and ECA, respectively. The timing of the frame is given in Fig. 4.8. The compounded speckle tracking and vector Doppler estimates are shown in the upper and lower panel, respectively, and the colors represent the estimated absolute velocity. The black squares indicate the sample volume for the absolute velocity plot in Fig. 4.8.

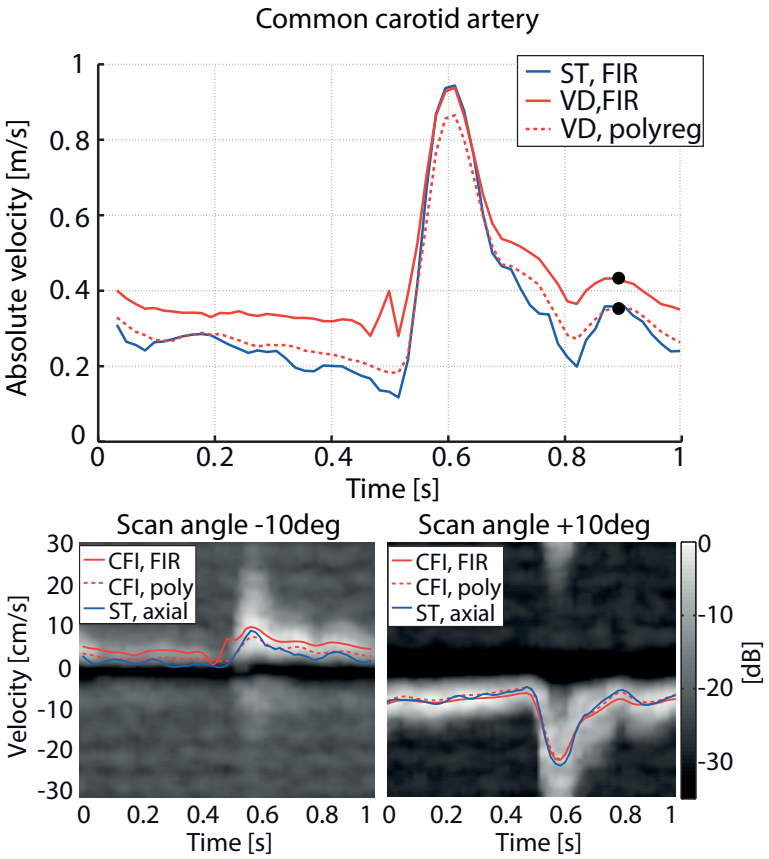

Figure 4.8: The top panel shows one heart cycle of the absolute velocity estimated from a 1 mm × 1 mm region in the middle of the common carotid artery (marked in Fig. 4.7).The black dots indicate the frame time used in Fig. 4.6 and 4.7. The FIR clutter filter was used for the ST and VD estimates given by the solid lines, and the polynomial regression filter was used for the VD estimates given by the dotted line. The bottom panel shows the corresponding PW spectra and Doppler estimates for scan angle $-10\,^\circ$ and $+10\,^\circ$. The PW spectra are made retrospectively from the IQ data filtered with the FIR filter. The ST velocity component in the given scan angle is plotted in blue.

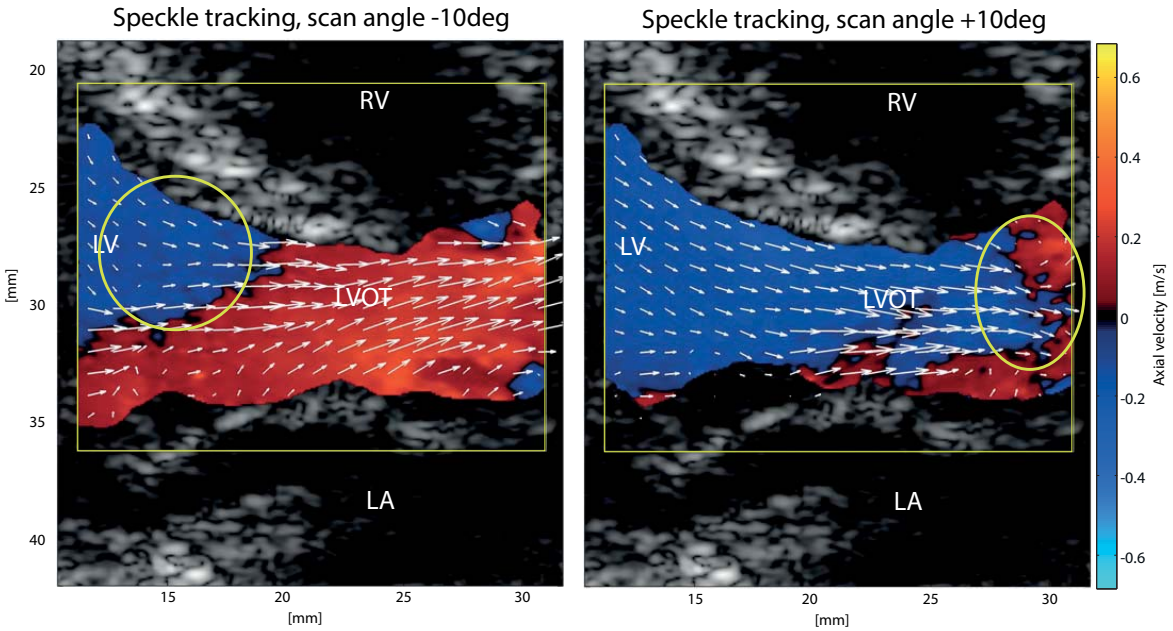

Figure 4.9: Blood flow in the left ventricular outflow tract in the heart of a newborn (15 days, 3065 g) from a parasternal long-axis view. The left atrium, ventricle and ventricular outflow tract are indicated as LA, LV and LVOT, respectively. The right ventricle is indicated as RV. The speckle tracking results for angle $-10°$ and $+10°$ are shown as arrows overlaid the corresponding color flow image. The yellow circles indicate areas where the clutter filter affects the velocity estimates.

the interpretation of flow images, especially for complex or abnormal flow patterns which can be present in diseased arteries and hearts.

In this work, we have investigated if dual-angle plane wave imaging and blood speckle tracking can be used to obtain robust angle-independent two-dimensional blood velocities, not limited by the beam-to-flow angle, and compared this with the corresponding vector Doppler performance from the same data.

The separation angle between the Doppler data affects the variance of the components estimated by VD. For our definition of the x- and z-directions, a larger separation angle would be beneficial for the V_x-component. The maximum steering angle is largely depending on the pitch of the transducer and the presence of grating lobes artifacts. For the transducer used in this work, the pitch was approximately equal to the wavelength, and only no steering would assure no grating lobes artifacts. The scan angles were chosen to be $\pm 10°$ to have a sufficient separation angle for VD and compounding ST estimation and a wide overlapping image area as deep as $5-6$ cm. A longer pulse length could increase the robustness of the VD estimates, but would decrease the resolution and degrade the ST estimates. The resulting compromise is in

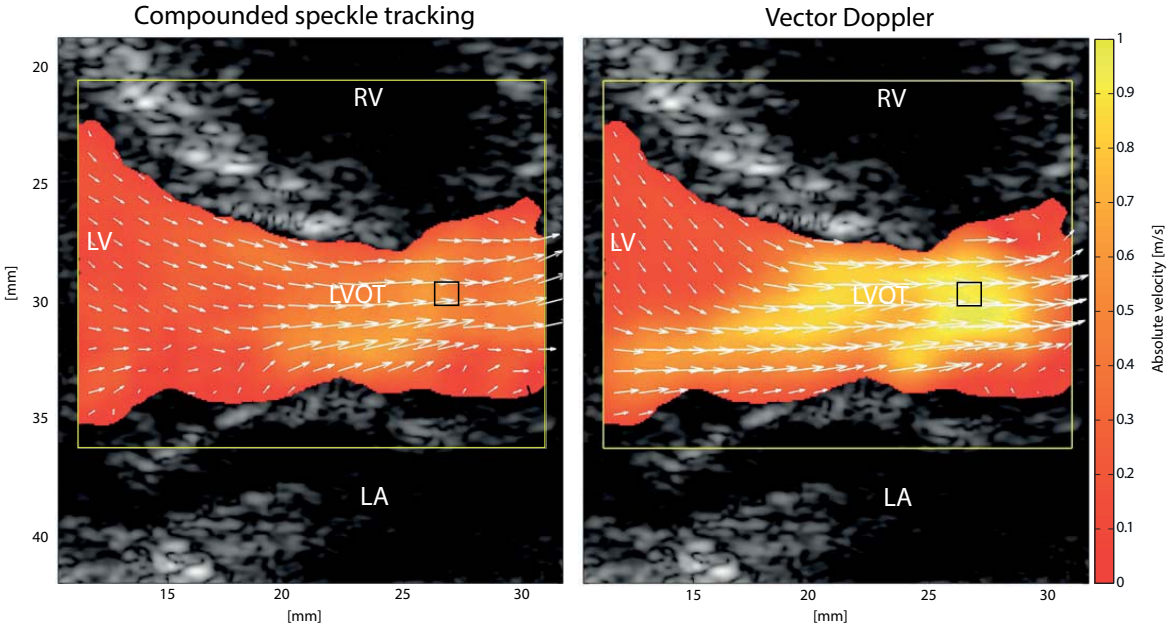

Figure 4.10: Blood flow in the left ventricular outflow tract in the heart of a newborn (15 days, 3065 g) from a parasternal long-axis view. The left atrium, ventricle and ventricular outflow tract are indicated as LA, LV and LVOT, respectively. The right ventricle is indicated as RV. The colors represent the estimated absolute velocity. The black squares indicate the sample volume for the absolute velocity plot in Fig. 4.11

this respect perhaps not optimal for either method. The same linear array and plane wave imaging were used both in the vascular and cardiac case. In cardiac imaging the standard probe is a smaller phased array which can image between the ribs and have a larger field-of-view, but on newborns it is possible to image through the ribs, and a linear array could therefore be used. Papadacci *et al.* [19] show that high frame rates and good image quality can be obtained using diverging beams and a phased array, however, it remains to be tested for blood velocity estimation.

The velocity variance increases below filter cutoff for all estimators (see Fig. 4.3 and Fig. 4.5). However, the compounded ST estimates had the lowest variance, and gave reduced variance even in regions where only one angle contributed to the final velocity estimate, since corrupted estimates were discarded. This results in an overall increase in estimator robustness, and increased velocity accuracy compared with the single angle ST and dual-angle VD. Combining ST and Doppler estimates could further increase the robustness of the velocity estimates, using the axial Doppler estimates and the lateral ST estimates as discussed by Swillens *et al.* [20].

In both *in vivo* cases investigated in this work, the VD estimator gave very regular vector fields for large beam-to-flow angles where the clutter filter has an influence.

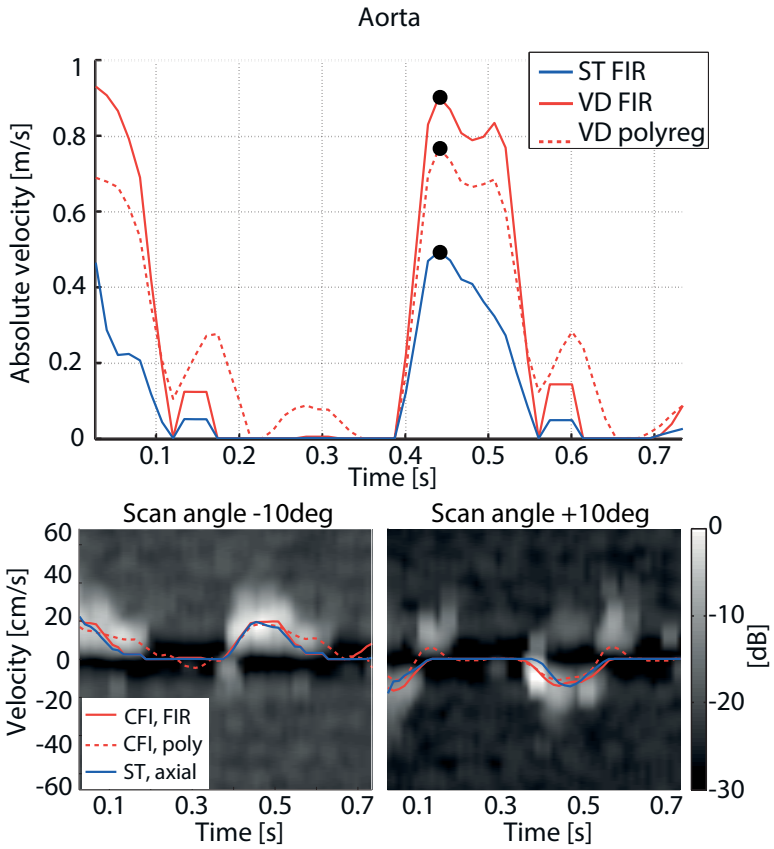

Figure 4.11: The top panel shows one heart cycle of the absolute velocity estimated from a 1 mm × 1 mm region right after the aortic valve (marked in Fig. 4.10).The black dots indicate the frame time used in Fig. 4.9 and 4.10. The FIR clutter filter was used for the ST and VD estimates given by the solid lines, and the polynomial regression filter was used for the VD estimates given by the dotted line. The bottom panel shows the corresponding PW spectra and Doppler estimates for scan angle $-10°$ and $+10°$. The PW spectra are made retrospectively from the IQ data filtered with the FIR filter. The ST velocity component in the given scan angle is plotted in blue.

This can be attributed to an overestimation in the Doppler estimates which through the triangulation formulas result in a severe overestimation of the lateral velocity component as was observed for the simulation results in Fig. 4.4. The clutter filter influence on the velocity estimates will depend on the chosen filter frequency response, and optimizing the clutter filter for the the given imaging scenario will decrease issues such as overestimation. In this work, a FIR-filter of order 10 and cut-off velocity of 5 cm/s was used as the standard clutter filter both for the vascular and the cardiac case, but the polynomial regression filter with a lower velocity cut-off resulted in less overestimation of the vector Doppler estimates and a better agreement between the VD and ST estimates as seen in Fig. 4.8.

The 2-D vector velocity estimation methods discussed in this paper have different advantages/disadvantages. The vector Doppler approach is computationally less demanding than ST, but is hampered by aliased velocities and biased velocities in the clutter filter transition region. The speckle tracking method can track beyond the Nyquist limit and is in our experience less influenced by the clutter filter in the transition region. The latter can be observed in Fig. 4.4 where the single angle ST estimator produce good estimates also below the clutter filter cut-off, and only overestimate for the highest beam-to-flow angles. The *in vivo* data also indicates this, as seen in Fig. 4.8, where the bias between the VD and ST estimates is removed when a clutter filter with a lower velocity cut-off is used for the Doppler estimates. The narrow-band autocorrelation method is known to be robust with regards to SNR, and will also work with longer pulses. On the other hand, ST is based on a wide-band approach where a short pulse is preferable. This may have implications for the range of clinical applications or imaging depth where ST can be utilized. The SNR in the left ventricular outflow tract was low (< 10 dB) which resulted in ST estimates with high variance. The ST estimates were probably underestimated in this region, which in addition to a possible overestimation of the VD estimates, resulted in a large deviation between the methods as seen in Fig. 4.11.

The ST compounding algorithm shows potential for sufficient SNR, partly because the variance in the velocity estimates is reduced when the ST estimates from two angles are averaged, but more importantly because the corrupted estimates are discarded. The success of the latter also depends on the segmentation maps used for discarding unreliable velocity estimates. In this work, the parameters for segmentation was adjusted for each case, but in further work a more robust segmentation algorithm should be developed. More than two angles on transit and/or on receive should also be exploited. With plane wave imaging it is possible to have multiple scan angles and a high frame rate. More scan angles could be beneficial both for vector Doppler [21] and compounding speckle tracking. For the latter, more samples to combine and choose between could make it easier to discard corrupted estimates. However, increasing the number of scan angles will lower the frame rate and/or Doppler PRF. The optimal number of scan angles will thus depend on the different clinical applications.

4.5 Conclusion

A compounding blood speckle tracking algorithm based on high frame rate plane wave imaging from two scan angles was investigated in a rotating simulation phantom and *in vivo*. In the simulations, the absolute velocity bias was reduced from 22% for the conventional ST estimates to 11% for the compounded ST estimates in a region where the clutter filter influenced the velocity estimates. In comparison, the VD estimates had an absolute velocity bias of 36% in the same region. *In vivo*, a more consistent flow depiction was seen in the compounded ST flow field compared to the ST flow field based on a single scan angle. The ST estimates were, however, sensitive to the SNR. The results demonstrated that both ST and VD velocity estimation were possible for vascular and neonatal cardiac imaging, and that clutter filter issues and corrupted velocity estimates could be avoided to achieve more robust velocity estimates with compounded ST.

References

[1] C. Tysoe and D. Evans, "Bias in mean frequency estimation of Doppler signals due to wall clutter filters," *Ultrasound in medicine & biology*, no. 5, pp. 671–677, 1995.

[2] D. Evans and W. McDicken, "Signal Processing for Colour Flow Imaging," in *Doppler Ultrasound: Physics, Instrumentation and Signal Processing*, pp. 246–250, 2000.

[3] L. N. Bohs, B. J. Geiman, M. E. Anderson, S. C. Gebhart, and G. E. Trahey, "Speckle tracking for multi-dimensional flow estimation.," *Ultrasonics*, vol. 38, pp. 369–75, Mar. 2000.

[4] B. Dunmire, K. W. Beach, K. Labs, M. Plett, and D. E. Strandness, "Cross-beam vector Doppler ultrasound for angle-independent velocity measurements.," *Ultrasound in medicine & biology*, vol. 26, pp. 1213–35, Oct. 2000.

[5] M. E. Anderson, "Multi-dimensional velocity estimation with ultrasound using spatial quadrature.," *IEEE transactions on ultrasonics, ferroelectrics, and frequency control*, vol. 45, pp. 852–61, Jan. 1998.

[6] J. A. Jensen and P. Munk, "A new method for estimation of velocity vectors.," *IEEE transactions on ultrasonics, ferroelectrics, and frequency control*, vol. 45, pp. 837–51, Jan. 1998.

[7] H. B. Kim, J. R. Hertzberg, and R. Shandas, "Development and validation of echo PIV," *Experiments in Fluids*, vol. 36, pp. 455–462, Mar. 2004.

[8] S. Ohtsuki and M. Tanaka, "The flow velocity distribution from the Doppler information on a plane in three-dimensional flow," *Journal of visualization*, vol. 9, no. 1, pp. 69–82, 2006.

[9] T. Uejima, A. Koike, H. Sawada, T. Aizawa, S. Ohtsuki, M. Tanaka, T. Furukawa, and A. Fraser, "A new echocardiographic method for identifying vortex flow in the left ventricle: numerical validation," *Ultrasound in Medicine and Biology*, vol. 36, no. 5, pp. 772–788, 2010.

[10] D. Garcia, J. C. Del Alamo, D. Tanne, R. Yotti, C. Cortina, E. Bertrand, J. C. Antoranz, E. Perez-David, R. Rieu, F. Fernandez-Aviles, and J. Bermejo, "Two-dimensional intraventricular flow mapping by digital processing conventional color-Doppler echocardiography images.," *IEEE transactions on medical imaging*, vol. 29, pp. 1701–13, Oct. 2010.

[11] F. Mehregan, F. Tournoux, S. Muth, P. Pibarot, R. Rieu, G. Cloutier, and D. Garcia, "Doppler Vortography: A Color Doppler Approach to Quantification of Intraventricular Blood Flow Vortices," *Ultrasound in Medicine and Biology*, no. 1, pp. 1–21, 2014.

[12] M. Tanter, J. Bercoff, L. Sandrin, and M. Fink, "Ultrafast compound imaging for 2-D motion vector estimation: application to transient elastography.," *IEEE transactions on ultrasonics, ferroelectrics, and frequency control*, vol. 49, pp. 1363–74, Oct. 2002.

[13] J. Udesen, F. Gran, K. L. Hansen, J. A. Jensen, C. Thomsen, and M. B. Nielsen, "High frame-rate blood vector velocity imaging using plane waves: simulations and preliminary experiments.," *IEEE transactions on ultrasonics, ferroelectrics, and frequency control*, vol. 55, pp. 1729–43, Aug. 2008.

[14] I. K. Ekroll, A. Swillens, P. Segers, T. Dahl, H. Torp, and L. Lovstakken, "Simultaneous quantification of flow and tissue velocities based on multi-angle plane wave imaging.," *IEEE transactions on ultrasonics, ferroelectrics, and frequency control*, vol. 60, pp. 727–38, Apr. 2013.

[15] I. Cespedes, Y. Huang, J. Ophir, and S. Spratt, "Methods for estimation of subsample time delays of digitized echo signals," *Ultrasonic imaging*, 1995.

[16] C. Kasai, K. Namekawa, A. Koyano, and R. Omoto, "Real-Time Two-Dimensional Blood Flow Imaging Using an Autocorrelation Technique," *IEEE Transactions on Sonics and Ultrasonics*, vol. 32, no. 3, pp. 458–464, 1985.

[17] S. Bjærum, H. Torp, and K. Kristoffersen, "Clutter filter design for ultrasound color flow imaging.," *IEEE transactions on ultrasonics, ferroelectrics, and frequency control*, vol. 49, pp. 204–16, Mar. 2002.

[18] J. A. Jensen, "Field : A Program for Simulating Ultrasound Systems," *Medical & Biological Engineering*, vol. 34, pp. 351–353, 1996.

[19] C. Papadacci, M. Pernot, M. Couade, M. Fink, and M. Tanter, "High-contrast ultrafast imaging of the heart.," *IEEE transactions on ultrasonics, ferroelectrics, and frequency control*, vol. 61, pp. 288–301, Mar. 2014.

[20] A. Swillens, P. Segers, and L. Lovstakken, "Two-dimensional flow imaging in the carotid bifurcation using a combined speckle tracking and phase-shift estimator: a study based on ultrasound simulations and in vivo analysis.," *Ultrasound in medicine & biology*, vol. 36, pp. 1722–35, Oct. 2010.

[21] J. Flynn, R. Daigle, L. Pflugrath, K. Linkhart, and P. Kaczkowski, "Estimation and display for Vector Doppler Imaging using planewave transmissions," *2011 IEEE International Ultrasonics Symposium*, pp. 413–418, Oct. 2011.

Chapter 5

Clutter Filtering Influence on Blood Velocity Estimation Using Speckle Tracking

Solveig Fadnes[1], Steinar Bjærum[2], and Lasse Løvstakken[1]
[1] MI Lab and Dept. of Circulation and Medical Imaging, NTNU, Norway
[2] GE Vingmed Ultrasound, Horten, Norway

Blood speckle tracking (BST) has shown potential for solving the angle-dependency limitation in color flow imaging (CFI). However, as clutter filtering is still Doppler-based, signal from flow at near perpendicular angles can still be severely attenuated. In this work, we investigate clutter filter design and its influence on speckle appearance and tracking performance.
The speckle pattern was significantly altered in the filter transition region due to a reduced imaging bandwidth, and a lateral amplitude modulation appears for near-perpendicular flow due to the inferred bandpass characteristics. Further, signal from grating lobes is less attenuated, leading to an equalization of the grating-to-main lobe level that is enhanced for large beam-to-flow angles and for unfocused transmit beams.
Analysis showed that time-variant clutter filters could be used to reduce variance in BST, but only for high slow-time ensembles (> 36). Compared to CFI we then found that BST could track blood velocities well below the filter cut-off where CFI becomes biased, and that BST is mainly limited by the high variance inferred by the potentially low signal-to-noise ratio (SNR) due to filter attenuation. Given a high lateral bandwidth (low F-number) and SNR of about 5 dB after filtering, reasonable tracking results could be achieved even for steep beam-to-flow angles.
Overall, given high Doppler ensembles as can be achieved using recent plane wave imaging or similar techniques, simulations and *in vitro* experiments indicate that reasonable speckle tracking estimates can be achieved also for near-perpendicular beam-to-flow angles.

5.1 Introduction

Blood velocity estimation and visualization using ultrasound color flow imaging (CFI) provides a parametric map of the mean axial blood velocities in a spatial region of interest, and is widely used when diagnosing cardiovascular disease, for the evaluation of organ perfusion and also in the context of tumor characterization [1]. In CFI, only the velocity component along the ultrasound beam axis can be measured, and the angle between the beam axis and the direction of blood flow must be known to find the true blood velocity vector. This angle-dependency is one of the fundamental limitations of Doppler methods and may result in color flow images which are difficult to interpret and therefore of limited clinical applicability.

One suggested method to overcome the angle-dependency has been to utilize the blood speckle pattern. The movement of blood speckle follows that of blood and is in principle not angle-dependent. Both qualitative methods for visualizing the speckle movement in CFI as well as approaches for *speckle tracking* have been proposed [2, 3]. Speckle tracking is based on estimating the displacement of smaller regions of speckle from frame to frame and can in principle provide quantitative angle-independent blood velocity estimates. Other methods proposed for 2-D blood velocity estimation includes vector-Doppler and transverse oscillation [4, 5], directional cross-correlation [6], a Doppler bandwidth approach [7], and Fourier-based methods [8].

Clutter filtering is required to attenuate the strong signal from surrounding tissue (e.g. vessel walls) which is typically 40-80 dB stronger than the signal from blood [9]. This is done using a high-pass filter in slow-time to attenuate the signal from (near) stationary scatterers. Clutter filter design and its influence for color flow imaging has been thoroughly investigated [9–11]. In conventional CFI, the slow-time ensemble size is kept low (8-16) to achieve acceptable frame rates, and one of the main challenges has been to design low order clutter filters with a sufficient stopband attenuation and a steep transition to pass band. This strict requirement is alleviated using more recent high frame rate acquisition techniques based on synthetic transmit aperture and plane wave imaging [12, 13], however, at near-perpendicular beam-to-flow angles the signal from blood will also be attenuated, leading to biased velocity estimates and signal drop-outs in CFI [11].

As the 1-D axial blood velocity component also determines the filter attenuation in BST, speckle tracking performance will be degraded for high beam-to-flow angles and is therefore in practice not truly angle-independent. Similar is true for all other multi-dimensional blood velocity estimators proposed, with exception of Fourier-based methods where attempts have been made to separated clutter and blood flow signal directly in the 2-D fast-time / slow-time frequency domain [8]. Still, previous work investigating clutter filter design and estimator influence is limited. For speckle tracking the advantage of using time-invariant filters has been underlined to avoid speckle decorrelation due to the filter itself [14], and adaptive clutter filtering techniques has been proposed to improve performance specifically for this approach [15].

In this work we investigate: 1) clutter filter design in the context of speckle tracking, and 2) how the clutter filter influences speckle appearance and subsequent tracking

performance in the filter transition and stop band region. The main motivation is to measure as low blood velocities as possible and at every beam-to-flow angle. Clutter filter designs for both conventional and the more recent plane wave imaging (PWI) approach, where longer Doppler ensembles are available, are considered. Theoretical considerations, simulations, and *in vitro* experiments are used to shed light on these subjects.

5.2 Background

5.2.1 Time-invariant vs time-variant clutter filters

High-pass filters commonly used for clutter rejection in ultrasound color flow imaging include finite impulse response (FIR) filters, infinite impulse response (IIR) filters with different types of initialization and polynomial regression filters [9–11, 16, 17]. A general linear filtering operation can be described as a matrix-vector multiplication [9]

$$\mathbf{y} = \mathbf{A}\mathbf{x}, \tag{5.1}$$

where $\mathbf{x} = [x(0), x(1), \ldots, x(N-1)]^T$ is the input vector of the complex demodulated Doppler signal with an ensemble size of N, $\mathbf{A}$ is an $N \times N$ matrix and $\mathbf{y} = [y(0), y(1), \ldots, y(N-1)]^T$ is the output vector.

For a FIR filter of order K, the filter matrix is given by

$$a(n,m) = \begin{cases} h(n-m) & n > K \text{ and } n-K \leq m \leq n \\ 0 & \text{elsewhere,} \end{cases} \tag{5.2}$$

where $h(n)$ is the filter impulse response. The first K output samples must be discarded due to initialization. The FIR filter is time-invariant and all output samples are filtered with the same impulse response. For velocity estimation based on signal correlation, the phase of the filter is not important and a nonlinear phase filter may therefore be used [11].

Regression filters approximate the clutter signal using a set of low-frequency and orthogonal basis functions, and subtract these from the original signal. The filter matrix is then given by [9]:

$$a(n,m) = \delta(n-m) - \sum_{p=0}^{P} b_p(n)^* b_p(m) \tag{5.3}$$

$$y(n) = \sum_{m=0}^{N-1} h_n(m)x(m), \tag{5.4}$$

where $b_0, b_1, ..b_P$ are orthonormal basis functions, e.g. Legendre polynomials, and P is the filter order. Regression filters are time-variant which implies that each row in the filter matrix A define individual FIR impulse responses $h_n(m)$, and each output sample $y(n)$ are therefore filtered differently in general. The overall frequency response of regression filters as used in CFI is given as the average over the ensemble.

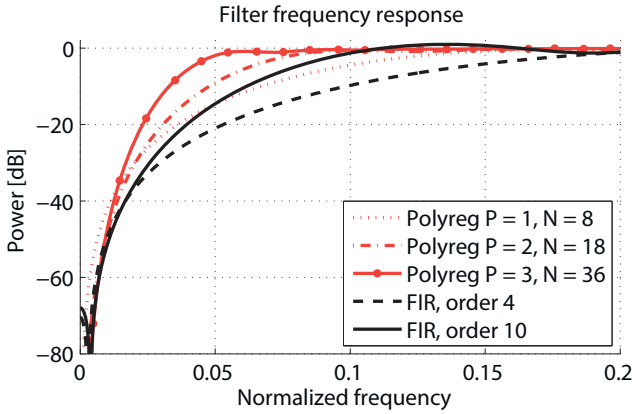

Figure 5.1: Frequency responses of two FIR and three polynomial regression filters (order 1, 2, 3 for ensemble size 8, 18, 36) with comparable stop band attenuation. The frequency axis is normalized to $[-0.5, 0.5]$.

Speckle tracking techniques depend on the similarity between subsequent image regions, and differences introduced by time-variant high-pass filtering should be avoided. Time-invariant FIR filters have therefore previously been preferred. In conventional CFI the ensemble size is limited by frame rate requirements to about 8-16 samples depending on the application. The recent introduction of parallel imaging using plane or diverging transmit pulses, allows for substantially longer signal ensembles. This means that more samples are available for clutter filtering, and FIR filters of higher order can for instance be used. However, it is also desired to retain as many valid output samples as possible for averaging to decrease the variance of the final velocity estimates.

In Fig. 5.1, the filter frequency responses are shown for two FIR filters and three polynomial regression filters with similar stop band characteristics. The frequency response of the polynomial regression filter varies with filter order P and ensemble size N. Steeper transition regions can be achieved for polynomial regression filters compared with corresponding FIR filters, and in addition are all filter output samples in principle valid.

In Fig. 5.2, the frequency responses for two polynomial regression filters are plotted for two consecutive output samples in the middle of the ensemble, $N/2 - 1$ and $N/2$. As can be seen, the frequency responses are different for the two output samples when using an ensemble size of $N = 8$, whereas they are close to identical for an ensemble size of $N = 36$. To further quantify the imposed decorrelation due to the time-variant nature of these filters, the normalized correlation between consecutive rows in the polynomial regression filter matrices were calculated and plotted in Fig. 5.3. It was observed that if the first and last output sample were discarded, all three cases have normalized correlations above 0.9, and for an ensemble size of $N = 36$

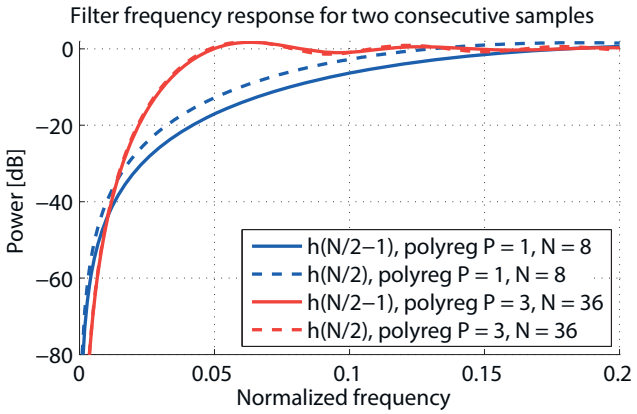

Figure 5.2: A comparison of the filter frequency responses for consecutive output samples for two polynomial regression filters. The two output samples are from the middle of the ensemble, $N/2-1$ and $N/2$. For a polynomial regression filter of order 3 and ensemble size $N = 36$, the frequency responses are close to identical for the two output samples, whereas for the polynomial regression filter of order 1 and ensemble size $N = 8$, a distinct difference is observed.

the correlation is above 0.95. Thus, the decorrelation introduced by a polynomial regression filter decreases significantly for high ensemble sizes. Similar is the case for the frequency bias introduced in the transition region for these filters using the autocorrelation approach in CFI [18].

5.2.2 Clutter filter influence on speckle pattern

In this section, theoretical considerations and simulations are used to illustrate the clutter filter influence on the blood speckle. The theoretical aspect has previously been discussed by Bjærum in [19, Paper H].

In an imaging system, x,y and z are the coordinates in the azimuth, elevation and axial directions, respectively. The system is assumed to be linear shift-invariant and the image plane is positioned at $y = 0$. Then, at time t_0, the image operation can be expressed by the convolution

$$i(x, z, t_0) = p(x, y, z) \underset{x,y,z}{*} o(x, y, z, t_0)|_{y=0}, \tag{5.5}$$

where $p(x, y, z)$ is the point-spread function of the imaging system and $o(x, y, z, t_0)$ is the object. Fourier transformation of the spatial variables gives

$$I(k_x, k_z, t_0) = \int P(\mathbf{k})O(\mathbf{k}, t_0)\mathrm{d}k_y, \tag{5.6}$$

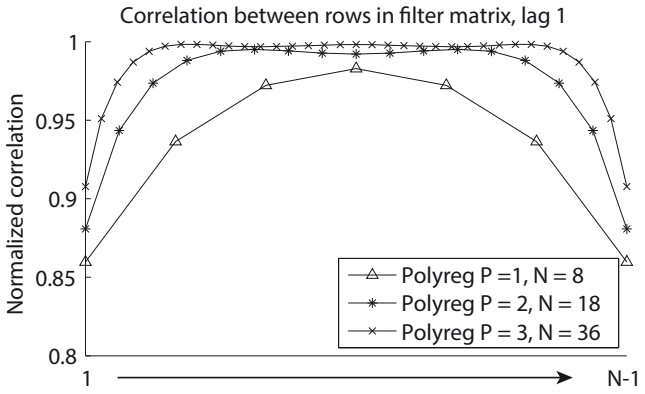

Figure 5.3: Normalized correlation of the impulse response functions $h_1, ..., h_{N-1}$ in the polynomial regression filter matrices with lag 1. The correlation is increasing for higher filter order and ensemble size.

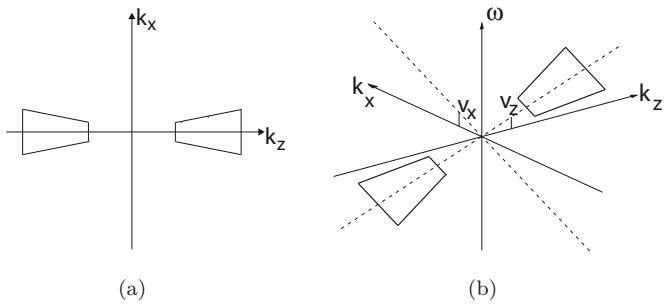

(a) (b)

Figure 5.4: Illustration of the Fourier spectrum of an ultrasound image prior to amplitude detection. (a) Imaging an object with zero velocity. (b) Imaging an object with axial and lateral velocity. The signal is projected onto a plane rotated around the x and z-axis according to the axial and lateral velocity of the object, where ω is the temporal angular frequency.

where $\mathbf{k} = (k_x, k_y, k_z)$. Equation 5.6 represents the image spectrum in the frequency domain and is illustrated schematically in Fig. 5.4a. Since the ultrasound pulse is a band-pass signal, the spectrum has band-pass characteristics in the k_z-direction.

An object moving with velocity $\mathbf{v}$ is imaged with pulse repetition time T. Assuming the velocity component transverse to the image plane, v_y, is zero, the resulting spectrum including the temporal angular frequency can be written as

$$I(k_x, k_z, \omega) = \int P(\mathbf{k}) O(\mathbf{k}, t_0) \delta(\omega - k_x v_x - k_z v_z) \mathrm{d}k_y, \tag{5.7}$$

where δ is the Dirac delta-function. The corresponding spectrum with lateral and axial

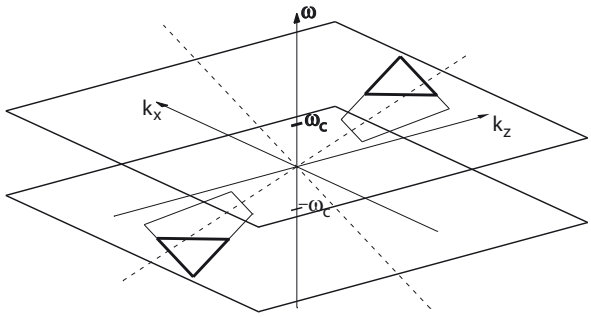

Figure 5.5: Clutter filtering is performed in the slow-time direction, and the effect of the high-pass filter on the spectrum in Figure 5.4b is illustrated here. The two planes, placed at the filter cut-off frequency ω_c, defines the frequencies removed by the filter.

motion is illustrated in Fig. 5.4b. The sampling frequency $1/T$ makes the spectrum periodic with period $2\pi/T$ in the temporal ω-direction, but only one period is included in the figure. The received signal is located in a plane rotated around the x and z axis according to the v_z and v_x velocity, respectively. A non-zero v_y-velocity will broaden the spectrum in the k_x- and k_z-direction.

The effect of high-pass filtering the signal with a 1-D, time-invariant filter is illustrated in Figure 5.5, where it is schematically represented by two planes removing the part of the signal contained in the interval $[-\omega_c, \omega_c]$. The filter transfer function, $H(\omega)$ is introduced to the image equation as:

$$I(k_x, k_z, \omega) = \int P(\mathbf{k})O(\mathbf{k}, t_0)\mathrm{d}k_y H(\omega)\delta(\omega - k_x v_x - k_z v_z). \tag{5.8}$$

The projection of the spectrum in Figure 5.5 onto the $k_x - k_z$-plane is shown in Figure 5.7a, where it is is seen that the total signal bandwidth is reduced when parts of the blood signal is within the stop band of the filter. This will in effect smear out the speckle pattern in the spatial domain. The latter is shown in Figure 5.6 for a straight-tube flow simulation using the simulation setup described in Sec. 5.3.3. The tube is tilted at a beam-to-flow angle of 80°, and the flow profile is parabolic with maximum velocity of 0.5 m/s. A fourth order minimum phase FIR filter with cut-off at $0.33 * V_{\text{Nyquist}}$ was used, as shown in Figure 5.1 with a black dashed line.

When the object is moving in the lateral (x) direction only, the 2-D projection of the filtered spectrum is shown in Fig. 5.7b. The Fourier imaging plane is only rotated around the z-axis and the high-pass filtering leads to a spectrum with bandpass characteristic for k_x. This results in amplitude modulation of the output speckle in the lateral direction after clutter filtering as seen in Fig. 5.8b. Due to of the lateral imaging bandwidth there is still remaining signal after filtering even for perpendicular beam-to-flow angles, but the total signal power will be significantly attenuated by the clutter filter. The effects on the speckle pattern using a time-variant clutter filter is similar to a time-invariant filter, but the correlation between the subsequent images

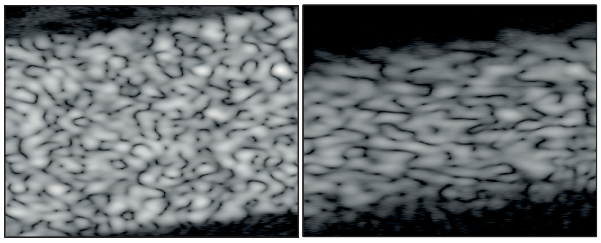

(a) No clutter filter applied (b) Clutter filter applied

Figure 5.6: Speckle patterns in a straight-tube flow simulation with beam-to-flow angle of 80 degrees, without and with clutter filtering. The speckle is smeared after clutter filtering.

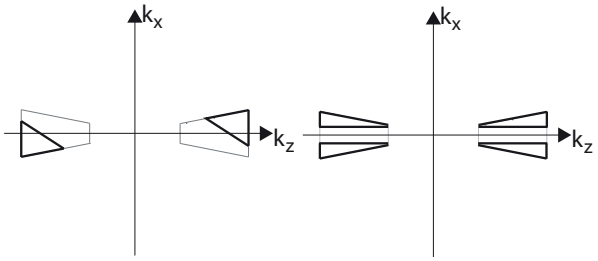

(a) Both axial and lateral velocity. (b) Only lateral velocity.

Figure 5.7: The effect of clutter filtering on the signal spectrum is illustrated here with the 2-D projection of the 3-D Fourier spectrum in Fig. 5.5 in (a). Both bandwidth and power is decreased after clutter filtering. (b) The corresponding spectrum when imaging an object with only lateral velocity. Clutter filtering leads to a bandpass characteristic spectrum for the k_x-frequencies.

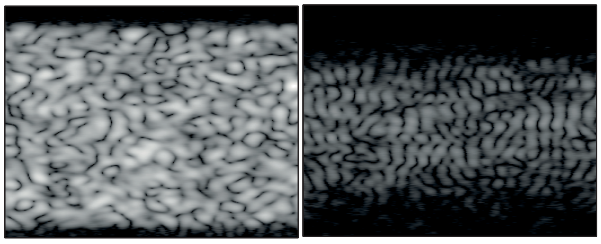

(a) No clutter filter applied (b) Clutter filter applied

Figure 5.8: Speckle patterns in a straight tube flow simulation with beam-to-flow angle of 90 degrees, without and with clutter filtering. An amplitude modulation is introduced in the speckle after clutter filtering.

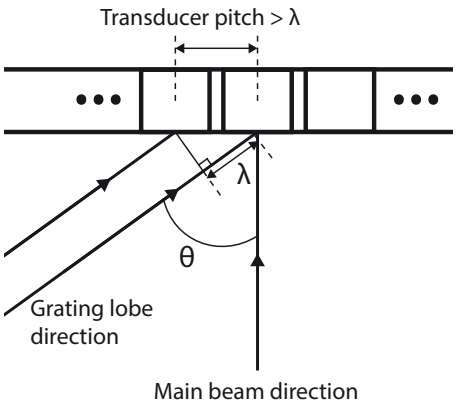

Figure 5.9: Grating lobes are replicas of the main beam which occur when neighboring elements interfere constructively in other direction than the main (receive or transmit) beam. The angle of the grating lobes depends on the wavelength, the pitch of the transducer and the steering of the main beam.

within an ensemble is affected as discussed in section 5.2.1. Visually this results in a flickering of the speckle images when displayed frame-by-frame.

5.2.3 Clutter filters and grating lobes

The regular element spacing of the ultrasound transducers infers unwanted constructive interference patterns in the imaging region called grating lobes, when the pitch (distance between element centers) of the transducer is larger than the pulse wavelength λ. The (first) grating lobes will occur at the angle θ where the received (or transmitted) ultrasound pulses of neighboring elements differ by one wavelength as sketched in Fig. 5.9. Including electronic steering of the beam will further bring the grating lobes into the imaging region [20]. The occurrence of grating lobes depends on the pulse wavelength, the pitch of the transducer and the steering angle of the beam as follows:

$$\sin\theta_k - \sin\theta_0 = k\frac{\lambda}{d}, \quad k = \pm 1, \pm 2, ..., \tag{5.9}$$

where θ_0 is the steering angle of the beam, θ_k is the angle of the grating lobe, λ is the wavelength, d is the pitch and k is an integer number [21].

For plane wave imaging, unfocused ultrasound waves insonify a wide region, and high frame rate, full field-of-view imaging is obtained by generating all receive beams in parallel. It should then also be noted that the grating lobes become more significant compared to focused transmit beams where most of the energy is concentrated in the main beam lobe. In Fig. 5.10, the two-way beam profiles for two linear arrays are compared. Dynamic focusing and Tukey window apodization is utilized on receive. To the left, the array has 128 elements and beam profiles for both unfocused and

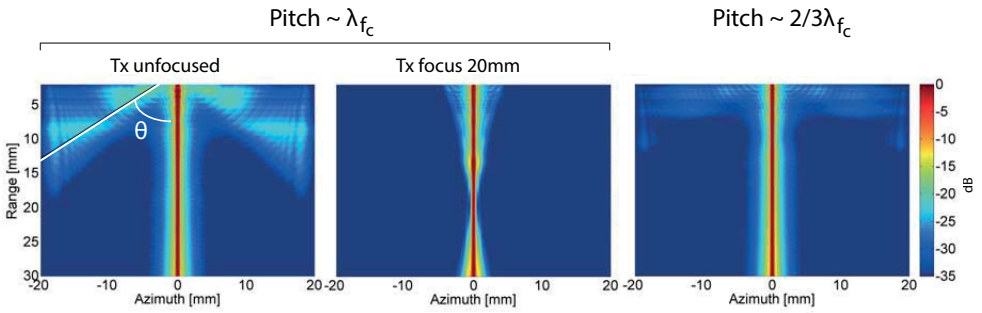

Figure 5.10: Two-way beam profiles for linear arrays with 128 elements and 192 elements, respectively. The 128 element array has a pitch approximately equal to the wavelength of the pulse center frequency. The pitch for the 192 element array is $\frac{2}{3}\lambda_{fc}$. The responses for both unfocused and focused transmissions are found for the 128 elements array, and are shown to the left. Grating lobes are observed at angles 56-90 degrees for unfocused transmission. To the right the beam profile for the 192 element array using unfocused transmission is shown. All beam profiles are normalized to maximum intensity at all depths.

focused transmission are shown. The pitch of this array is approximately equal to the wavelength of the pulse center frequency of 5 MHz, implying grating lobes at 90 deg. However, when using a pulse of 50% bandwidth (as is quite common in CFI) the highest frequency components are around 6MHz, and grating lobes will therefore occur at $\theta = \arcsin(\lambda_{f\max}/d) \approx 56°$. The grating lobes in the simulation was 20 dB below the main lobe when using unfocused transmissions, while below 35 dB when the transmitted waves were focused at 2 cm depth. To the right, the beamprofile for unfocused transmission using a 192 element linear array is shown. The pitch of this array is equal to $\frac{2}{3}\lambda_{fc}$, and as can be seen, this results in significantly reduced grating lobe levels for the same imaging pulse.

In the context of clutter filtering and blood velocity estimation, the grating lobes may register blood signal from a different effective beam-to-flow angle than the main beam, and may thus bias the blood velocity estimates coming from the main lobe, a known effect in Doppler imaging. The potential influence of grating lobes on the speckle tracking accuracy has not been investigated, and is in this work evaluated using the simulation setup described in Sec. 5.3.3.

5.3 Methods

5.3.1 The blood speckle tracking method

The basic principle in speckle tracking is shown schematically in Figure 5.11. A 2-D kernel region is defined in an initial frame, and the displacement of the kernel is then searched for in a subsequent frame of data. The displacement is found using a

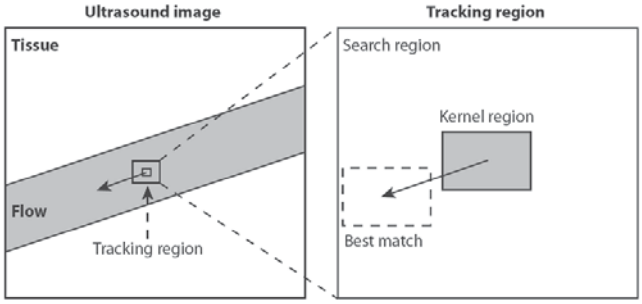

Figure 5.11: The basic principle of speckle tracking.

template matching search among all possible locations in a limited search region [3]. A velocity vector can be calculated using the estimated displacement and the known time between the frames. When all the defined kernels in the image have been tracked, a full velocity vector map of the flow is obtained. Temporal and spatial averaging is used to reduce the variance of the estimates. Tracking can be done on both RF and envelope (detected) data. The type of ultrasound data utilized affect computational demands (higher for RF), it may affect the tracking performance [3], and the clutter filter influence may be different.

The pattern matching algorithms used in this work were normalized 2-D cross-correlation (NCC) and sum-of-squared-differences (SSD). The NCC is given by

$$\rho(u,v) = \frac{\sum\limits_{x,y}\left(I(x+u,y+v) - \overline{I}_{u,v}\right)\left(K(x,y) - \overline{K}\right)}{\sqrt{\sum\limits_{x,y}(I(x+u,y+v) - \overline{I}_{u,v})^2 \sum\limits_{x,y}(K(x,y) - \overline{K})^2}}, \tag{5.10}$$

where K is the original kernel and I is the search region displaced (u,v) from the kernel K position for a subsequent frame. The averages are defined as

$$\begin{aligned} \overline{I}_{u,v} &= \frac{1}{N_x N_y}\sum_{x,y} I(x+u,y+v) \\ \overline{K} &= \frac{1}{N_x N_y}\sum_{x,y} K(x,y), \end{aligned} \tag{5.11}$$

where N_x and N_y are the kernel dimensions, so $x = [0, N_x - 1]$ and $y = [0, N_y - 1]$. The index of the maximum correlation value determines the most likely displacement of the kernel.

The SSD algorithm is given by

$$d(u,v) = \sum_{x,y}\left(I(x+u,y+v) - K(x,y)\right)^2, \tag{5.12}$$

where the minimum SSD-coefficient $d(u_{\min}, v_{\min})$ reveals the most likely displacement of the kernel. The SSD is substantially less computationally demanding and therefore attractive from a real-time imaging perspective.

The size of the search region determines the maximum measurable velocity and is in practice limited by the correlation length of the signal. The minimum measurable velocity is initially limited by the grid resolution in the correlation or matching matrix. In this work the IQ data was linearly interpolated both laterally and radially to achieve a velocity resolution of 0.1 m/s in both directions. Parabolic subsample interpolation of the estimated grid displacement was further used in the x and z directions respectively to improve the velocity resolution. The offset correction is then given by [22]:

$$\hat{\delta} = \frac{d_0 - d_2}{2(d_0 - 2d_1 + d_2)}, \tag{5.13}$$

where $d_1 = \rho_{max}$ was the displacement location with the highest correlation and d_0 and d_2 were the two nearest neighbors. The velocity estimates were finally averaged over the temporal ensemble and in a 1 mm×1 mm spatial region.

5.3.2 The autocorrelation method

The autocorrelation method (ACM) is conventionally used to estimate the mean axial velocity in color flow imaging [23]. The autocorrelation function is estimated as follows,

$$\hat{R}(l) = \frac{1}{N-l} \sum_{k=1}^{N-1} x(k)^* x(k+l), \tag{5.14}$$

where $x(k)$ is the Doppler ensemble from a fixed spatial position, * denotes the complex conjugate and N is the ensemble size. The autocorrelation estimates were spatially averaged as for ST estimates and the velocity estimates were calculated using:

$$\hat{v}_d = \frac{c \cdot \mathrm{PRF}}{4\pi f_0} \angle(\hat{R}(1)), \tag{5.15}$$

where the c is the speed of sound, PRF is the pulse repetition frequency and f_0 is the pulse center frequency.

5.3.3 Ultrasound simulation setup

The ultrasound simulation tool, Field II [24], was used to investigate clutter filter influence on speckle tracking performance. The imaging set up is shown in Fig. 5.12. Channel data from two different linear arrays transmitting unfocused (plane) waves covering the whole transducer width were simulated, and 256 receive beams were beamformed for each transmission with an F-number of 1.4. The pulse repetition frequency (PRF) was 4 kHz and the temporal ensemble size varied from 8 and 48. The sampling frequency of the radio-frequency (RF) data was 100 MHz, and the RF data were IQ demodulated at a demodulation frequency of 5 MHz and decimated to

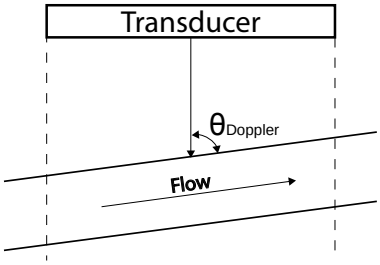

Figure 5.12: Simulation setup of straight tube flow. The tube is tilted to obtain beam-to-flow angles from 60-90°. Unfocused waves are transmitted using all elements of the transducer. All receive beams are simulated in parallel.

Table 5.1: Simulation parameters

Probe	#1: UX L9-4/38	#2
Probe type	Linear array	Linear array
Number of elements	128	192
Pitch [μm]	304	203
Elevation focus [mm]	19	19

Pulse center frequency [MHz]	5
Pulse length	2.5
PRF [Hz]	4000
ensemble size	8-48
Receive F-number	1.4
Doppler angle [degrees]	60-90
SNR [dB]	5, 30
Straight tube length [cm]	6
Straight tube radius [cm]	0.5

a sampling frequency of 20 MHz. Dynamic focusing and Tukey window apodization was used on receive. Two transducers were simulated, a 128 element linear array and a modified version with 192 elements and 2/3 times the pitch. The transducer specifications and other simulation parameters are listed in Table 5.1.

The straight tube model was 6 cm long with a radius of 5 mm, and placed at a depth of 2 cm. The tube was tilted with beam-to-flow angles varying between $60-90°$, moving the blood signal gradually into the filter transition and stop band region for the different filters. The blood signal was simulated with 10 point scatterers per resolution cell to ensure a Gaussian distributed signal amplitude as expected from blood scatterers. The blood scatterers followed a parabolic velocity profile with a maximum velocity of 0.5 m/s. White noise was added to yield two cases of low SNR (5 dB) and high SNR (30 dB). The simulations did not include clutter signal, and we therefore assume that the filters remove the clutter signal sufficiently.

5.3.4 *In vitro* setup

To confirm the simulation results, we used a SonixMDP ultrasound scanner (Ultraonix, Richmond, BC, Canada) with the UX L9-4/38 probe to acquire *in vitro* data. A Sonix DAQ was connected to the scanner to acquire channel data and the beamforming was done off-line. The plane wave data was acquired continuously at a PRF of 4000 Hz. The *in vitro* setup consisted of a pump (PhysioPulse 100 Flow System, Shelley Medical Imaging Technologies, London, ON, Canada) connected to a straight-tube flow phantom (ATS Laboratories, Bridgeport, CT, USA) using a blood-mimicking fluid [25]. The tube had a diameter of 6 mm, and a pulsatile sinusoidal flow pattern was setup at beam-to-flow angles of 63° and 83°. The maximum velocity was approximately 0.8 m/s. We otherwise used the same processing setup as for the simulations.

To validate the velocity estimates in the *in vitro* case, PW-Doppler spectra were generated from the same data used for speckle tracking and the autocorrelation method. The PW-Doppler spectra were averaged in a 1mm×1mm region in the middle of the tube, and calculated using the conventional Welch spectral estimation approach.

5.3.5 Performance evaluation

The clutter filter influence on blood velocity estimation using 2-D speckle tracking was investigated as follows:

1. The performance of ST was investigated in the clutter filter transition and stop band region for varying ensemble sizes and clutter filters available using both conventional and plane wave acquisition strategies.

2. The performance of time-invariant (FIR) versus time-variant (polyreg) filters was compared, particularly relevant when considering duplex modalities with a separate B-mode acquisition.

3. As grating lobes are significantly higher for plane wave imaging, the effect of clutter filtering when grating lobes are present was investigated.

4. The potential difference in tracking performance using RF or envelope data was evaluated, a choice with significant impact on computational demands and future real-time implementation.

The straight-tube simulation setup and transducer #2 (without grating lobes) were used to investigate the influence of clutter filtering on ST performance for both high (30dB) and low (5dB) signal-to-noise scenarios, and for varying beam-to-flow angles. Unless otherwise specified, envelope data and SSD matching were utilized for tracking. The 4th order FIR filter was used for ensembles from 8-18, while the 10th order FIR filter was used for the longer ensembles. The first and last output samples from the polynomial regression filters were discarded to decrease the decorrelation introduced by the filter. Finally, speckle tracking performance was investigated for the described *in vitro* setup using a beam-to-flow angle of 63° and 83°, respectively.

The overall accuracy of the velocity measurements was evaluated using the mean absolute bias and mean standard deviation, as well as the root-mean-squared error (RMS) for all realizations in a 2 cm length of the tube and for a radius < 4 mm. The exact ground truth velocity in the *in vitro* setup was not know, and in this case the PW-Doppler spectrum from the most parallel beam-to-flow angle (63°) was used as reference.

5.4 Results

The RMS error of the V_x estimates for ST and V_z estimates for both ST and ACM for varying beam-to-flow angles and for both high and low SNR, when using a high ensemble size $N = 36$, is shown in Fig. 5.13. For high SNR, the V_z RMS error for ST stays relatively constant for all angles while ACM exhibits an increasing error when approaching 90 deg. The latter can be attributed to the expected bias in the filter transition region as shown previously [11]. The ACM method is in general more robust for low SNR, however, for a high initial SNR (30dB) and when using the polynomial regression filter the performance is comparable. The RMS error of the V_x component is approximately least twice that of the V_z for ST, but with an increasing error when entering the filter transition region. For the low SNR scenario using the FIR filter, the performance is substantially worsened for V_x, however, it should be noted that the V_x component increases for higher beam-to-flow angles, and is substantially higher than V_z.

The RMS error of the V_x and V_z estimates for an increasing ensemble size (8-48) and a near-perpendicular beam-to-flow angle (85°) is shown in Fig. 5.14. For a short ensemble size and a high initial SNR the polyreg filter gave larger errors despite the overall improved frequency response. When increasing the ensemble size this gradually changed, and for $N = 40 - 50$ the polynomial regression filter was generally preferred, and in particular for reducing the RMS error of the V_x component. For low initial SNR the polyreg was consistently better for the V_z component, and comparable or better for the V_x component except for very low ensemble sizes. The corresponding RMS error for the V_z estimates from the ACM is plotted in the rightmost panel. The ACM is in general less influenced by SNR compared to ST, but the RMS error is approximately twice that of ST when using a high ensemble size.

The influence of grating lobes is shown in Fig. 5.15, where higher Doppler phase shifts and large speckle movements were observed outside and partly inside the simulated tube. As expected, the grating lobes artifacts were greatly reduced when a transducer with a lower pitch was used. The Doppler spectra from the red and blue squares inside the tubes are plotted in the lower panel, where a significant difference between the transducers can be observed. The bias of the velocity estimates inside the squares are plotted in Fig. 5.16. The absolute velocity bias increased for increasing beam-to-flow angle and was worst for the clutter filter with highest velocity cut-off. The bias was significantly reduced when transducer #2 was used where the grating lobes were insignificant.

A comparison of ST performance using RF and envelope data is shown in Fig. 5.17.

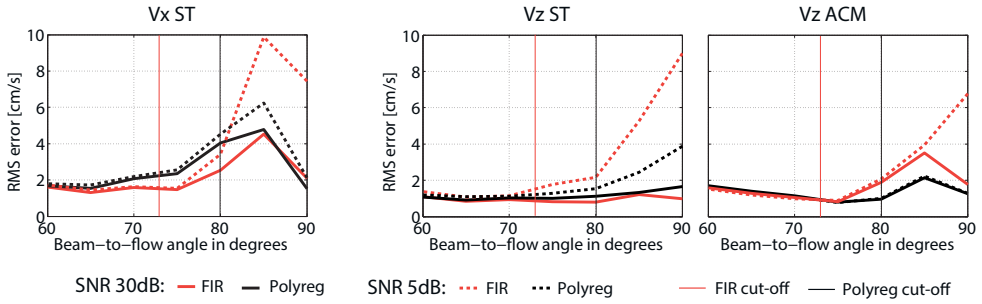

Figure 5.13: A comparison of the velocity estimates using the 10th order finite impulse response (FIR) and polynomial regression (polyreg) filters. The root-mean-square error of the velocity estimates is plotted as a function of beam-to-flow angle for signal-to-noise ratios of 5 dB and 30 dB. The ensemble size is $N = 36$. Left: V_x-estimates from speckle tracking (ST). Right: V_z-estimates from speckle tracking and autocorrelation (ACM), respectively. The true velocities range from $V_x = 0.43 - 0.5\,\mathrm{m/s}$ and $V_z = 0.25 - 0\,\mathrm{m/s}$ when the beam-to-flow angle is increased from 60° to 90°.

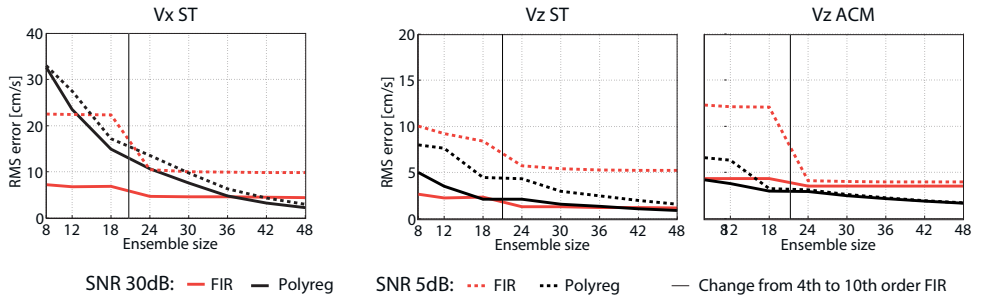

Figure 5.14: A comparison of the velocity estimates using finite impulse response (FIR) and polynomial regression (polyreg) filters. The root-mean-square error of the velocity estimates is plotted as a function of ensemble size for signal-to-noise ratios of 5 dB and 30 dB. The beam-to-flow angle is 85°and the true velocities are $V_x \approx 0.5\,\mathrm{m/s}$ and $V_z \approx 0\,\mathrm{m/s}$. Left: V_x-estimates from speckle tracking (ST). Right: V_z-estimates from speckle tracking and autocorrelation (ACM), respectively. Note: The plots have different scaling.

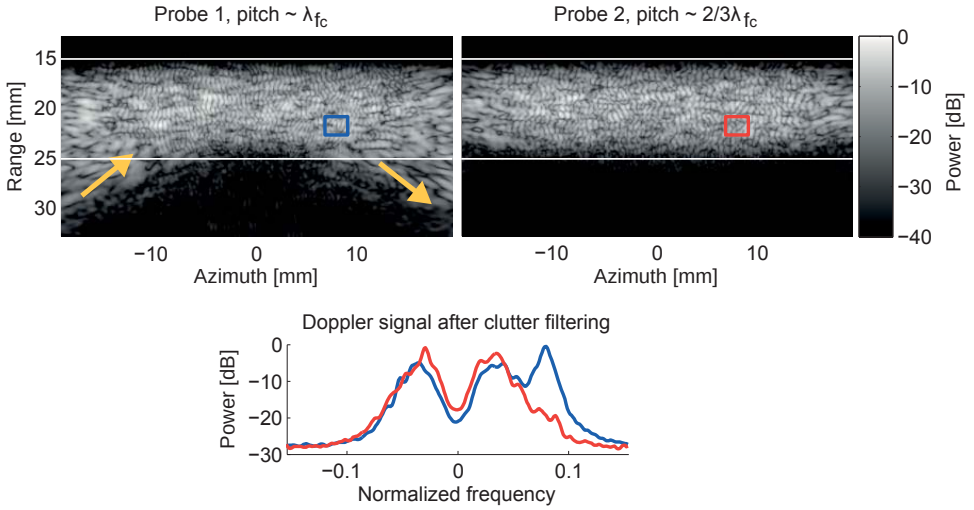

Figure 5.15: A comparison of the grating lobe influence between the two transducer simulated. No noise was added and the 4th order finite impulse response filter was used as clutter filter. The speckle below the tube is only due to the grating lobes and the movement of this speckle is indicated by the yellow arrows. The averaged Doppler signals from the blue and red square (after clutter filtering) are plotted in the lower panel.

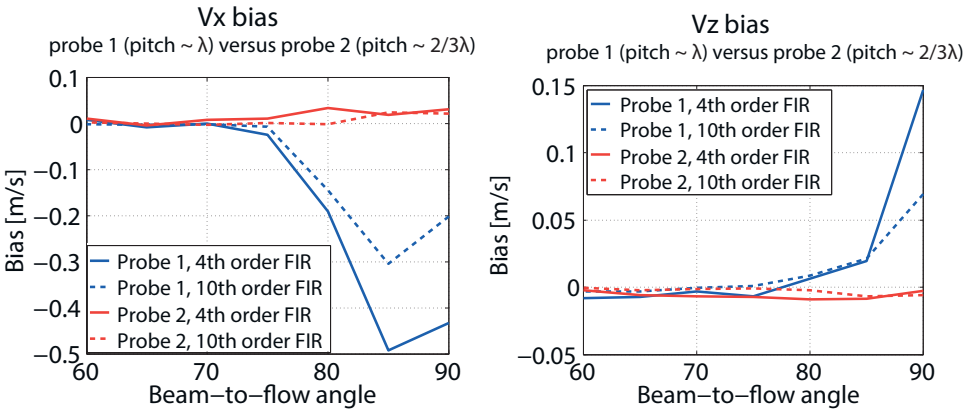

(a) (b)

Figure 5.16: A comparison of the bias of the V_x- and V_z-estimates from the blue and red squares in Fig. 5.15 for the two transducers. The true velocities range from $V_x = 0.43 - 0.5\,\mathrm{m/s}$ and $V_z = 0.25 - 0\,\mathrm{m/s}$ when the beam-to-flow angle is increased from 60° to 90°. No noise was added and the 4th order finite impulse response filter was used as clutter filter.

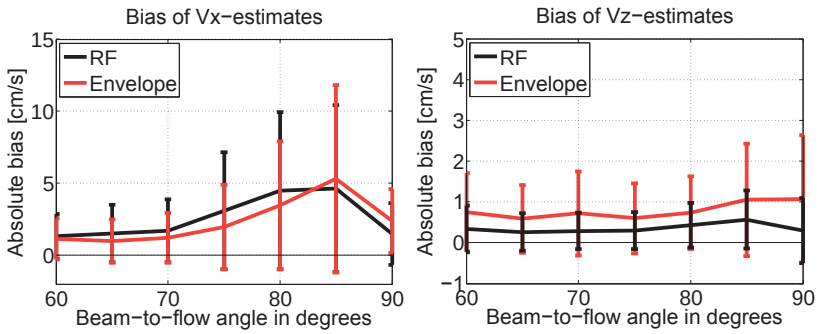

(a) (b)

Figure 5.17: The accuracy of RF and envelope tracking is compared using the speckle tracking (ST) estimates absolute bias as a function of the beam-to-flow angle. The ensemble size was 36 and the 4th order finite impulse response filter was used as clutter filter. The true velocities range from $V_x = 0.43 - 0.5\,\mathrm{m/s}$ and $V_z = 0.25 - 0\,\mathrm{m/s}$ when the beam-to-flow angle is increased from 60° to 90°. Note: The plots have different scaling.

The absolute bias and standard deviation of V_z estimates are approximately halved for RF tracking, while comparable for the V_x-estimates. It can also be observed that the standard deviation in general is substantially lower for the V_z component. Normalized cross-correlation was used for both the RF and envelope data in this case.

The *in vitro* setup used to confirm the findings from the simulations is shown in Fig. 5.18. The two setups with beam-to-flow angles of $\theta = 63°$ and $\theta = 83°$, and the corresponding PW-Doppler spectra are shown below in the leftmost panel. As expected, the spectrum for $\theta = 83°$ is of much poorer quality than the spectrum for $\theta = 63°$ due to the high beam-to-flow angle. To the right in the figure, the PW spectrum for the best beam-to-flow angle was angle-corrected and used as a reference for the velocity traces. Only the autocorrelation estimate from $\theta = 63°$ was angle-corrected and compared to ST. The best filter overall for low and high ensemble size respetively was selected based on the simulation results. This corresponded to a conventional acquisition low ensemble size setup ($N = 12$) using the 4th order FIR filter, and the polynomial regression filter for the high ensemble scenarios ($N = 36$). In the high ensemble case, the ST estimates for both beam-to-flow angles are similar and match the angle-corrected spectrum and ACM estimates, except when the ACM estimates are aliased. In the low ensemble scenario, the ST estimates for $\theta = 83°$ (blue dashed line) are generally underestimated compared to estimates at $\theta = 63°$ (red dashed line), with significant estimation bias in the very low velocity regions for both angles. In this region the (angle-corrected) ACM estimates are significantly overestimating the low velocities when filtered with the 4th order FIR filter (black dashed line).

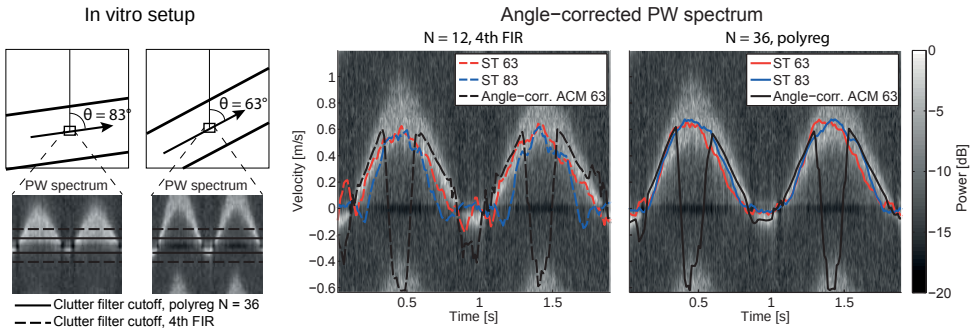

Figure 5.18: Left: *In vitro* straight-tube setup with two beam-to-flow angles, 83° and 63°, respectively. The resulting PW spectra from a sample volume in the middle of the tube for each beam-to-flow angle is shown below. Right: Results from conventional ensemble size and clutter filter are compared with results from a high ensemble size and polynomial regression filter. The angle-corrected PW spectrum from the smallest beam-to-flow angle is used as a reference specter. The absolute velocity found from speckle tracking (ST) for the two Doppler angles are compared with the angle-corrected autocorrelation estimates (ACM) from Doppler angle 63°.

5.5 Discussion

We have investigated how clutter filtering affects blood speckle appearance and speckle tracking performance when parts of the blood signal is attenuated by the filter. The overall motivation is to achieve a true angle-independent blood velocity estimator for a given minimum blood velocity. This will currently require special care for near-perpendicular beam-to-flow angles due to the Doppler-based clutter filtering. A series of simulations and *in vitro* experiments were used to investigate and evaluate tracking performance for different clutter filter designs. In particular, the possibility for improved clutter filtering using longer Doppler ensembles was considered, as can be obtained for instance based on plane wave imaging or synthetic transmit aperture imaging [12, 13].

Speckle tracking performance is influenced by the filter through the inferred decrease in SNR and imaging bandwidth, worsened for increasing beam-to-flow angles. These factors respectively lead to an increased variance and a lateral smearing of the speckle pattern. For RF-tracking it has also been reported that the clutter filter may introduce false or secondary peaks in the correlation function [9]. The smearing of speckle increases the tracking error (potentially both bias and variance) if the kernel region eventually becomes very small relative to the speckle size. This effect may be limited by increasing the kernel size. For stationary flows, a large kernel size is beneficial, whereas the optimal kernel size is difficult to predict when both spatial and temporal flow gradients are present [3]. The lateral bandwidth reduction ultimately leads to a lateral bandpass signal, where the associated amplitude modulation may increase tracking performance. Given a low F-number (wide lateral bandwidth), the

remaining signal after filtering may thus be sufficient to give reasonable tracking estimates also at perpendicular angles. The minimum velocity limit and required conditions for *in vivo* application remains to be investigated.

Results indicates that the overall RMS error for ST is comparable or better than the ACM for the V_z component when approaching the stop band of the clutter filter. Further, ST was not influenced by the bias that hampers the mean frequency estimate due to the skewed Doppler spectrum when the blood signal is partly attenuated, and ST can therefore be expected to yield more consistent estimates in the filter transition region. It should be noted that the performance evaluation was based on data from a large region in the vessel which included both low and high velocities, and that the velocity estimator performance as such has not been isolated. While other authors have also evaluated the speckle tracking estimator [14, 15, 26], we find it difficult to directly compare results as previous work has not focused on the blood velocities in the filter transition region.

The high acquisition rate provided by plane wave imaging (or related techniques) allows for high Doppler ensembles and thus clutter filters can be designed with steep transition regions. As seen in Fig. 5.13 and Fig. 5.14, the performance is substantially improved for high ensembles. Simulation results showed that this also allows for the use of the polynomial regression filters which has a steeper transition region and yields more valid output samples. The time-variant property of regression filters introduce a decorrelation between the output samples not present for FIR filters. However, as seen in Fig. 5.3, if the first and last output samples from the polynomial regression filter is discarded the decorrelation is kept insignificant for high ensemble sizes.

The use of polynomial regression filters is particularly advantageous for duplex modalities using a separate B-mode acquisition. Although both modalities can be generated from the same data acquired continuously, the B-mode image quality will often be compromised unless transmit focusing can be retained using a synthetic transmit aperture or coherent plane wave compounding approach [27]. This is often not the case, for instance when 2nd harmonic imaging is desired, or for phased-array imaging using small apertures in general.

While plane wave imaging is beneficial to achieve improved clutter filtering and instantaneous snapshots of blood speckle for 2-D tracking, the technique also introduce particular challenges for speckle tracking and blood velocity estimation in general. The reduced output pressure results in a reduction in SNR which may limit the final clinical applicability. For vascular imaging, coherent compounding of several transmitted plane waves from different angles could be used to retain SNR as well as transmit focusing. These aspects have not been investigated in this study. Plane wave imaging also increase grating lobes artifacts as seen in Fig. 5.9 and 5.15. Grating lobes artifacts become particular significant for high beam-to-flow angles, because the blood signal in the main lobe is more attenuated than the signal picked up by the grating lobes. A large velocity bias and variance may therefore be introduced for the highest beam-to-flow angles, and care should be taken to avoid grating lobes when setting up the acquisition scheme for a given transducer.

In the pursuit of real-time multi-dimensional velocity estimation based on speckle tracking, the computational demands should also be minimized. In our study, results

indicated that RF tracking may be more accurate for V_z-estimates, while similar for the V_x-estimates. Overall, envelope tracking may be used to decrease computation time without significantly compromising tracking accuracy.

5.6 Conclusion

Blood speckle tracking performance can be severely degraded by the current Doppler-based clutter filter scheme and is therefore not a true angle-independent 2-D blood velocity estimator. Compared to the autocorrelation approach, the speckle tracking estimator was in general less biased in the filter transition region, but more influenced by low signal-to-noise ratios. To improve tracking accuracy for near-perpendicular angles, a low F-number (large aperture) should be used to increase the lateral bandwidth. When high Doppler ensembles can be used, improved clutter filters such as the time-variant polynomial regression filter can be used to improve tracking performance. For this case, robust tracking performance could be achieved also in the filter transition and stop band region in our simulations and *in vitro* experiments.

References

[1] K. Ferrara and G. DeAngelis, "Color flow mapping," *Ultrasound in Medicine & Biology*, vol. 23, pp. 321–345, 1997.

[2] L. Lovstakken, S. Bjærum, D. Martens, and H. Torp, "Blood flow imaging - A new real-time, 2-D flow imaging technique.," *IEEE transactions on ultrasonics, ferroelectrics, and frequency control*, vol. 53, pp. 289–99, Feb. 2006.

[3] L. N. Bohs, B. J. Geiman, M. E. Anderson, S. C. Gebhart, and G. E. Trahey, "Speckle tracking for multi-dimensional flow estimation.," *Ultrasonics*, vol. 38, pp. 369–75, Mar. 2000.

[4] B. Dunmire, K. W. Beach, K.-H. Labs, M. Plett, and D. E. Strandness Jr., "Cross-beam vector Doppler ultrasound for angle-independent velocity measurements," *Ultrasound in Medicine & Biology*, vol. 26, no. 8, pp. 1213–1235, 2000.

[5] J. A. Jensen and P. Munk, "A new method for estimation of velocity vectors," *IEEE Transactions on Ultrasonics, Ferroelectrics, and Frequency Control*, vol. 45, pp. 837–851, 1998.

[6] J. A. Jensen and N. Oddershede, "Estimation of velocity vectors in synthetic aperture ultrasound imaging," *IEEE Transactions on Medical Imaging*, vol. 25, pp. 1637–1644, 2006.

[7] K. W. Yeung, "Angle-insensitive flow measurement using Doppler bandwidth.," *IEEE Trans Ultrason Ferroelectr Freq Control*, vol. 45, pp. 574–80, 1998.

[8] N. Oddershede, L. Lø vstakken, H. Torp, and J. r. A. Jensen, "Estimating 2-D vector velocities using multidimensional spectrum analysis.," *IEEE transactions on ultrasonics, ferroelectrics, and frequency control*, vol. 55, pp. 1744–54, Aug. 2008.

[9] H. Torp, "Clutter Rejection Filters in Color Flow Imaging: A theoretical approach," *IEEE Transactions on Ultrasonics Ferroelectrics and Frequency Control*, vol. 44, no. 2, pp. 417–424, 1997.

[10] A. P. G. Hoeks, J. J. W. Vandevorst, A. Dabekaussen, P. J. Brands, and R. S. Reneman, "An efficient algorithm to remove low-frequency doppler signals in digital doppler systems," *Ultrason. Imaging*, vol. 13, pp. 135–144, 1991.

[11] S. Bjærum, H. Torp, and K. Kristoffersen, "Clutter filter design for ultrasound color flow imaging," *IEEE Trans. Ultrason., Ferroelec., Freq. Contr.*, vol. 49, pp. 204–216, 2002.

[12] S. I. Nikolov and J. A. Jensen, "In-vivo synthetic aperture flow imaging in medical ultrasound," *IEEE Transactions on Ultrasonics, Ferroelectrics, and Frequency Control*, vol. 50, pp. 848–856, 2003.

[13] J. Bercoff, G. Montaldo, T. Loupas, D. Savery, F. Mézière, M. Fink, and M. Tanter, "Ultrafast compound doppler imaging: Providing full blood flow characterization," *IEEE Transactions on Ultrasonics, Ferroelectrics, and Frequency Control*, vol. 58, pp. 134–147, 2011.

[14] A. Swillens, P. Segers, and L. Lovstakken, "Two-dimensional flow imaging in the carotid bifurcation using a combined speckle tracking and phase-shift estimator: a study based on ultrasound simulations and in vivo analysis.," *Ultrasound in medicine & biology*, vol. 36, pp. 1722–35, Oct. 2010.

[15] C. M. Gallippi and G. E. Trahey, "Adaptive clutter filtering via blind source separation for two-dimensional ultrasonic blood velocity measurement," *Ultrason. Imaging*, vol. 24, pp. 193–214, 2002.

[16] E. S. Chornoboy, "Initialization for improved iir filter performance," *IEEE Trans. Signal Process.*, vol. 40, pp. 543–550, 1992.

[17] A. P. Kadi and T. Loupas, "On the performance of regression and step-initialized iir clutter filters for color doppler systems in diagnostic medical ultrasound," *IEEE Trans. Ultrason., Ferroelec., Freq. Contr.*, vol. 42, pp. 927–937, 1995.

[18] L. Lovstakken and H. Torp, "Extended velocity range in color flow imaging using parallel receive beamforming," *2010 IEEE International Ultrasonics Symposium*, pp. 1198–1201, 2010.

[19] S. Bjærum, *Detection and Visualization of Moving Targets in Medical Ultrasound Imaging.* PhD thesis, Norwegian University of Science and Technology, Department of Computer and Information Science, 2001. Paper IV reproduced with kind permission of Elsevier, sciencedirect.com.

[20] T. A. Whittingham, "Transducers and beam-forming," in *Diagnostic Ultrasound: Physics and Equipment* (P. Hoskins, K. Martin, and A. Thrush, eds.), pp. 32–33, Cambridge University Press, 2nd ed., 2010.

[21] B. Angelsen, "Ultrasonic beam forming with arrays," in *Ultrasound Imaging - Waves, Signals and Signal processing in Medical Ultrasonics*, ch. 6, pp. 6.20—-6.25, Trondheim: Emantec, 2000.

[22] I. Cespedes, Y. Huang, J. Ophir, and S. Spratt, "Methods for estimation of subsample time delays of digitized echo signals," *Ultrasonic imaging*, 1995.

[23] C. Kasai, K. Namekawa, A. Koyano, and R. Omoto, "Real-time two-dimensional blood flow imaging using an autocorrelation technique," *IEEE Transactions on Sonics and Ultrasonics*, vol. 32, pp. 458–464, 1985.

[24] J. Jensen, "Field: A program for simulating ultrasound systems," *Med.Biol.Eng.Comput.*, vol. 34, no. 5, pp. 351–352, 1996.

[25] K. V. Ramnarine, D. K. Nassiri, P. R. Hoskins, and J. Lubbers, "Validation of a new blood-mimicking fluid for use in Doppler flow test objects," *Ultrasound in Medicine and Biology*, vol. 24, no. 3, pp. 451–459, 1998.

[26] J. Udesen, F. Gran, K. H. Hansen, J. A. Jensen, C. Thomsen, and M. B. Nielsen, "High Frame-Rate Blood Vector Velocity Imaging Using Plane Waves: Simulations and Preliminary Experiments," *Ultrasonics, Ferroelectrics and Frequency Control, IEEE Transactions on*, vol. 55, no. 8, pp. 1729–1743, 2008.

[27] G. Montaldo, M. Tanter, J. Bercoff, N. Benech, and M. Fink, "Coherent plane-wave compounding for very high frame rate ultrasonography and transient elastography," *IEEE Transactions on Ultrasonics, Ferroelectrics, and Frequency Control*, vol. 56, pp. 489–506, 2009.